ABSTRACT

Title of thesis	Performance of Two-Stage CO_2 Refrigeration Cycles
Degree Candidate	Aydin Celik
Degree and Year	Master of Science, 2004
Thesis directed by	Professor Reinhard Radermacher, Ph.D. Department of Mechanical Engineering

The performance of four CO_2 cycle options was measured for three different evaporating temperatures, 7.2, -6.7, and -23.3°C under the ARI Standard 520 for condensing units. The four cycle options were the baseline cycle, the cycle with suction line heat exchanger, the cycle with intercooler, and two-stage split cycle. The cycle operation at the low evaporating temperature was limited by the high discharge temperature for most cycle options except the two-stage split cycle. The compressor used in the testing was a hermetic, rotary type two-stage compressor.

The effect of cycles and individual cycle components on system capacity and performance was investigated. Cycle optimization was conducted by using mass flow rate ratio, intermediate pressure coefficient and power ratio.

Modeling of these four cycles by EES showed similar results with the test data and provided information on sizing the system components for different system capacities for maximum performance.

PERFORMANCE OF TWO-STAGE CO_2 REFRIGERATION CYCLES

By

Aydin Celik

Thesis submitted to the Faculty of the Graduate School of the University of Maryland, College Park in partial fulfillment
of the requirements for the degree of
Master of Science
2004

Advisory Committee:

Professor Reinhard Radermacher, Ph.D., Chairman/Advisor

Associate Professor Gregory Jackson, Ph.D., Committee Member

Associate Professor Jungho Kim, Ph.D., Committee Member

Dedication

This is lovingly dedicated to my parents and friends for their endless love, support, and encouragement that made this work possible

Acknowledgement

I would first like to thank my advisor Dr. Reinhard Radermacher for providing me with the opportunity to work at the Center for Environmental Energy Engineering. I am also very grateful for the support of Dr. Yunho Hwang whose guidance was very helpful to carry on my work.

Special thanks also goes to the Heat Pump Lab team members, both past and present – namely, Jun-Pyo Lee, Amr Gado, Hajo Huff, J.K. Hong, John Linde, Lorenzo Cremaschi, Layla Monajemi, Kai Huebner and James Kalinger. It was a pleasure working with each and every one of you.

Special thanks are extended to Sanyo Co. who supported the research presented in this thesis.

Finally, I would like to express my gratitude to my parents and my friends who supported and trusted me with encouragement, devotion, and love.

Table of Contents

List of Tables vii

List of Figures ix

1 Introduction 1

1.1 Overview 1

1.2 Literature Review 6

1.3 Objectives 7

2 Experimental Setup 8

2.1 Compressor 8

2.2 Heat Exchangers 9

2.2.1 Gas Cooler and Intercooler 9

2.2.2 Suction Line Heat Exchanger and Internal Heat Exchanger 10

2.3 Electrically Heated Evaporator 11

2.4 Expansion Valves 12

2.5 Fans 13

3 Instrumentation and Measurement 14

3.1 Temperature Measurement 14

3.2 Pressure Measurement 15

3.3 Power Measurement 16

3.4 Mass Flow Rate Measurement 16

3.5 Data Acquisition System 17

4 Cycle Configurations and Test Conditions 18

4.1 Baseline Cycle 18

4.2 Cycle with Suction Line Heat Exchanger 19
4.3 Intercooler Cycle 20
4.4 Two-stage Split Cycle 21
4.5 Test Conditions 23
5 Experimental Results 24
5.1 Baseline Cycle 25
5.1.1 Test Condition A 26
5.1.2 Test Condition B 28
5.2 Cycle with Suction Line Heat Exchanger 29
5.2.1 Condition 1 30
5.2.2 Condition 2 32
5.3 Intercooler Cycle 34
5.3.1 Test Condition A 34
5.3.2 Test Condition B 36
5.4 Split Cycle 38
5.4.1 Test Condition A 38
5.4.2 Test Condition B 41
5.4.3 Test Condition C 45
5.5 Comparison of Test Results 48
6 Heat Exchanger Performances 56
6.1 Gas Cooler 59
6.2 Intercooler 62
6.3 SLHX 64

6.3.1 Condition 1 64
6.3.2 Condition 2 65
6.4 IHX 67
7 Compressor Performance Data 69
7.1 Volumetric Efficiencies 71
7.2 Compressor Efficiency 72
8 Optimization of Split Cycle 73
8.1 Optimum Mass Flow Ratio 76
8.2 Optimum Intermediate Pressure Coefficient 77
8.3 Optimum Power Ratio 79
9 Cycle Modeling 81
9.1 Baseline Cycle 83
9.2 SLHX Cycle 97
9.3 Intercooler Cycle 101
9.4 Split Cycle 109
10 Conclusions 116
11 Future Work 118
12 Uncertainty Analysis 119
13 References 121

List of Tables

Table 1: HCFC regulation schedule 2
Table 2: Environmental properties of common and alternative refrigerants 3
Table 3: Expansion valves for CO_2 refrigeration systems 12
Table 4: Specifications of the gas cooler and intercooler fans 13
Table 5: Specifications of thermocouples 14
Table 6: Specifications of pressure transducers 16
Table 7: Specifications of the power transducers 16
Table 8: Specifications of the refrigerant mass flow meter 17
Table 9: ARI test conditions for condensing units for refrigeration applications 23
Table 10: Tested conditions for CO_2 cycles 24
Table 11: Effect of different fan settings to system performance 26
Table 12: Properties of each state point at condition A for baseline cycle 27
Table 13: Performance of the baseline cycle at condition A 28
Table 14: Properties of each state point at condition B for baseline cycle 28
Table 15: Performance of the baseline cycle at condition B 29
Table 16: Properties of each state point at condition 1 for SLHX cycle 31
Table 17: Performance of the SLHX cycle at condition A-1 32
Table 18: Properties of each state point at condition 2 for SLHX cycle 33
Table 19: Performance of the SLHX cycle at condition A-2 34
Table 20: Properties of each state point at condition A for the intercooler cycle 35
Table 21 Performance of the intercooler cycle at condition A 36
Table 22: Properties of each state point at condition B for the intercooler cycle 37
Table 23: Performance of the intercooler cycle at condition A 38
Table 24: Two-stage split cycle test results at condition A 39
Table 25: Two-stage split cycle test results at condition B 42
Table 26: Two-stage split cycle test results at condition C 45
Table 27: Summary of test results – condition A 53
Table 28: Summary of test results – condition B 53
Table 29: Conventional condensing units 55

Table 30: Sensitivity analysis for the baseline cycle 83
Table 31: System performance at two different approach temperatures 89
Table 32: Comparison of experimental and simulation results for the baseline cycle 97
Table 33: Comparison of experimental and simulation results for the SLHX cycle 101
Table 34: Comparison of experimental and simulation results for the intercooler cycle 109
Table 35: Comparison of experimental and simulation results for the intercooler cycle 115
Table 36: Estimated uncertainties of characteristic parameters 120

List of Figures

Figure 1: Typical single-stage CO_2 cycle 4
Figure 2: R134a and CO_2 refrigeration cycles 5
Figure 3: Two-stage CO_2 compressor (Yamasaki et al. 2001) 9
Figure 4: Schematic of the heat exchanger for gas cooler and intercooler 10
Figure 5: Heat exchanger for SLHX and IHX 11
Figure 6: Electrically heated evaporator 12
Figure 7: Baseline cycle configuration 19
Figure 8: The cycle configuration for cycle with SLHX 20
Figure 9: Intercooler cycle configuration 21
Figure 10: Two-stage CO_2 cycle configuration 22
Figure 11 COP as a function of intermediate and discharge pressures for two-stage split cycle at condition A 40
Figure 12 Evaporating capacity vs. discharge pressure for two-stage split cycle–A 41
Figure 13 COP as a function of intermediate and discharge pressures for two-stage split cycle at condition B 44
Figure 14 Evaporating capacity vs. discharge pressure for two-stage split cycle–B 44
Figure 15 COP as a function of intermediate and discharge pressures for two-stage split cycle at condition C 47
Figure 16 Evaporating capacity vs. discharge pressure for two-stage split cycle–C 47
Figure 17: Comparison of CO_2 cycles in pressure-enthalpy diagram 49
Figure 18: COP variation with discharge pressure for baseline and SLHX cycles 50
Figure 19: COP variation with discharge temperature for baseline and SLHX cycles 50
Figure 20: System capacity of different CO_2 cycles at different test conditions 51
Figure 21: COP of different CO_2 cycles at different test conditions 52
Figure 22: Effect of evaporating temperature on COP 54
Figure 23: Specific heat variation of CO_2 with pressure and temperature 58
Figure 24: Pseudo-critical temperatures at different pressures 59
Figure 25: Approach temperature vs. gas cooling pressure 60

Figure 26: Gas cooling capacity vs. gas cooling pressure 61
Figure 27: Approach temperature vs. intercooling pressure 62
Figure 28: Intercooler capacity vs. intercooling pressure 63
Figure 29: SLHX effectiveness vs. refrigerant mass flow rate at condition 1 65
Figure 30: SLHX effectiveness and refrigerant mass flow rate vs. gc outlet pressure at condition 1 65
Figure 31 SLHX effectiveness vs. refrigerant mass flow rate at condition 2 66
Figure 32: SLHX effectiveness and refrigerant mass flow rate vs. gc outlet pressure at condition 2 67
Figure 33 Internal heat exchanger capacity vs. internal heat exchanger inlet pressure 68
Figure 34 Volumetric efficiency of 1st stage at different test conditions 71
Figure 35 Volumetric efficiency of the 2nd stage for different test conditions 72
Figure 36 Compressor efficiency at different test conditions 72
Figure 37 State points of split cycle on p-h diagram 73
Figure 38: Optimum mass flow rate ratios 76
Figure 39: Optimum intermediate pressure coefficients 77
Figure 40: Optimum power ratios at different suction pressures 79
Figure 41: Effect of gas cooler approach temperature to COP 85
Figure 42: Effect of gas cooler approach temperature to the capacity 86
Figure 43: Effect of gas cooler approach temperature to the compressor power 87
Figure 44: Enthalpy-pressure and temperature relationships for CO_2 88
Figure 45: Optimum gas cooler outlet pressures for the baseline cycle 90
Figure 46: Effect of gas cooler pressure drop to capacity and compressor power 91
Figure 47: COP variation with gas cooler pressure drop and approach temperature 92
Figure 48: Effect of compressor efficiency to COP 93
Figure 49: Effect of variable compressor efficiency to COP 94
Figure 50: Effect of compressor efficiency to the optimum discharge presssure 95
Figure 51: Effect of SLHX effectiveness to COP 98
Figure 52: Effect of SLHX effectiveness to system capacity 99
Figure 53: Effect of SLHX effectiveness to compressor power 100
Figure 54: P-h diagram of ideal intercooler cycle 102
Figure 55: COP variation with gas cooler and intercooler approach temperatures 103
Figure 56: Results for 2nd approach of intercooler cycle modeling 105

Figure 57: Optimum discharge pressures for the intercooler cycle 106
Figure 58: Required heat exchanger capacities for AT_{ic}=0K 107
Figure 59: Required gas cooler capacity ratios for the intercooler cycle 108
Figure 60: Comparison of optimum pressures for intercooler and split cycles 112
Figure 61: Comparison of COP values for intercooler and split cycles 113
Figure 62: Effect of internal heat exchanger effectiveness on COP for the split cycle .. 114

1 Introduction

1.1 Overview

The first studies with CO_2 started in 1850 with Alexander Twining's proposed use of carbon dioxide (CO_2) in vapor compression systems. Franz Windhausen designed the first CO_2 compressor in 1886, and carbon dioxide was widely used as a refrigerant in the early part of this century (Bodinus 1999).

Its popularity was based on its low cost, nonflammability, low toxicity and universal availability. However, it had the disadvantages such as low cycle efficiency and high operating pressure. Other refrigerants such as ammonia, sulfur dioxide and methylene chloride could achieve much higher cycle efficiencies, but they had their own disadvantages, such as toxicity, that limited their application. Therefore, CO_2 was used in refrigeration applications until the implementation of chlorofluorocarbons (CFCs) and hydrogenated chlorofluorocarbons (HCFCs) in 1930's, which had low toxicities, high cycle efficiencies and low operating pressures.

Although CFCs and HCFCs were considered perfect refrigerants, they had a negative effect on the environment because of their ozone depletion potential (ODP). "When these refrigerants leak from refrigeration and air–conditioning equipment and migrate to the stratosphere, they deplete the ozone layer. Ozone depletion harms living creatures on earth, increases the incidence of skin cancer and cataracts, and poses risks to the human immune system" (Hwang and Radermacher 2000). Therefore, usage of these refrigerants

caused a great concern.

Concern over the potential environmental impacts of ozone depletion led to the development of an international agreement, the Montreal Protocol, in 1987 to reduce the production of ozone-depleting substances such as CFCs, HCFCs, and Halons. After the Montreal Protocol was signed in 1987 to regulate the production and trade of ozone-depleting substances such as CFCs and Halons, the regulation was extended in a follow-up conference. At the fourth meeting of the parties to the Montreal Protocol in November 1992, new controls were required to phase out CFCs at the end of 1995 and HCFCs by 2030 as shown in Table 1 (Reed, 1993). Now the regulation of HCFCs is being tightened on a faster schedule. Some countries already have more severe regulation plans. In the United States, the phase out of R22 in new machinery is set for the year 2010 (Allied Signal, 1999) and in Germany it is set for January 1, 2000 (Kruse, 1993).

Table 1: HCFC regulation schedule

Year	2004	2010	2015	2020	2030
Reduction	35%	65%	90%	99.5%	100%

Although Hydrofluorocarbons (HFCs) with zero ODP seem like a logical replacement for both CFCs and HCFCs, the global warming potential (GWP) of these refrigerants is too high as shown on Table 2. The use of energy has been adding gases to the atmosphere that trap heat radiation and warm the earth, known as “greenhouse gases.” The impact on our health by global warming is likely to be significant. In Table 2, by agreement, the

ODP of R-12 is defined as 1, and the GWP of CO_2 is 1.

Table 2: Environmental properties of common and alternative refrigerants

Refrigerant	R-12	R-22	R-134a	CO_2
Type	CFC	HCFC	HFC	Natural
ODP	1	>.05	0	0
GWP	7100	1500-4100	1200-3100	1
First Use	1931	1936	1990	1869

In 1997, the Parties to the United Nation Framework Convention on Climate Change agreed to an historic Kyoto Protocol to reduce greenhouse gas emissions and set emission reduction targets for developed nations: 8% below 1990 emissions levels for the European Union, 7% for the U.S., and 6% for Japan. Emission reduction targets include HFCs, which were introduced in response to ozone depletion.

Finally, environmental concerns lead to the re-usage of CO_2 due to its zero ODP and extremely low GWP. However, the two drawbacks of CO_2, which are lower cycle efficiency and higher operating pressures, still remain a challenge for using CO_2 as a refrigerant.

Evaporating pressures for typical air conditioning duty using carbon dioxide are about 3.4 MPa to 4.8 MPa (490 to 790 psia) while high side pressures are about 8.3 MPa to 13.8 MPa (1,200 to 2000 psia). These pressures are about five times higher than with

conventional refrigerants. This presents obvious problems of providing thicker walls for piping, heat exchangers, receivers and compressor shells. On the other hand, higher fluid densities lead to lower velocities and lower pressure drops. In his study, Pettersen showed that higher densities of CO_2 also lead to more compact heat exchangers (Pettersen 1994). Compared with other refrigerants COP has better transfer characteristics such as higher latent heat, higher specific heat, higher thermal conductivity and lower viscosity.

Figure 1 shows the characteristics of a typical single-stage CO_2 cycle. In this figure "CP" represents the critical point at the critical pressure (Pc) and critical temperature (Tc).

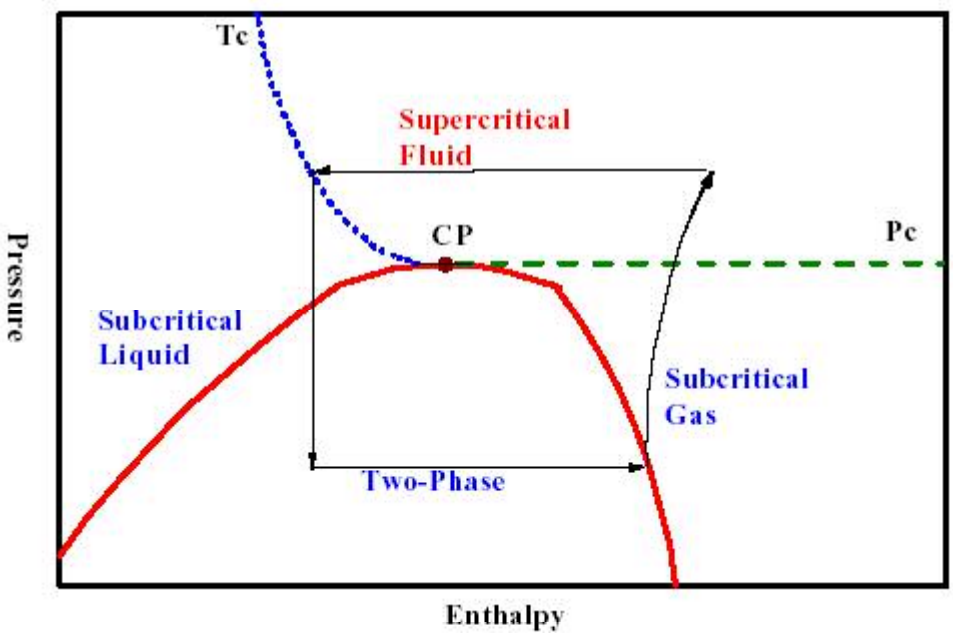

Figure 1: Typical single-stage CO_2 cycle

Critical pressure for CO_2 is 7.4 MPa and critical temperature is 31.1°C. The state of the refrigerant above this critical pressure and temperature is called "supercritical fluid".

For R-134a, which is a commonly used HFC in air-conditioning and refrigeration

applications, the critical temperature is 101.2°C. Therefore, while it is typical for CO_2 cycles to be in supercritical region, R-134a condenses and remains below its critical point. A schematic comparison of these two cycles is shown on Figure 2. Since CO_2 cycle operates between subcritical and supercritical regions, the cycle is named as "transcritical cycle". Moreover, the heat exchanger, which works above the critical point, is named as "gas cooler" instead of "condenser" in conventional cycles since no condensation occurs above that point.

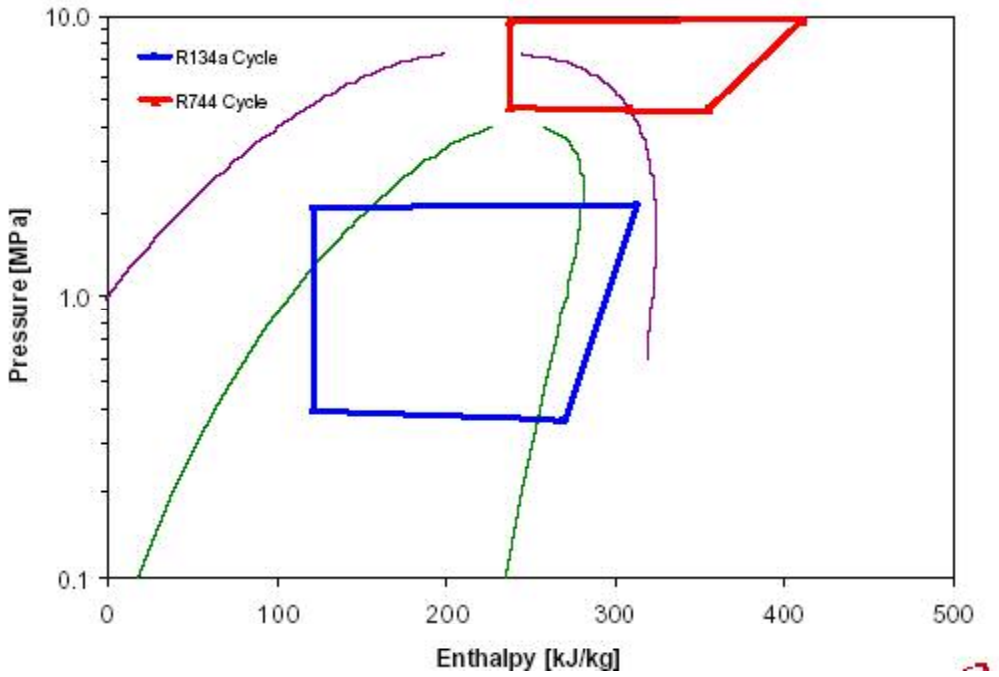

Figure 2: R134a and CO_2 refrigeration cycles

The second drawback of the CO_2 cycles, which is lower cycle efficiency, can be altered by improving the cycle efficiency by additional components such as suction line heat exchanger (SLHX), intercooler (IC) and internal heat exchanger (IHX) with or without

two-stage compression. This thesis represents the cycle efficiency improvements by designing the cycles combining one or two of the mentioned additional heat exchangers.

1.2 Literature Review

Since the research on the CO_2 cycles were recently revived in early 1990's, considerable work and investigation has been devoted to the use of single stage CO_2 cycles in various applications. While initial experimentation and simulation concentrated on the use of CO_2 in a transcritical cycle for mobile air conditioning applications (Lorentzen et al. 1993; Pettersen et al. 1994; Hafner et al. 1998; Hirao et al. 2000; Preissner et al. 2000), the potential of CO_2 in other applications such as water heating systems (Hwang and Radermacher 1998a; Mukaiyama et al. 2000) and a few air-to-air heat pumping systems (Aarlieln et al. 1998; Rieberer et al. 1998; Richter et al. 2000) was also investigated.

Design issues with hermetic-type CO_2 compressors was investigated (Fagerli 1996a; Fagerli 1997; Tadano et al. 2000) while some researchers focused on the modification of existing HCFC-22 compressors for operation with CO_2 (Fagerli 1996b; Koehler et al. 1998; Hwang and Radermacher 1998b).

In the more recent studies, Connaghan (2002) reported the results of tests for a basic CO_2 cycle at various gas cooler air entering temperatures. Connaghan observed that higher discharge pressures increased evaporator capacity at all conditions tested and generally increased system efficiency. Baek et al. (2002) performed a thermodynamic analysis of the transcritical CO_2 cycle with two-stage compression and intercooling by a computer

model. Baek et al. (2002) observed that the maximum COP of the intercooler cycle occurred at a pressure ratio across the 1st-stage compressor that was significantly larger than the pressure ratio across the 2nd-stage compressors due to the characteristics of the transcritical cycle. In addition to the intercooler cycle, baseline, suction line heat exchanger and two-stage split CO_2 cycles were designed, tested and analyzed in this thesis.

This review of the literature indicates that the previous studies on the performance improvement of the CO_2 cycle by employing two-stage cycles does not include work using the split cycle for refrigeration applications.

1.3 Objectives

The objectives of this thesis are summarized as follow:

1. Designing and building the experiments
2. Investigating performance improvements for each cycle option
    - Providing methods for optimization of system parameters to maximize performance
    - Investigating parametric study of CO_2 cycles
    - Comparing the performance of CO_2 refrigeration systems with that of refrigeration systems with conventional refrigerants

2 Experimental Setup

In this section, the components of the two-stage CO_2 systems are described. The condensing unit of the system was designed by using an axial fan, a 2-stage 1100 W CO_2 compressor, an expansion valve, a gas cooler, an intercooler and an Internal Heat Exchanger (IHX).

Electrically heated evaporators were used for system capacity measurement. A PID controller was implemented to control the electrical heaters for maintaining the same refrigerant temperature at the compressor inlet.

2.1 Compressor

The compressor used in system design is a hermetic rotary type CO_2 compressor, which has two rolling pistons designed to ensure low-vibration and low-noise operation. It is also able to work at the compressor speeds of 30 Hz to 120 Hz.

Rotary compressors are best suited for low compression ratios. A Two-stage compression cycle is required to achieve the large pressure difference needed to use CO_2 as the working fluid. Two rotary compression units are mounted on a single drive shaft but with a 180°phase difference. Low-pressure gas is taken into the first stage compression unit and compressed to a pressure of 5 to 8 MPa. This gas is directed both into the compressor case and a piping loop outside the case. The two channels merge outside the case where the gas is directed into the second stage compression unit. The high pressure gas from the second stage is then discharged to the refrigeration cycle. A schematic of the two-stage

CO_2 compressor is shown in Figure 3.

Figure 3: Two-stage CO_2 compressor (Yamasaki et al. 2001)

Intermediate pressure is implemented inside the shell to minimize gas leakage between the compression rooms and the inner space of the shell case. The case is maintained at the intermediate pressure, rather than the usual discharge pressure, to avoid having to strengthen the case. As a result of these design features, the compressor achieves high efficiency and high-reliability (Yamasaki et al. 2001).

2.2 Heat Exchangers

2.2.1 Gas Cooler and Intercooler

The same type of heat exchangers was used for both gas cooler and intercooler. Two heat exchangers were connected in parallel with the refrigerant flow for the gas cooler while only one heat exchanger was used for intercooler.

Design for CO_2 Heat exchanger is a staggered plate fin-and-tube heat exchanger having 4

rows with 7 tubes per row as shown on Figure 4. The dimensions in this figure are in mm. The specifications of the heat exchanger are as follows:

- Tube: OD 6.35 mm, ID 4.96 mm, tube pitch 22 mm
- Fin: thickness 0.152 mm, fin pitch 3.67 mm (136 ea for each row)
- Dimension: width 500 mm, height 265 mm, depth 50 mm
- Maximum operating pressure: 14 MPa
- Air side area: 3.2 m^2 Material: Aluminum

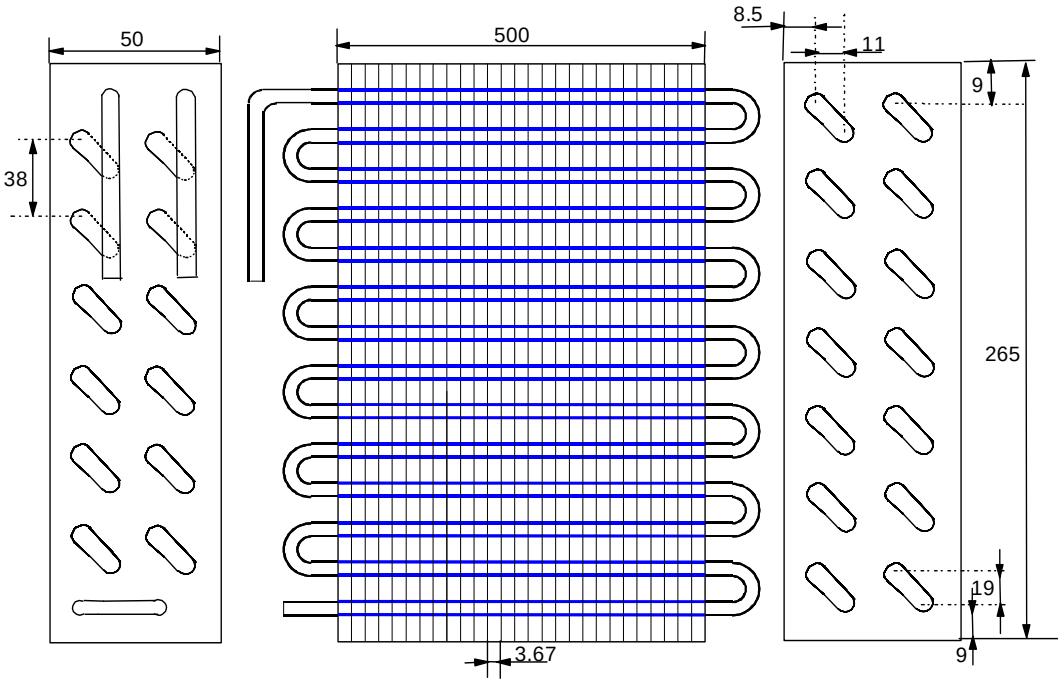

Figure 4: Schematic of the heat exchanger for gas cooler and intercooler

2.2.2 Suction Line Heat Exchanger and Internal Heat Exchanger

The same type of heat exchanger was used as both SLHX and IHX. The heat exchanger is a co-axial type (tube-in-tube) aluminum heat exchanger. The specifications of the heat

exchanger are shown on Figure 5.

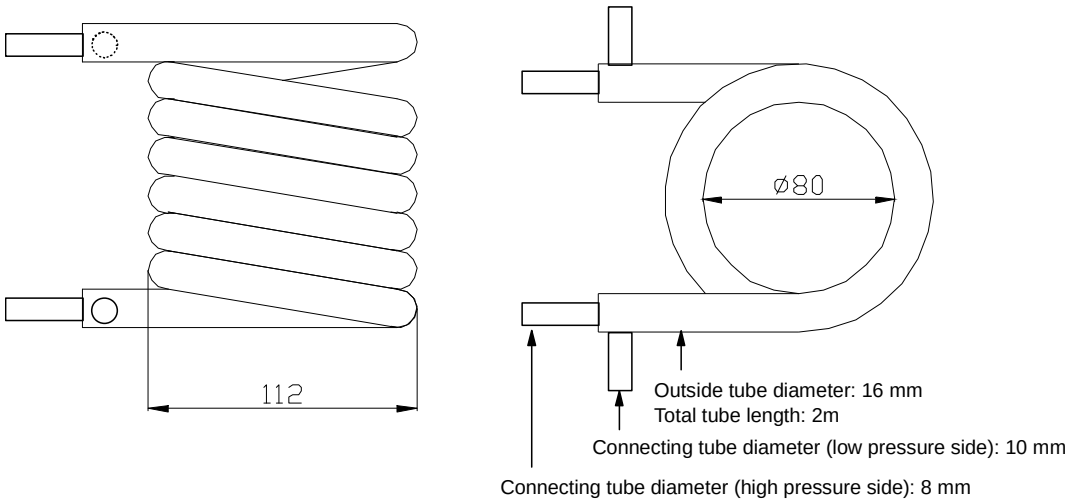

Figure 5: Heat exchanger for SLHX and IHX

2.3 Electrically Heated Evaporator

The construction of electrically heated evaporators included the following phases:

- 6 copper tubes (each 3’ long, 3/8” OD, 1/16” thick) were connected in series.
- 6 electrical heaters were wrapped around these tubes. These heaters included one “Omegalux Rope Heater” (maximum temperature 900°F, 120 V, 400 W, 8 ft) and five “Amptek Heavy Amox Insulated Duo-Tapes” (maximum temperature 1400 °F, 120 V, 5.2 A, 8 ft).
- “McMaster Melamine Insulations” were used to insulate the heaters (temp. range -150 to 400 °F, Insulation ID: 1/2”, Thickness: 1”).

A photograph of the electrically heated evaporator is shown on Figure 6.

Figure 6: Electrically heated evaporator

A PID controller was used for regulating the power input to the heaters to keep the suction (evaporator outlet) temperature constant as required in ARI Standard 520. The model number of the PID controller is Omega CN9121A.

2.4 Expansion Valves

Two different expansion valves were implemented for different cycle configurations. The specifications of these expansion devices are shown in Table 3.

Table 3: Expansion valves for CO_2 refrigeration systems

Model	SS-1RS4	SS-31RS4
Type	Integral-bonnet needle valve	Metering valve
Material	Steel	Stainless steel
Flow Coefficient	0.37	0.04
Orifice Diameter	4.4 mm	1.6 mm
Operating Temperatures	-20°C to 100°C	-65°C to 100°C
Maximum Operating Pressure	3000 psig (20.7 MPa)	5000 psig (34.4 MPa)
Manufacturer	Swagelok Inc.	Swagelok Inc.

SS-31RS4 was used for all cycle configurations, although SS-1RS4 was used for only sub cycle of the split cycle, which is described in more detail in Chapter 4.4.

2.5 Fans

Different fans were used for cooling the refrigerant passing through the gas cooler and intercooler. Table 4 summarizes their specifications.

Table 4: Specifications of the gas cooler and intercooler fans

Name	Gas Cooler Fan	Intercooler Fan
Type	Twin window fan	Single fan
Voltage rating	120 V	120 V
Setting	1	3
Power Consumption	37 W	63 W, 76 W, 90 W
Air velocity-facial	1.5 m/s	1.1 m/s
Manufacturer	Honeywell	-

3 Instrumentation and Measurement

Accurate measurements of temperature and pressure of the refrigerant at each state point, mass flow rate and total power consumption are quite important to analyze the system cooling capacity and performance. The instrumentation and measurement points are described in the following chapters.

3.1 Temperature Measurement

Thermocouples were used to measure temperatures at several locations in the test facility. The data acquisition system uses hardware and software compensation to simulate the reference junction, therefore eliminating the need for physical reference junction at constant reference temperature. The voltages from the thermocouples are converted into temperature values using appropriate correlations in the data acquisition program. Table 5 shows the detailed specifications of the thermocouples.

Table 5: Specifications of thermocouples

Item	Specification
Thermocouple type	T-type
Alloy Combination	Copper-Constantan
Temperature range	-270 to 400 ºC
Accuracy	± 0.5 ºC
Manufacturer	Omega Engineering, Inc.

In order to understand the behavior of the cycle characteristics, 10 different temperatures at inlet and outlet of each component were measured as listed below.

1. Compressor Inlet (in stream thermocouple)

2. Compressor 1st Stage Outlet (in stream thermocouple)
3. Intercooler Outlet (in stream thermocouple)
4. Compressor 2nd Stage Inlet (in stream thermocouple)
5. Compressor 2nd Stage Outlet (in stream thermocouple)
6. Gas Cooler Inlet (attached thermocouple)
7. Secondary Expansion Valve Outlet (in stream thermocouple)
8. Internal Heat Exchanger (IHX) Outlet (in stream thermocouple)
9. Main Expansion Valve Inlet (in stream thermocouple)
10. Evaporator Inlet (in stream thermocouple)

3.2 Pressure Measurement

Seven absolute pressure transducers were installed in the following locations for refrigerant pressure measurement.

1. Compressor Inlet (Range: 0-1000 psi)
2. Compressor 1st Stage Outlet (Range: 0-3000 psi)
3. Compressor 2nd Stage Outlet (Range: 0-3000 psi)
4. Secondary Expansion Valve Outlet (Range: 0-3000 psi)
5. Main Expansion Valve Inlet (Range: 0-3000 psi)
6. Evaporator Inlet (Range: 0-1000 psi)
7. Evaporator Outlet (Range: 0-1000 psi)

Detailed specifications of these pressure transducers are shown in Table 6.

Table 6: Specifications of pressure transducers

Item	Specification
Model	280E
Pressure Range	0-3000 psia and 0-1000 psia
Accuracy	± 0.11 % Full Scale
Output	0-5 VDC
Excitation	24 VDC Nominal
Manufacturer	Setra System, Inc.

3.3 Power Measurement

Compressor, gas cooler fan and evaporator fan power consumptions were measured to obtain the total power consumption and system performance. The power consumption by electrical heaters was also measured to determine the system cooling capacity. The specifications for these power transducers are shown in Table 7. Two of the power transducers given in the table were used for electrical heaters.

Table 7: Specifications of the power transducers

Item	Compressor	Fans	Electrical heaters
Model	GH-011D	PC8-003-080	GH-019D/10K
Current Rating	0-10 A	0-5 A	0-20 A
Voltage Rating	0-300 V	0-150 V	0-150 V
Capacity	2 kW	0.75 kW	2 kW
Frequency	60 Hz	60 Hz	60 Hz
Accuracy	0.2% RDG	0.2% RDG	0.2% RDG
System	Single-phase	Single-phase	Single-phase
Output (DC)	0-10 V	0-10 V	0-10 V
Manufacturer	Ohio Semitronics	Ohio Semitronics	Ohio Semitronics

3.4 Mass Flow Rate Measurement

One Coriolis mass flow meter was used to measure the refrigerant mass flow rate. The refrigerant mass flow meter was installed at the condenser outlet. The specifications of the mass flow meter are shown in Table 8.

Table 8: Specifications of the refrigerant mass flow meter

Item	Specification
Sensor Model	DH025S119SU
Transmitter Model	1700C11ABUEZZZ
Type of Sensor	Coriolis Mass Flow Meter
Flow Range	0 – 30 g/s
Accuracy	± 0.5 % of rate
Maximum Operating Pressure	3000 psig (20.7 MPa)
Maximum Operating Temperature	150 ºC
Output	1 to 5 V
Manufacturer	Micro Motion Inc.

3.5 Data Acquisition System

All the temperature, pressure and power measurement sensors were connected to a Hewlett Packard (HP) 3497A data acquisition and control unit and they are displayed in real time by Quick Basic software program interface with three second time intervals.

4 Cycle Configurations and Test Conditions

Four different CO_2 cycles were designed to evaluate the best cycle performance and to investigate the advantages and disadvantages of additional system components.

These four cycles were:

1. Baseline cycle
2. Cycle with SLHX
3. Intercooler Cycle
4. Two-stage Split Cycle with Intercooler

4.1 Baseline Cycle

This cycle consists of two-stage CO_2 compressor, gas cooler, expansion valve and electrically heated evaporator. The COP and capacity of other cycles and additional heat exchangers were compared with the baseline cycle. Figure 7 shows the baseline cycle configuration.

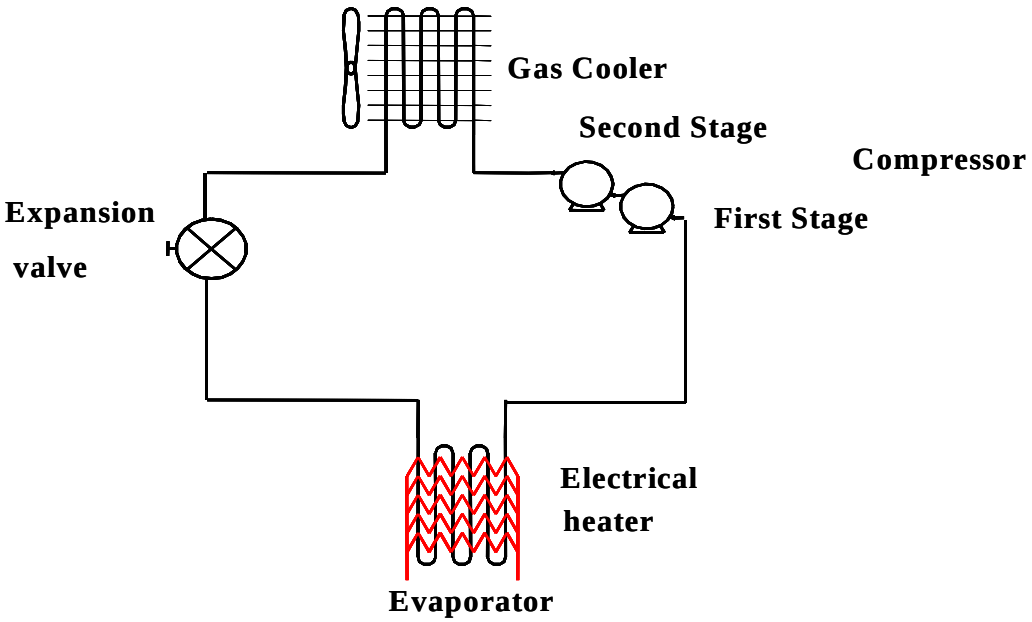

Figure 7: Baseline cycle configuration

In most cases, the state point of the refrigerant at the compressor outlet lies in the supercritical region rather than the superheated vapor region. Therefore, the cooling process after the compressor does not condense the refrigerant. Thus, the heat exchanger after the compressor is called a “gas cooler” instead of a “condenser”.

4.2 Cycle with Suction Line Heat Exchanger

In this cycle design, a suction-line heat exchanger (SLHX) was added to the baseline cycle configuration. This provides capacity increase by lowering the refrigerant temperature after the gas cooler. However, the refrigerant temperature at the compressor suction also increases causing an increase in compressor discharge temperature. Therefore, the cycle with SLHX is limited by the maximum compressor discharge temperature specified by the manufacturer.

Since, SLHX is the only addition to the baseline cycle, the effect of SLHX on the system

capacity and COP can be obtained. Moreover, the effectiveness of the SLHX can be evaluated. The cycle configuration for cycle with SLHX is shown in Figure 8.

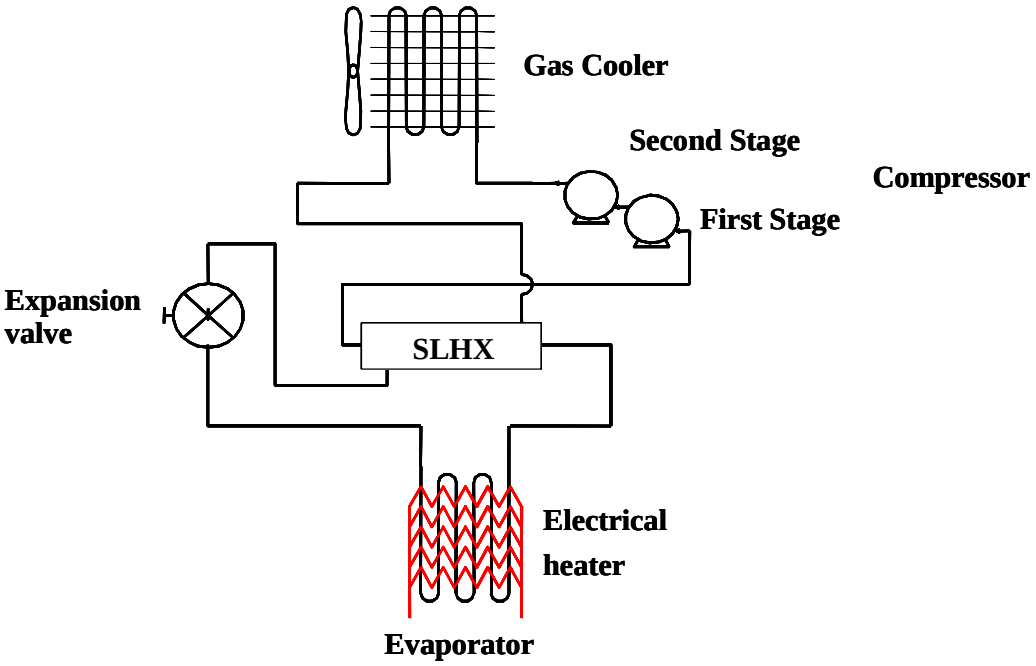

Figure 8: The cycle configuration for cycle with SLHX

4.3 Intercooler Cycle

One other advantage of two-stage compression is that, the refrigerant after the first stage compression can be cooled down to provide lower inlet temperatures to the second stage compression inlet. This process not only decreases compressor discharge temperature, but also improves compressor efficiency by allowing for operation at lower temperatures. Thus, actual compressor power decreases. Moreover, since the gas cooler inlet temperature decreases, a lower temperature at the gas cooler outlet can be obtained which results in higher capacity and COP.

The heat exchanger used to cool down the refrigerant between the first and second

compression stages is called the “intercooler”. Figure 9 shows the configuration for the intercooler cycle.

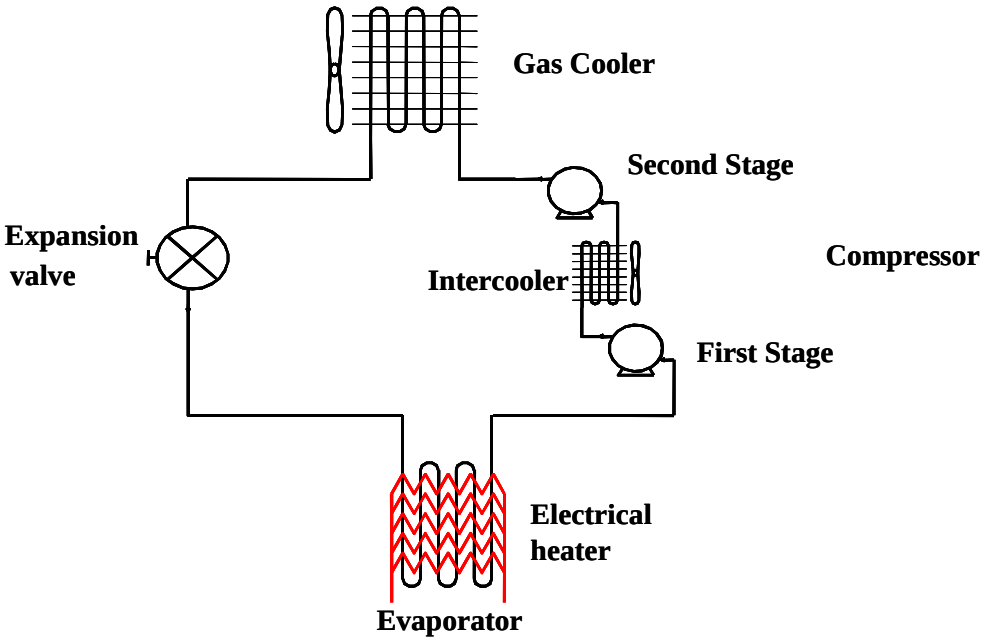

Figure 9: Intercooler cycle configuration

4.4 Two-stage Split Cycle

Two-stage split cycle configuration is shown in Figure 10.

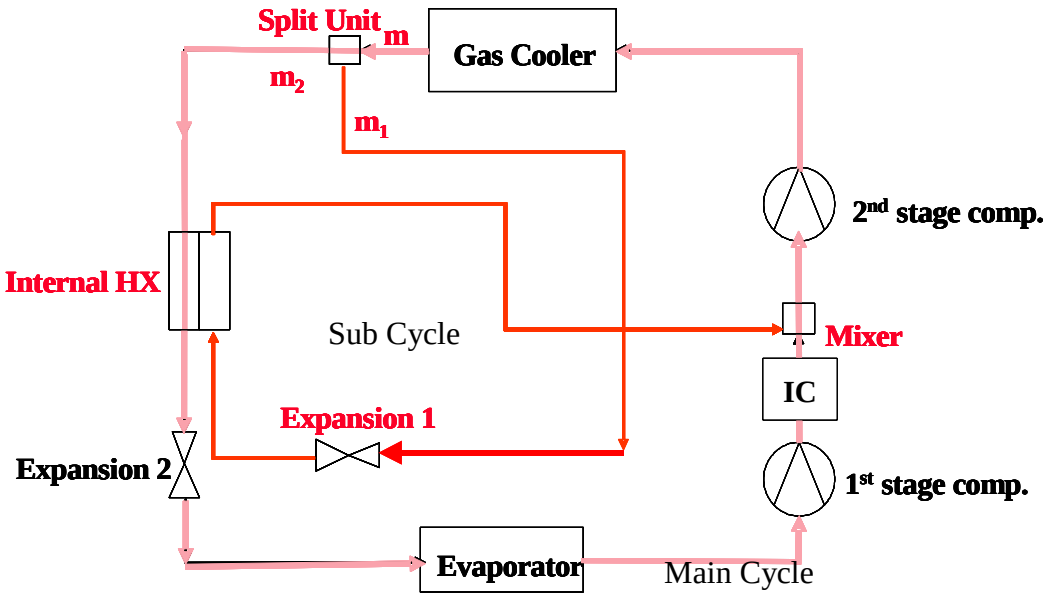

Figure 10: Two-stage CO_2 cycle configuration

As seen from this figure, the split cycle includes two cycles. These are named as “sub cycle” and “main cycle”. The main cycle includes the same system components as the intercooler cycle. The sub cycle includes the internal HX, additional expansion valve, splitter and mixer units.

After the gas cooler, the refrigerant stream is divided into two separate streams with a splitter unit. One of these streams is the main stream, which goes directly to the internal HX while the sub stream enters the expansion valve. The sub stream becomes colder as it is expanded. Therefore, by utilizing an internal HX, the refrigerant temperature at the main stream can be lowered to provide lower temperatures at the main cycle’s expansion valve inlet. Thus, the system capacity is increased. However, this is not the only benefit of the split cycle. The intermediate pressure is adjusted by the sub cycle’s expansion valve at each refrigerant charge. This provides another opportunity to optimize the COP.

With baseline, intercooler and SLHX cycles, only the discharge pressure is varied for optimum COP. However, with the split cycle, both the intermediate and discharge pressures can be varied. Therefore, the compressor efficiencies and power consumption of the first and second stages can be altered for optimum COP.

The refrigerant stream at the sub cycle after the internal HX then mixes with the main flow after the intercooler and enters the second stage compression.

4.5 Test Conditions

ARI Standard 520-97 was used to test the designed cycle configurations. The test conditions are shown in Table 9.

Table 9: ARI test conditions for condensing units for refrigeration applications

Condition	$T_{ambient}$ (°C)	$P_{suction}$ (kPa)	$T_{suction}$ (°C)	SH (°C)
A	32.2	4,198 (7.2°C)	18.3	11.1
B	32.2	2,906 (-6.7°C)	4.4	11.1
C	32.2	1,777 (-23.3°C)	4.4	27.7
D	32.2	1,348 (-31.7°C)	4.4	36.1
E	32.2	1,005 (-40°C)	4.4	44.4

The compressor discharge temperatures of the cycles were above 120°C for test conditions C, D and E. Therefore, tests were conducted only at conditions A and B. The compressor frequency was fixed at 60Hz (3600 rpm) during the tests. Tests were conducted at different refrigerant charges. The opening of the main expansion valve was adjusted for each charge to keep the suction pressure constant.

5 Experimental Results

In this chapter, experimental results for each cycle configuration will be provided at the standard test conditions. Table 10 shows the cycles and tested test conditions.

Table 10: Tested conditions for CO_2 cycles

Cycle Configuration	Condition
Baseline Cycle	A, B
Cycle with SLHX	A
Intercooler Cycle	A, B
Split Cycle	A, B, C

The limitation for test conditions was the high side compressor discharge temperatures. The refrigerant-side evaporator capacity is calculated by Equation 1.

$$Q_{evap} = m_{ref} * (h_2 - h_1) \quad (1)$$

Where m_{ref}: Mass flow rate of the refrigerant (kg/s)

h_1: Enthalpy of the refrigerant (CO_2) at evaporator inlet (kJ/kg)

h_2: Enthalpy of the refrigerant (CO_2) at compressor inlet (kJ/kg)

Q_{evap}: Evaporator capacity (kW)

Enthalpy values are calculated by using Engineering Equation Solver (EES) software from the measured temperature and pressure values.

Evaporator capacity is also determined by two other methods. The second method is

averaging the output of the watt-hour meter over time as shown in Equation 2.

$$Q_{evap} = \frac{\sum(P_i * \Delta t_i)}{\sum(\Delta t_i)} \quad (2)$$

where, P_i: Power reading from watt-hour meter (W)

Δt_i: Time interval for each different power reading (s)

The third method uses the output of the watt-hour meter directly as shown in Equation 3.

$$Q_{evap} = \frac{0.2(Whr/Counts) * \Delta n(Counts)}{\Delta t(hr)} \quad (3)$$

where, Δn: Number of counter relay switches (Counts)

Δt: Sampling time (hr)

For the last two methods, the test was conducted for 30 minutes after the cycle reached steady-state.

5.1 Baseline Cycle

Because the gas cooler fan had three fan settings, air velocity across the heat exchanger was measured for each setting prior to testing. The effect of fan settings to the cycle parameters was also investigated. Table 11 shows the results for 430 g refrigerant charge at test condition A for the baseline cycle.

Table 11: Effect of different fan settings to system performance

Setting	Q_{evap} (W)	COP	P_{fan} (W)	P_{comp} (W)	P_{total} (W)	T_{GCOut} (°C)	$T_{compOut}$ (°C)	$P_{compOut}$ (kPa)
High	1,331	1.215	88	1,008	1,096	41.4	80.7	9,170
Medium	1,282	1.164	77	1,025	1,102	42.4	82.2	9,302
Low	1,076	0.974	64	1,041	1,105	43.4	83.3	9,470

From this table, it was found that the discharge pressure, discharge temperature, gas cooler outlet temperature and compressor power decrease as the fan power increases. Since the evaporating capacity increased more than the increase of the fan power, the COP value increased by 25% as the fan setting changed from “low” to “high”. Therefore, the remaining tests were conducted at the highest fan setting.

5.1.1 Test Condition A

Tests were conducted at 430, 460, 490, 520 and 550 g refrigerant charges at Condition A. Table 12 shows the cycle temperatures and pressures during the steady-state. As the refrigerant charge increased, the optimum gas cooling pressure was found at 11.4 MPa, which resulted in higher evaporating capacity and the compressor discharge temperature rose to 99°C. However, it should be noted that the enthalpy of the gas cooler outlet did not change much when the charge was increased from 520 g to 550 g.

Table 12: Properties of each state point at condition A for baseline cycle

Charge (g)	Cycle Points	Temperature (°C)	Pressure (kPa)
430	Evaporator Inlet	8.2	4,242
	Compressor Inlet	18.4	4,100
	Compressor Outlet	80.7	9,170
	Gas Cooler Outlet	41.4	8,950
	Expansion Valve Inlet	41.2	8,910
460	Evaporator Inlet	7.4	4,285
	Compressor Inlet	18.2	4,126
	Compressor Outlet	86.1	9,815
	Gas Cooler Outlet	45.2	9,650
	Expansion Valve Inlet	44.9	9,608
490	Evaporator Inlet	7.6	4,250
	Compressor Inlet	18.1	4,100
	Compressor Outlet	91.5	10,520
	Gas Cooler Outlet	47.5	10,376
	Expansion Valve Inlet	47.1	10,340
520	Evaporator Inlet	8.0	4,300
	Compressor Inlet	18.3	4,150
	Compressor Outlet	98.5	11,400
	Gas Cooler Outlet	49.3	11,270
	Expansion Valve Inlet	49.1	11,249
550	Evaporator Inlet	7.8	4,280
	Compressor Inlet	18.3	4,130
	Compressor Outlet	104.5	11,920
	Gas Cooler Outlet	51.0	11,730
	Expansion Valve Inlet	50.8	11,695

The system performance results for test condition A are provided in Table 13. The optimum charge is 520 g where the COP is at its maximum.

Table 13: Performance of the baseline cycle at condition A

Charge (g)	P_{comp} (W)	P_{fan} (W)	P_{total} (W)	Q_{evap} (W)	COP
430	1,008	88	1,096	1,331	1.215
460	1,090	92	1,182	1,539	1.302
490	1,182	92	1,274	1,759	1.380
520	1,288	92	1,380	1,959	1.420
550	1,372	93	1,465	2,001	1.366

5.1.2 Test Condition B

Tests were conducted at Condition B with three refrigerant charges: 430, 460 and 490 g. Table 14 shows the cycle temperatures and pressures during steady state. As the refrigerant charge increased, the optimum gas cooling pressure was found at 11.3 MPa, which resulted in higher evaporating capacity and the compressor discharge temperature rose to 111°C. However, it should be noted that the enthalpy of the gas cooler outlet did not change much when the charge was increased from 460 g to 490 g.

Table 14: Properties of each state point at condition B for baseline cycle

Charge (g)	Cycle Points	Temperature (°C)	Pressure (kPa)
430	Evaporator Inlet	-5.0	3,037
	Compressor Inlet	4.5	2,864
	Compressor Outlet	101.8	10,080
	Gas Cooler Outlet	44.7	9,921
	ExpansionValve Inlet	44.2	9,882
460	Evaporator Inlet	-5.2	3,025
	Compressor Inlet	4.6	2,906
	Compressor Outlet	110.8	11,304
	Gas Cooler Outlet	46.0	11,140
	Expansion Valve Inlet	45.7	11,102
490	Evaporator Inlet	-4.4	3,100
	Compressor Inlet	4.1	2,965
	Compressor Outlet	115.9	11,640
	Gas Cooler Outlet	47.1	11,526
	Expansion Valve Inlet	46.8	11,500

The system performance results for test condition B are provided in Table 15. The optimum charge is 460 g where the COP is at its maximum.

Table 15: Performance of the baseline cycle at condition B

Charge	P_{comp} (W)	P_{fan} (W)	P_{total} (W)	Q_{evap} (W)	COP
430 g	1,157	91	1,248	1,188	0.952
460 g	1,290	92	1,382	1,502	1.087
490 g	1,345	92	1,437	1,505	1.047

5.2 Cycle with Suction Line Heat Exchanger

The condensing unit with SLHX was tested only at Condition A because the discharge temperatures exceeded the limit at other test conditions. Since there is no available test standard for the system with the SLHX, two sets of tests were conducted at different suction conditions. These are:

- Condition 1: Setting the evaporator outlet temperature to be 18.3°C (so the suction temperature is higher than 18.3°C)
- Condition 2: Setting the compressor suction temperature to be 18.3°C

It should be noted that inlets and outlets of the SLHX mean specific state points of the cycle as indicated below:

- Hot refrigerant inlet: Gas cooler outlet, high pressure side
- Hot refrigerant outlet: Expansion valve inlet, high pressure side
- Cold refrigerant inlet: Evaporator outlet, low pressure side
- Cold refrigerant outlet: Compressor suction, low pressure side

5.2.1 Condition 1

Tests were conducted at five different refrigerant charges (400, 430, 460, 490 and 520 g). The opening of the expansion valve was adjusted for each charge to keep the suction pressure constant. The PID controller was integrated with an electric heater, which was installed on the evaporator pipe to keep the refrigerant temperature at the evaporator outlet constant. For all the refrigerant charges, the refrigeration cycle operated as a transcritical cycle.

Table 16 shows the cycle temperatures and pressures during the steady state. As the refrigerant charge increased, the optimum gas cooling pressure was found at 10.5 MPa, which resulted in higher evaporating capacity and the compressor discharge temperature rose to 114°C.

Table 16: Properties of each state point at condition 1 for SLHX cycle

Charge (g)	Cycle Points	Temperature (°C)	Pressure (kPa)
400	Evaporator Inlet	9.1	4398
	Evaporator Outlet	18.7	4290
	Compressor Inlet	33.5	4150
	Compressor Outlet	83.6	7947
	Gas Cooler Outlet	39.7	7738
	Expansion Valve Inlet	34.6	7697
430	Evaporator Inlet	9.8	4454
	Evaporator Outlet	18.0	4356
	Compressor Inlet	37.1	4223
	Compressor Outlet	93.1	8701
	Gas Cooler Outlet	42.4	8522
	Expansion Valve Inlet	38.2	8487
460	Evaporator Inlet	9.7	4447
	Evaporator Outlet	18.1	4359
	Compressor Inlet	38.6	4225
	Compressor Outlet	98.0	9151
	Gas Cooler Outlet	43.9	8988
	Expansion Valve Inlet	39.8	8957
490	Evaporator Inlet	9.2	4396
	Evaporator Outlet	18.1	4310
	Compressor Inlet	40.1	4177
	Compressor Outlet	107.0	9901
	Gas Cooler Outlet	46.4	9755
	Expansion Valve Inlet	41.4	9731
520	Evaporator Inlet	8.7	4351
	Evaporator Outlet	18.3	4273
	Compressor Inlet	40.4	4145
	Compressor Outlet	113.5	10543
	Gas Cooler Outlet	47.9	10408
	Expansion Valve Inlet	41.5	10385

The system performance results for test condition A and at special condition 1 are provided in Table 17. The optimum charge is 520 g where the COP is at its maximum.

Table 17: Performance of the SLHX cycle at condition A-1

Charge (g)	P_{comp} (W)	P_{fan} (W)	P_{total} (W)	Q_{evap} (W)	COP
400	830	93	913	1,084	1.175
430	925	93	1,018	1,462	1.438
460	984	92	1,076	1,675	1.556
490	1,086	92	1,178	1,952	1.657
520	1,173	92	1,265	2,113	1.671

5.2.2 Condition 2

Similar to condition 1, the expansion valve opening was adjusted for each charge to keep the suction pressure constant. However, the PID controller integrated with an electric heater was used to keep the refrigerant temperature at the compressor inlet constant.

Tests at condition 2 were conducted at six different refrigerant charges (430, 460, 500, 600, 640 and 690 g), which were higher than those used at condition 1. The first three refrigerant charges resulted in a subcritical cycle, while the last three refrigerant charges resulted in a transcritical cycle. Table 18 shows the cycle temperatures and pressures during steady-state operation.

Table 18: Properties of each state point at condition 2 for SLHX cycle

Charge (g)	Cycle Points	Temperature (°C)	Pressure (kPa)
430	Evaporator Inlet	8.4	4332
	Evaporator Outlet	7.6	4246
	Compressor Inlet	18.4	4140
	Compressor Outlet	53.8	6372
	Gas Cooler Outlet	34.1	5998
	Expansion Valve Inlet	21.3	5932
460	Evaporator Inlet	8.4	4322
	Evaporator Outlet	7.7	4263
	Compressor Inlet	18.3	4168
	Compressor Outlet	58.1	6596
	Gas Cooler Outlet	35.4	6249
	Expansion Valve Inlet	24.1	6197
500	Evaporator Inlet	8.2	4309
	Evaporator Outlet	7.7	4267
	Compressor Inlet	18.3	4175
	Compressor Outlet	58.1	6847
	Gas Cooler Outlet	35.4	6532
	Expansion Valve Inlet	24.1	6492
600	Evaporator Inlet	8.1	4298
	Evaporator Outlet	7.8	4264
	Compressor Inlet	18.2	4138
	Compressor Outlet	85.2	9601
	Gas Cooler Outlet	44.5	9406
	Expansion Valve Inlet	20.1	9381
640	Evaporator Inlet	8.3	4320
	Evaporator Outlet	8.0	4285
	Compressor Inlet	18.1	4160
	Compressor Outlet	93.9	10593
	Gas Cooler Outlet	47.3	10419
	Expansion Valve Inlet	19.8	10396
690	Evaporator Inlet	9.2	4417
	Evaporator Outlet	8.9	4385
	Compressor Inlet	18.1	4259
	Compressor Outlet	104.1	12006
	Gas Cooler Outlet	50.7	11826
	Expansion Valve Inlet	19.6	11804

The system performance results for test condition A and at special condition 2 are

provided in Table 19. The optimum charge is 640 g where the COP is at its maximum.

Table 19: Performance of the SLHX cycle at condition A-2

Charge (g)	P_{comp} (W)	P_{fan} (W)	P_{total} (W)	Q_{evap} (W)	COP
430	616	93	709	68	0.096
460	646	93	737	147	0.199
500	683	93	776	240	0.310
600	1,069	92	1,161	1,466	1.263
640	1,194	92	1,286	1,745	1.357
690	1,369	92	1,461	1,918	1.313

5.3 Intercooler Cycle

5.3.1 Test Condition A

Tests were conducted at different refrigerant charges (490, 550, 615, 645, 675 and 700 g). For each charge, the opening of the expansion valve was adjusted to keep the suction pressure constant. At all the refrigerant charges, the refrigeration cycle was operated in the transcritical region. The best performance of the cycle was obtained at 700 g charge. The optimum COP of the system was 1.76, which is 24% higher than that of the baseline cycle. Table 20 shows the cycle temperatures and pressures during the steady-state.

Table 20: Properties of each state point at condition A for the intercooler cycle

Charge (g)	Cycle Points	Temperature (°C)	Pressure (kPa)
490	Evaporator Inlet	9.2	4351
	Compressor Inlet	18.3	4131
	Compressor 1st Outlet	56.7	6835
	IC Outlet	35.5	6560
	Compressor 2nd Outlet	53.3	7713
	GC Outlet	36.3	7440
	Expansion Valve Inlet	36.1	7415
550	Evaporator Inlet	9.3	4372
	Compressor Inlet	18.0	4172
	Compressor 1st Outlet	59.3	7063
	IC Outlet	37.2	6785
	Compressor 2nd Outlet	61.6	8953
	GC Outlet	41.0	8740
	Expansion Valve Inlet	40.8	8712
615	Evaporator Inlet	9.4	4403
	Compressor Inlet	18.4	4205
	Compressor 1st Outlet	63.3	7393
	IC Outlet	39.1	7101
	Compressor 2nd Outlet	69.3	10195
	GC Outlet	45.0	10020
	Expansion Valve Inlet	44.8	9998
645	Evaporator Inlet	9.1	4370
	Compressor Inlet	18.0	4174
	Compressor 1st Outlet	65.4	7572
	IC Outlet	39.8	7290
	Compressor 2nd Outlet	71.4	10668
	GC Outlet	45.5	10497
	Expansion Valve Inlet	45.3	10476
675	Evaporator Inlet	9.3	4395
	Compressor Inlet	18.0	4200
	Compressor 1st Outlet	67.4	7864
	IC Outlet	40.5	7578
	Compressor 2nd Outlet	73.1	11185
	GC Outlet	46.2	11010
	Expansion Valve Inlet	46.0	10991
700	Evaporator Inlet	9.2	4388
	Compressor Inlet	18.1	4190
	Compressor 1st Outlet	68.0	7944
	IC Outlet	39.0	7659
	Compressor 2nd Outlet	73.5	11404
	GC Outlet	45.7	11242
	Expansion Valve Inlet	45.5	11225

The system performance results for test condition A are provided in Table 21. Since, separate fans were used for the gas cooler and intercooler, the power consumption for intercooler cycle was higher than the baseline and SLHX cycles.

Table 21 Performance of the intercooler cycle at condition A

Charge (g)	P_{comp} (W)	P_{fan} (W)	P_{total} (W)	Q_{evap} (W)	COP
490	820	128	948	808	0.852
550	968	128	1,096	1,509	1.377
615	1,103	127	1,230	2,054	1.669
645	1,162	127	1,289	2,191	1.700
675	1,230	127	1,357	2,314	1.705
700	1,258	127	1,385	2,437	1.759

5.3.2 Test Condition B

Tests were conducted at different refrigerant charges (430, 490, 550, 580, and 610 g). For each charge, the opening of the expansion valve was adjusted to keep the suction pressure constant. At all the refrigerant charges, a transcritical cycle was maintained. The best performance of the cycle was obtained at 550 g charge. The optimum COP of the system was 1.19, which is 10% higher than that of the baseline cycle. Table 22 shows the cycle temperatures and pressures during steady state.

Table 22: Properties of each state point at condition B for the intercooler cycle

Charge (g)	Cycle Points	Temperature (°C)	Pressure (kPa)
430	Evaporator Inlet	-4.7	3060
	Compressor Inlet	4.4	2860
	Compressor 1st Outlet	59.0	5484
	IC Outlet	36.4	5283
	Compressor 2nd Outlet	73.3	8401
	GC Outlet	38.8	8280
	Expansion Valve Inlet	38.6	8253
490	Evaporator Inlet	-4.7	3064
	Compressor Inlet	4.0	2881
	Compressor 1st Outlet	62.0	5697
	IC Outlet	37.4	5496
	Compressor 2nd Outlet	79.6	9413
	GC Outlet	41.8	9310
	Expansion Valve Inlet	41.6	9282
550	Evaporator Inlet	-4.8	3054
	Compressor Inlet	4.2	2878
	Compressor 1st Outlet	66.2	5942
	IC Outlet	37.2	5743
	Compressor 2nd Outlet	86.8	10626
	GC Outlet	43.2	10530
	Expansion Valve Inlet	43.0	10501
580	Evaporator Inlet	-5.1	3023
	Compressor Inlet	4.4	2850
	Compressor 1st Outlet	68.7	6072
	IC Outlet	37.4	5876
	Compressor 2nd Outlet	89.8	11137
	GC Outlet	43.5	11040
	Expansion Valve Inlet	43.3	11010
610	Evaporator Inlet	-5.1	3026
	Compressor Inlet	4.3	2855
	Compressor 1st Outlet	71.8	6446
	IC Outlet	37.6	6252
	Compressor 2nd Outlet	91.2	11817
	GC Outlet	43.9	11715
	Expansion Valve Inlet	43.7	11691

The system performance results for test condition B are provided in Table 23.

Table 23: Performance of the intercooler cycle at condition A

Charge (g)	P_{comp} (W)	P_{fan} (W)	P_{total} (W)	Q_{evap} (W)	COP
430	956	128	1,084	792	0.731
490	1,055	128	1,183	1,260	1.065
550	1,176	128	1,304	1,552	1.190
580	1,236	128	1,344	1,612	1.182
610	1,311	128	1,439	1,674	1.163

5.4 Split Cycle

Tests were conducted at three different conditions as shown previously in Table 10. The split cycle allowed for testing at the low evaporating temperatures required in test condition C, in addition to allowing for A and B test conditions.

5.4.1 Test Condition A

Tests for the split cycle at condition A were conducted at three different refrigerant charges (670, 770, and 850 g). The opening of the main cycle's expansion valve was adjusted for each charge to keep the suction pressure constant. At each charge, the opening of the sub cycle's expansion valve was adjusted to optimize the system performance by changing the intermediate pressure. At all the refrigerant charges, the refrigeration cycle operated as a transcritical cycle.

The best performance of the cycle was obtained at 770 g charge. The optimum COP of the system was 1.86, which is 31% higher than that of the baseline cycle. Two-stage split cycle test results at Condition A are summarized in Table 24.

Table 24: Two-stage split cycle test results at condition A

Charge (g)	Cycle Points	Temperature (°C)	Pressure (kPa)
670	Evaporator Inlet	8.9	4,340
	Compressor 1st Inlet	18.5	4,160
	Compressor 1st Outlet	64.2	7,570
	Intercooler Outlet	37.4	7,300
	Compressor 2nd Inlet	38.0	7,300
	Compressor 2nd Outlet	59.0	9,030
	Gas Cooler Outlet	41.0	8,780
	Exp. Valve 1 Inlet	39.9	8,715
	Exp. Valve 2 Outlet	31.0	7,330
	IHX Outlet: Mixer Inlet	39.8	7,300
770	Evaporator Inlet	8.9	4,360
	Compressor 1st Inlet	18.4	4,165
	Compressor 1st Outlet	71.1	8,570
	Intercooler Outlet	41.5	8,315
	Compressor 2nd Inlet	42.3	8,315
	Compressor 2nd Outlet	60.8	10,185
	Gas Cooler Outlet	45.0	9,930
	Exp. Valve 1 Inlet	41.7	9,880
	Exp. Valve 2 Outlet	37.0	8,360
	IHX Outlet: Mixer Inlet	43.6	8,315
850	Evaporator Inlet	9.2	4,380
	Compressor 1st Inlet	18.6	4,206
	Compressor 1st Outlet	76.4	9,090
	Intercooler Outlet	44.3	8,826
	Compressor 2nd Inlet	44.3	8,826
	Compressor 2nd Outlet	67.6	11,766
	Gas Cooler Outlet	47.7	11,520
	Exp. Valve 1 Inlet	44.6	11,466
	Exp. Valve 2 Outlet	38.7	8,878
	IHX Outlet: Mixer Inlet	44.2	8,826

The effects of the discharge and intermediate pressures on the COP are shown in Figure 11. As shown, the COP of the split cycle is related to both the discharge and intermediate pressures. Two-stage split cycle optimizes both these pressures while the other cycle options optimizes only the discharge pressure for the maximum COP. The maximum

COP was found at 10.2 MPa discharge pressure and at 8.6 MPa intermediate pressure.

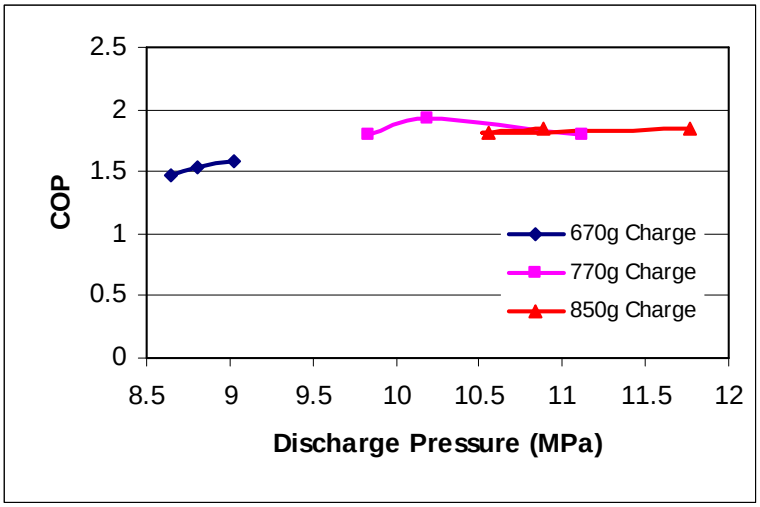

(a) COP vs. discharge pressure

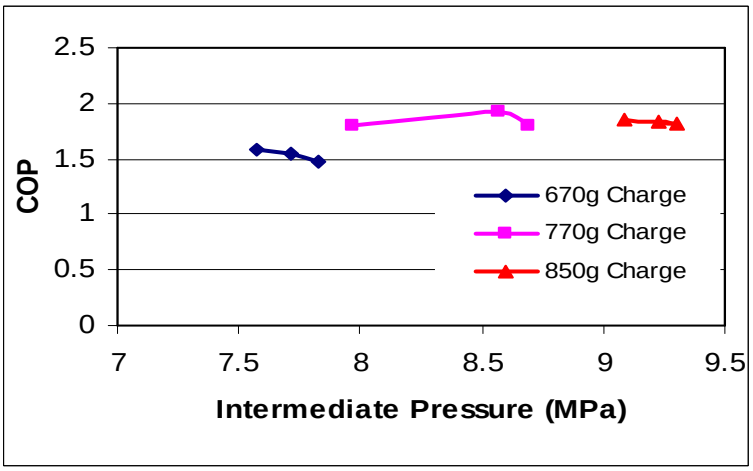

(b) COP vs. intermediate pressure

Figure 11 COP as a function of intermediate and discharge pressures for two-stage split cycle at condition A

The effect of the discharge pressure on evaporator capacity is shown in Figure 12. As

shown in Figures 11a and 12, the evaporating capacity shows a similar behavior with the COP with increasing compressor discharge pressures. The COP and the evaporator capacity usually increase with the increasing discharge pressure. However, they both have a maximum point at 770 g refrigerant charge, which coincides with about 10 MPa discharge pressure.

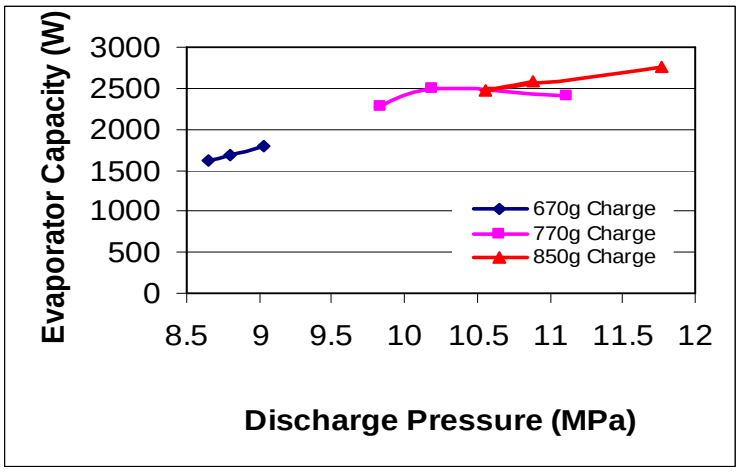

Figure 12 Evaporating capacity vs. discharge pressure for two-stage split cycle–A

5.4.2 Test Condition B

Tests for the split cycle at Condition B were conducted at four different refrigerant charges (600, 700, 800 and 900 g). The best performance of the cycle was obtained at 800 g charge. The optimum COP of the system was 1.53, which is 40% higher than that of the baseline cycle. The two-stage split cycle test results at Condition B are summarized in Table 25.

Table 25: Two-stage split cycle test results at condition B

Charge (g)	Cycle Points	Temperature (°C)	Pressure (kPa)
600	Evaporator Inlet	-4.5	3,058
	Compressor 1st Inlet	4.1	2,887
	Compressor 1st Outlet	67.2	6,198
	Intercooler Outlet	35.0	6,004
	Compressor 2nd Inlet	36.3	6.004
	Compressor 2nd Outlet	63.7	8,441
	Gas Cooler Outlet	38.8	8,216
	Exp. Valve 2 Inlet	37.0	8,201
	Exp. Valve 1 Outlet	22.3	6,042
	IHX Outlet: Mixer Inlet	38.6	6,004
700	Evaporator Inlet	-5.0	3.021
	Compressor 1st Inlet	4.1	2,860
	Compressor 1st Outlet	71.4	6,971
	Intercooler Outlet	36.1	6,807
	Compressor 2nd Inlet	38.6	6.807
	Compressor 2nd Outlet	69.7	9,603
	Gas Cooler Outlet	42.6	9,378
	Exp. Valve 2 Inlet	36.7	9,363
	Exp. Valve 1 Outlet	27.6	6,861
	IHX Outlet: Mixer Inlet	41.8	6,807
800	Evaporator Inlet	-5.0	3,026
	Compressor 1st Inlet	4.4	2,860
	Compressor 1st Outlet	73.7	7,492
	Intercooler Outlet	36.7	7,337
	Compressor 2nd Inlet	37.8	7,337
	Compressor 2nd Outlet	62.8	9,631
	Gas Cooler Outlet	42.6	9,406
	Exp. Valve 2 Inlet	34.9	9,391
	Exp. Valve 1 Outlet	30.9	7,396
	IHX Outlet: Mixer Inlet	38.5	7,337
900	Evaporator Inlet	-4.8	3,065
	Compressor 1st Inlet	4.3	2,900
	Compressor 1st Outlet	72.8	8,008
	Intercooler Outlet	37.8	7,813
	Compressor 2nd Inlet	34.3	7,813
	Compressor 2nd Outlet	56.5	10,959
	Gas Cooler Outlet	42.4	10,736
	Exp. Valve 2 Inlet	34.1	10,721
	Exp. Valve 1 Outlet	33.1	7,873
	IHX Outlet: Mixer Inlet	33.7	7,813

The effect of the discharge and intermediate-pressures on COP is shown in Figure 13. As shown, the COP of the split cycle at condition B is also related to both the discharge and intermediate pressures, similar to condition A. The maximum COP was found at 9.6 MPa discharge pressure and at 7.5 MPa intermediate pressure. The effect of the discharge pressure on the evaporating capacity is shown in Figure 14.

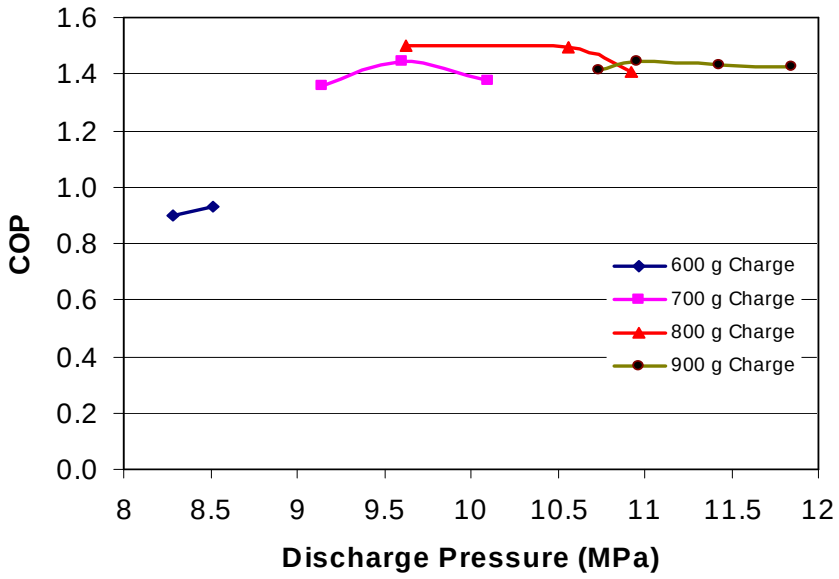

(a) COP vs. discharge pressure

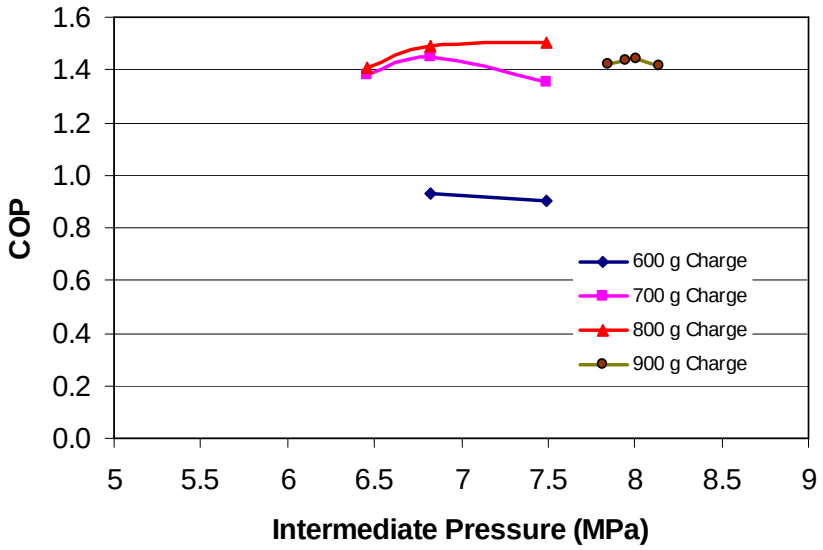

(b) COP vs. intermediate pressure

Figure 13 COP as a function of intermediate and discharge pressures for two-stage split cycle at condition B

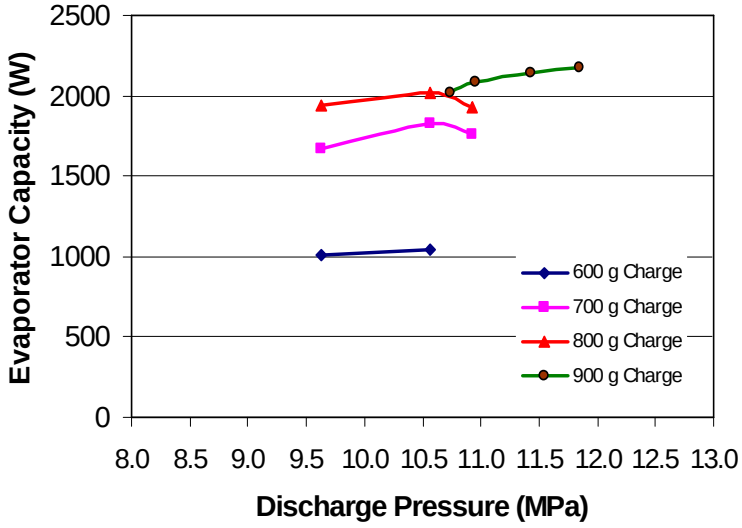

Figure 14 Evaporating capacity vs. discharge pressure for two-stage split cycle–B

5.4.3 Test Condition C

Tests for the split cycle at Condition C were conducted at three different refrigerant charges (450, 550 and 650 g). The best performance of the cycle was obtained at 550 g charge. The maximum COP of the system was 1.13. The two-stage split cycle test results at Condition C are summarized in Table 26.

Table 26: Two-stage split cycle test results at condition C

Charge (g)	Cycle Points	Temperature (°C)	Pressure (kPa)
450	Evaporator Inlet	-20.0	1,939
	Compressor 1st Inlet	4.6	1,782
	Compressor 1st Outlet	81.5	6,273
	Intercooler Outlet	35.5	6,192
	Compressor 2nd Inlet	35.7	6,192
	Compressor 2nd Outlet	67.9	8,442
	Gas Cooler Outlet	38.5	8,203
	Exp. Valve 2 Inlet	32.3	8,188
	Exp. Valve 1 Outlet	23.5	6,254
	IHX Outlet: Mixer Inlet	35.9	6,192
550	Evaporator Inlet	-20.1	1,936
	Compressor 1st Inlet	4.4	1,772
	Compressor 1st Outlet	79.4	6,184
	Intercooler Outlet	35.3	6,095
	Compressor 2nd Inlet	25.8	6,095
	Compressor 2nd Outlet	66.5	9,572
	Gas Cooler Outlet	41.6	9,367
	Exp. Valve 2 Inlet	24.1	9,352
	Exp. Valve 1 Outlet	22.7	6,150
	IHX Outlet: Mixer Inlet	23.3	6,095
650	Evaporator Inlet	-20.0	1,963
	Compressor 1st Inlet	4.1	1,793
	Compressor 1st Outlet	79.0	6,339
	Intercooler Outlet	35.5	6,240
	Compressor 2nd Inlet	23.8	6,240
	Compressor 2nd Outlet	66.0	10,380
	Gas Cooler Outlet	42.5	10,230
	Exp. Valve 2 Inlet	24.8	10,214
	Exp. Valve 1 Outlet	23.6	6,291
	IHX Outlet: Mixer Inlet	23.6	6,240

The effect of the discharge and intermediate-pressures on COP is shown in Figure 15. As shown, the COP of the split cycle at condition C is also related to both the discharge and intermediate pressures, similar to conditions A and B. However, at the same refrigerant charge, the COP of the cycle changes more than 23% at condition C while it changes less than 8% at conditions A and B. Therefore, the split cycle is more sensitive to the discharge and intermediate pressures at condition C than conditions A and B. This can be explained by the decreased refrigerant mass flow rate in the main stream at condition C because of lower suction pressure than the other conditions. Therefore, the refrigerant mass flow rate of the sub stream becomes important. Since this mass flow rate is determined by the intermediate and discharge pressures, split cycle at condition C becomes more sensitive to both discharge and intermediate pressures. The maximum COP was found at 9.6 MPa discharge pressure and at 6.2 MPa intermediate pressure. The effect of the discharge pressure on the evaporating capacity is shown in Figure 16, which is similar to COP.

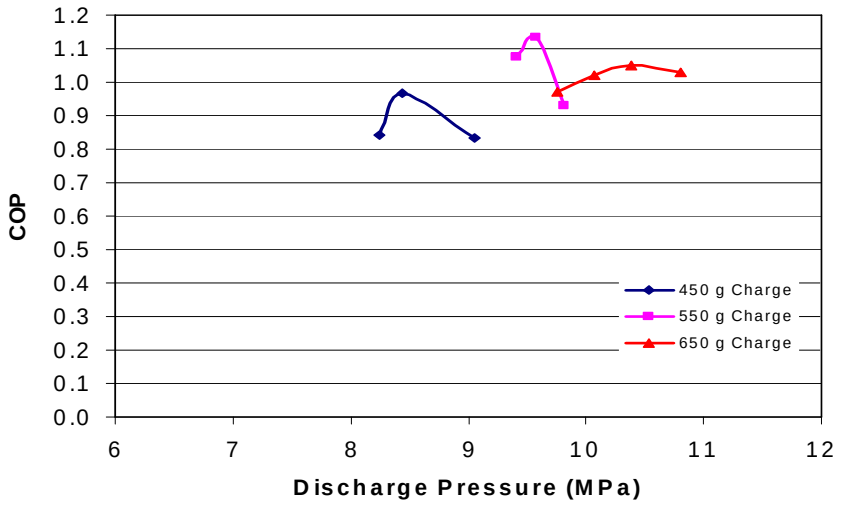

(a) COP vs. discharge pressure

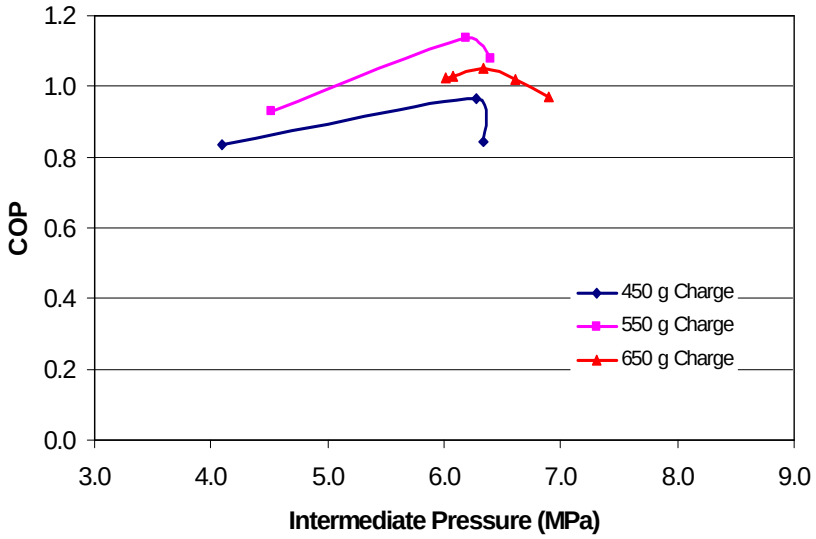

(b) COP vs. intermediate pressure

Figure 15 COP as a function of intermediate and discharge pressures for two-stage split cycle at condition C

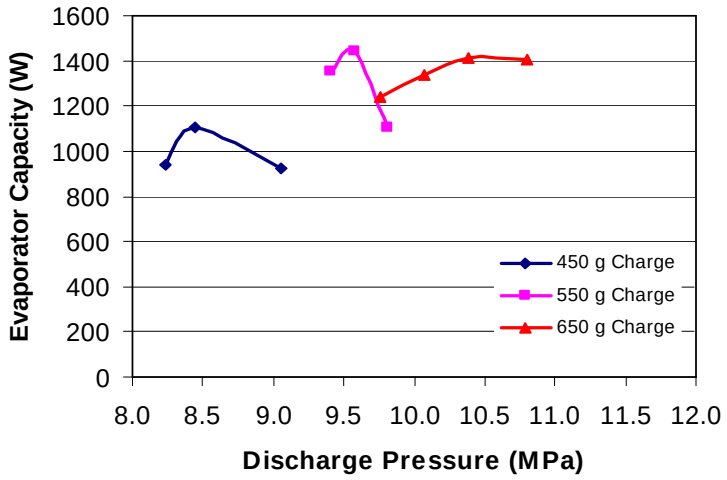

Figure 16 Evaporating capacity vs. discharge pressure for two-stage split cycle–C

5.5 Comparison of Test Results

The four cycles are compared in Figure 17 in a pressure-enthalpy diagram for test condition A. As shown, the SLHX cycle provides the lowest refrigerant enthalpy at the expansion valve inlet. Therefore, the enthalpy difference across the evaporator is the highest for the SLHX cycle. However, the refrigerant temperature at the compressor inlet for the SLHX cycle is higher than other cycle options. Therefore, refrigerant density is lower which results in lower refrigerant mass flow rate. The evaporator capacity is the multiplication of the refrigerant mass flow rate and the enthalpy difference across the evaporator as given in Equation 1. Depending on the change in these variables, the evaporator capacity for the SLHX cycle may be lower or higher than the other cycles. The experimental values for the evaporator capacity at test condition A are provided later in Table 27.

Figure 17 also shows that the intercooler capacity doesn't increase the evaporator capacity directly as the SLHX does. Only 20% of the intercooler capacity is used for extra cooling, The gas cooler can cool down to lower temperatures from the extra cooling provided. The size of the gas cooler is a limiting factor on the percentage of the intercooler capacity used for extra cooling.

The split cycle has higher intermediate pressures compared to that of intercooler cycle. This is mainly because of the additional refrigerant mass flow rate of the sub stream. This figure also shows that the split cycle provides more capacity than the other cycles

because of the IHX capacity in addition to the indirect effect of the intercooler capacity.

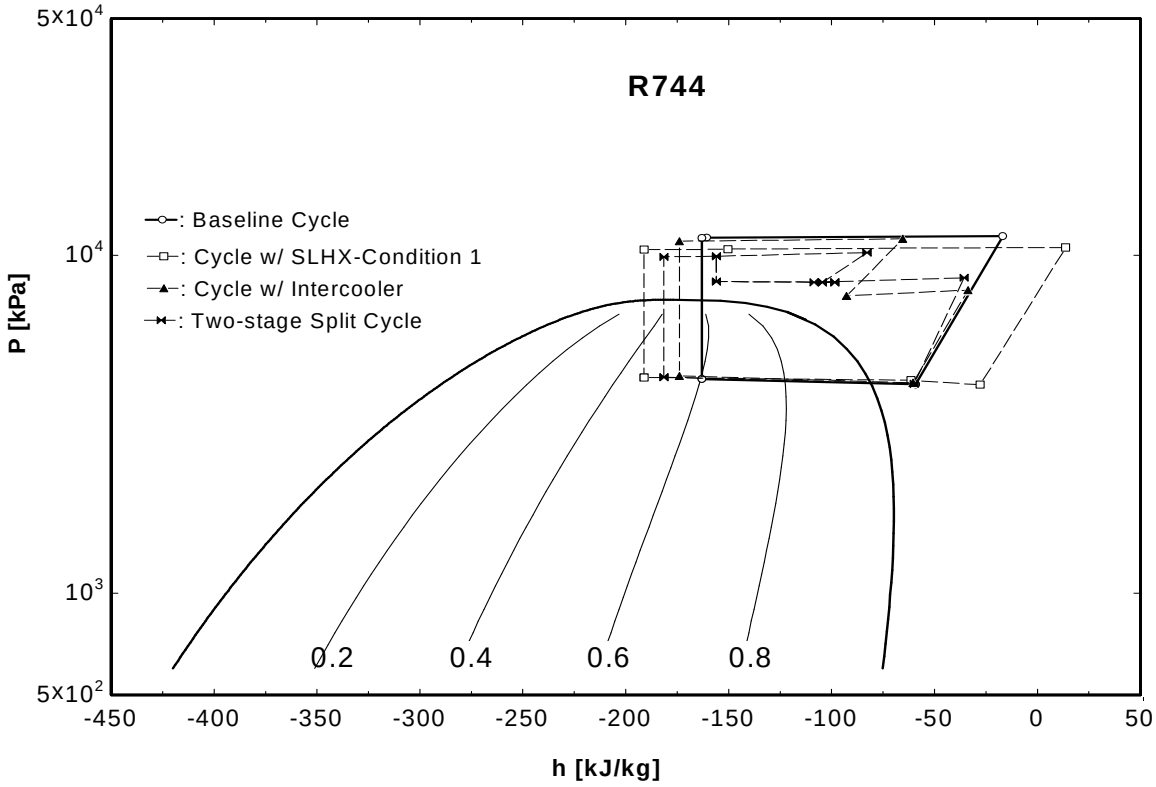

Figure 17: Comparison of CO_2 cycles in pressure-enthalpy diagram

The test results for the cycle with SLHX are compared with the test results for the baseline cycle as shown in Figures 18 and 19. As shown here, the cycle with SLHX performs better under the condition 1 than under the condition 2. Moreover, the cycle with SLHX shows 18% higher COP than that of the baseline cycle because of increased cooling capacity by the SLHX. The cycle with SLHX under condition 1 has a discharge pressure which is 0.9 MPa less than that of the baseline cycle at optimum charge. However, it also shows that the discharge temperature of the cycle with SLHX is about 15 K higher than that of the baseline cycle at optimum charge.

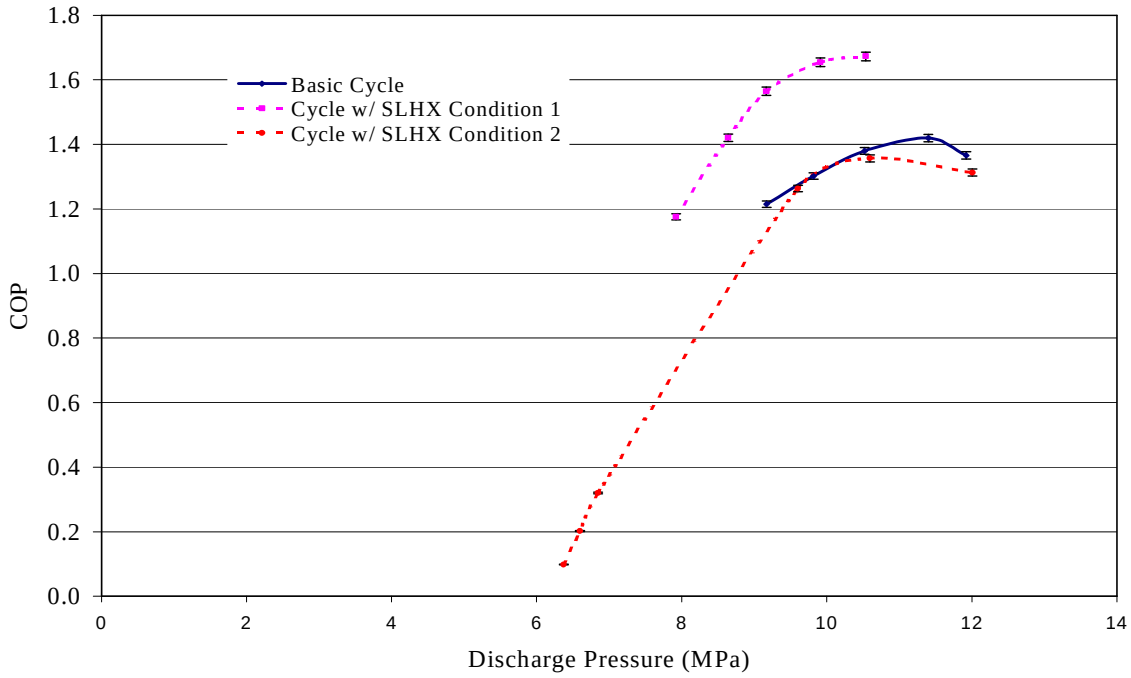

Figure 18: COP variation with discharge pressure for baseline and SLHX cycles

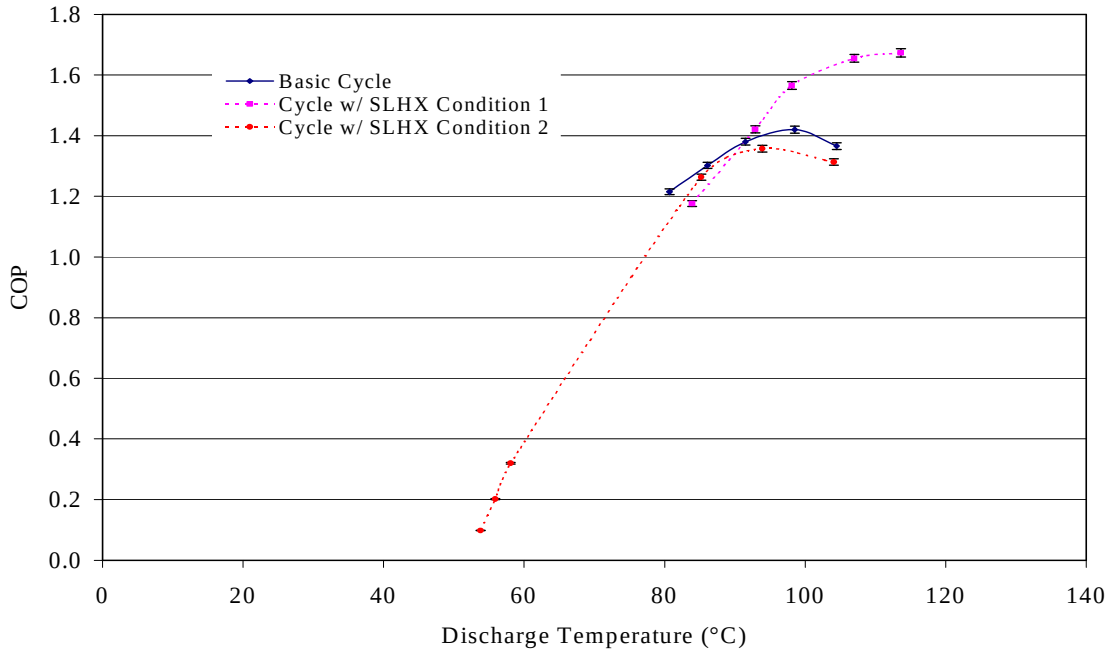

Figure 19: COP variation with discharge temperature for baseline and SLHX cycles

Test results of four different cycle options under test conditions A and B are displayed at various discharge pressures in Figures 20 and 21. In these figures, data with closed symbols and open symbols are for test condition A and B, respectively. The cycle with SLHX and the cycle with intercooler have a similar effect on the capacity of the system over the baseline cycle under the test condition A. The split cycle showed the most improvement in terms of COP and capacity among the cycle options and provided greater capacity increase for the test condition B than the test condition A over the baseline cycle.

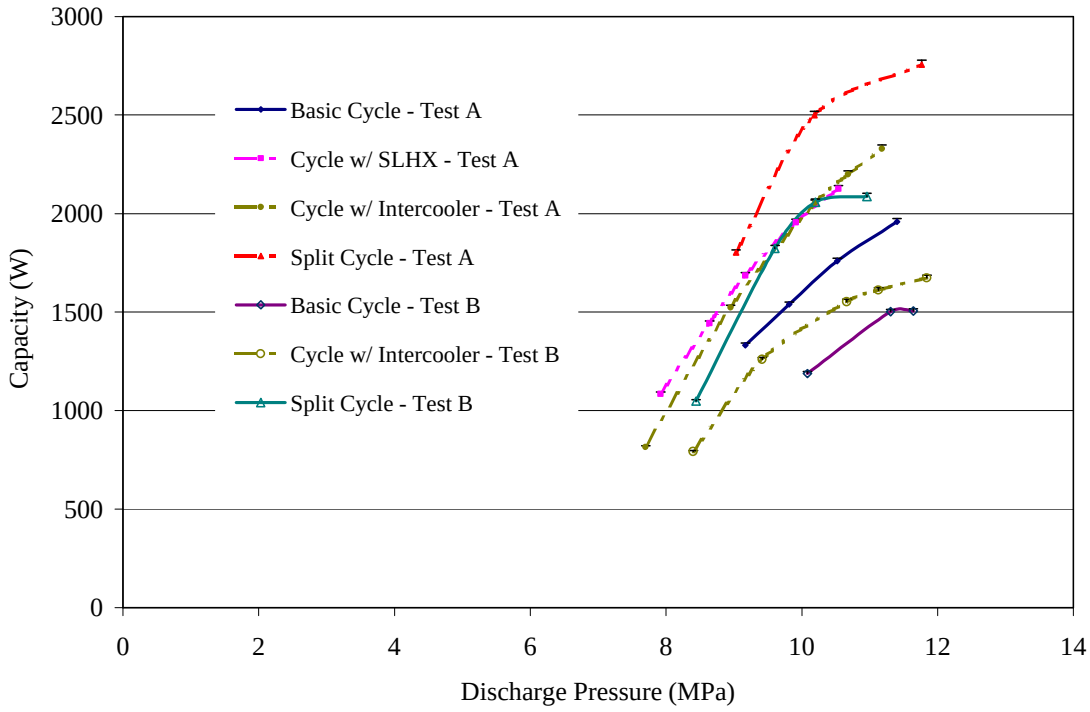

Figure 20: System capacity of different CO_2 cycles at different test conditions

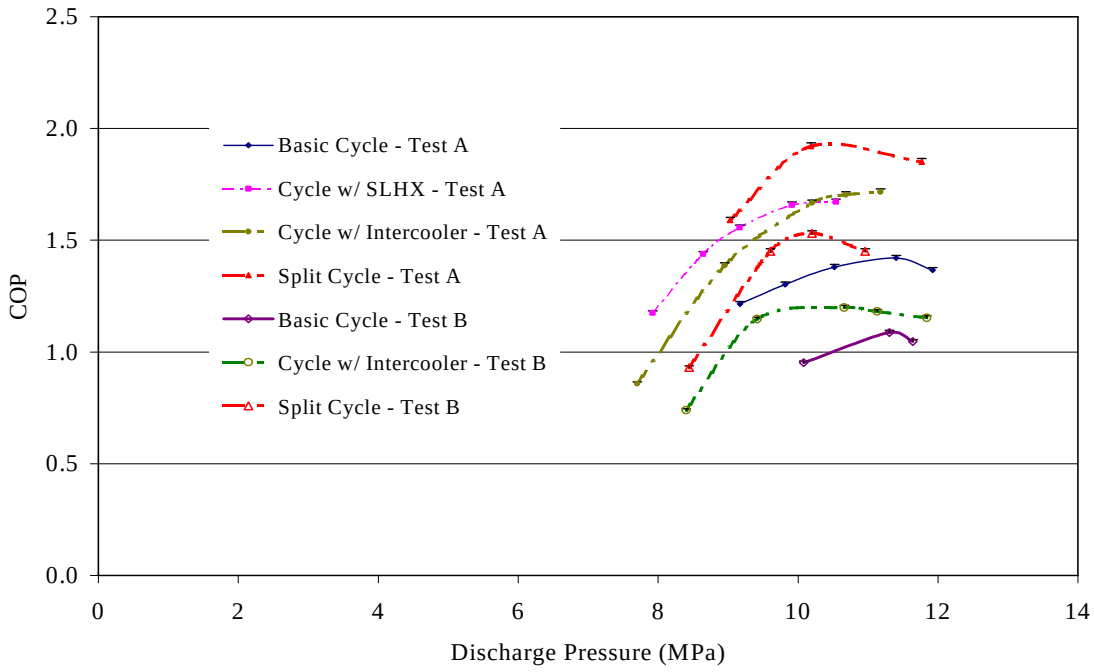

Figure 21: COP of different CO_2 cycles at different test conditions

The optimum test results of four cycles under test condition A are summarized in Table 27. The cycle with SLHX has a reduced discharge pressure but has the negative effect of increased discharge temperature. However, the cycle with intercooler reduced the discharge temperature. The split cycle has both the reduced discharge pressure and temperature. The improvement of the COP of the cycle with SLHX, the cycle with intercooler, and the split cycle over the baseline cycle is 18, 24, and 31%, respectively.

Table 27: Summary of test results – condition A

Cycle Option	P_{dis} (MPa)	T_{dis} (°C)	Q_{evap} (kW)	W_{comp} (kW)	COP	Improvement (%)
Baseline	11.42	98.5	1.959	1.290	1.42	-
SLHX	10.52	113.6	2.125	1.175	1.67	18
Intercooler	11.42	73.5	2.400	1.260	1.76	24
Split Cycle	10.18	60.8	2.430	1.177	1.86	31

The optimum test results of cycles for test condition B are summarized in Table 28. Tests were not run for SLHX cycle option because of high discharge temperatures. As shown here, the cycle with intercooler has a reduced discharge temperature and pressure as compared to the baseline cycle. The split cycle provides further reduced discharge temperature and pressure by 38 K and 1.1 MPa, respectively, as compared with the baseline cycle. The improvement of the COP of the cycle with intercooler and the split cycle over the baseline cycle is 10 and 40%, respectively.

Table 28: Summary of test results – condition B

	P_{dis} (MPa)	T_{dis} (°C)	Q_{evap} (kW)	W_{comp} (kW)	COP	Improvement (%)
Baseline	11.3	110.8	1.501	1.290	1.09	-
Intercooler	10.7	87.0	1.720	1.307	1.20	10
Split	10.2	62.8	2.058	1.215	1.53	40

The optimum COPs of four cycle options at each evaporating temperature are compared at various evaporating temperatures as shown in Figure 22. As shown here, the split cycle shows the highest COP over the entire range of evaporating temperatures investigated,

followed by the cycle with intercooler and the cycle with SLHX. Moreover, the baseline cycle and the cycle with intercooler were in operation for the evaporating temperature down to -6.7°C. The split cycle was in operation for the evaporating temperature down to -23.3°C, which is the widest range of operation. However, the cycle with SLHX was in operation only for the evaporating temperature at 7.2°C. The limiting factor for the operation in low evaporating temperature is the compressor discharge temperature.

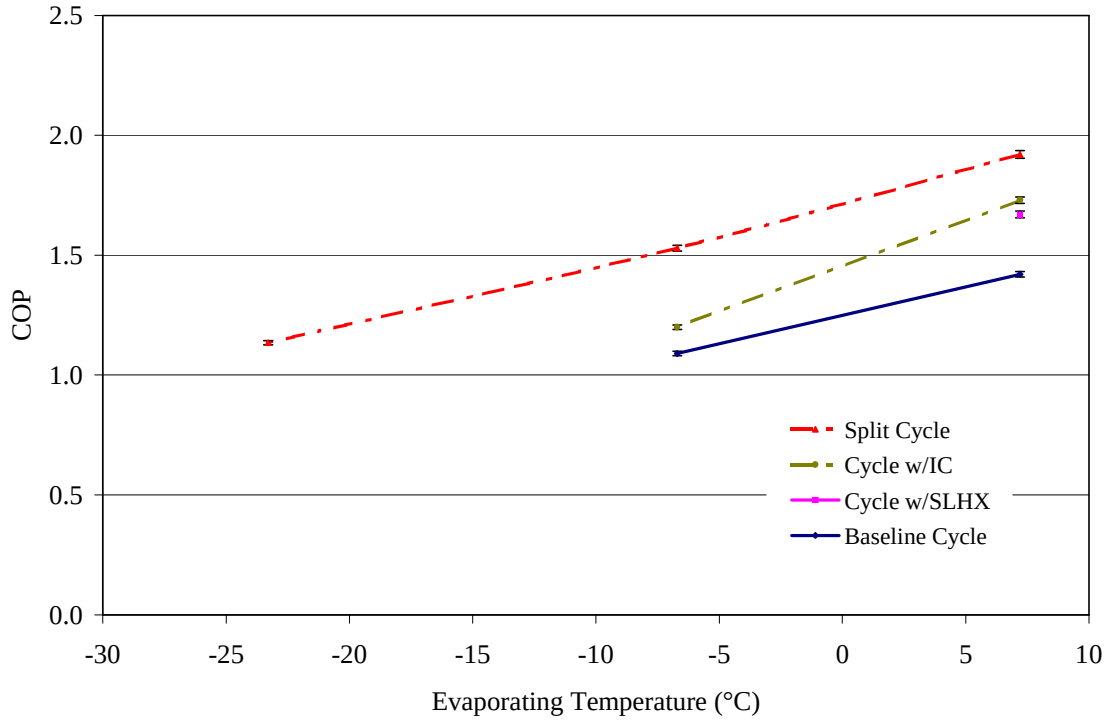

Figure 22: Effect of evaporating temperature on COP

One of the main purposes of this project is to make the CO_2 cycles competitive with conventional cycles. Table 23 shows some of the conventional condensing units which are working with different refrigerants. Capacity, power and COP values on this table are

from test results at test condition A. Red colored units have a similar system capacity as the two-stage split CO_2 system tested here. As seen from here, the two-stage split CO_2 cycle's COP of 1.86 makes it competitive with these units.

Table 29: Conventional condensing units

Company	**Model**	**Refrigerant**	**Q_{evap} (W)**	**W_{comp} (W)**	**COP**
Danfoss	SC18CNX-BG4	R-290	1,885	1,202	1.57
Danfoss	SC15CNX-BG4	R-290	1,713	915	1.87
Danfoss	SC12CNX-BG4	R-290	1,501	699	2.15
Embraco	UF8,58K	R-12	773	409	1.87
Embraco	UFI12HBX	R-134a	1,447	670	2.12
Embrac	UT6215Z	R-134a	1,962	1,022	1.87
Embraco	UJ6220Z	R-134a	2,673	1,330	1.97
Tecumseh	AEA4444YXA	R-134a	1,299	792	1.64

6 Heat Exchanger Performances

In this chapter, performance characteristics of various heat exchangers used in the tests are investigated. These characteristics are approach temperature, effectiveness and capacity.

The term “subcooling” cannot be used for a transcritical CO_2 cycle because the high side pressure is higher than the critical pressure of CO_2. Instead, the term “approach temperature” is used, and is defined by the following equation.

$$\Delta T_{app}=T_{hxo}-T_{amb} \quad (4)$$

where

ΔT_{app}: Approach temperature of the refrigerant (°C)

T_{hxo}: Refrigerant temperature at heat exchanger outlet (°C)

$T_{amb:}$ Ambient temperature (°C)

The effectiveness of the SLHX is calculated by Equation 5.

$$\varepsilon = \frac{Q}{Q_{max}} \quad (5)$$

where ε : Effectiveness of the SLHX

Q: Actual heat transfer rate (kW)

Q_{max}: Maximum possible heat transfer rate (kW)

Actual heat transfer rate (Q) is given by

$$Q= \dot{m} * c_{p,h} * (t_{hi} - t_{ho}) = \dot{m} * c_{p,c} * (t_{co} - t_{ci}) \quad (6)$$

where $\dot{m}$: Mass flow rate of the fluid (kg/s)

$c_{p,h}$: Specific heat of the hot fluid (kJ/kg°C)

$c_{p,c}$: Specific heat of the cold fluid (kJ/kg°C)

t_{hi} : Hot fluid inlet temperature (°C)

t_{ho} : Hot fluid outlet temperature (°C)

t_{ci} : Cold fluid inlet temperature (°C)

t_{co} : Cold fluid outlet temperature (°C)

The maximum possible heat transfer rate is expressed by

$$Q_{max} = \dot{m} * c_{p,min} * (t_{hi} - t_{ci}) \quad (7)$$

The parameters "P" and "R" are used to simplify the calculation of the effectiveness of the SLHX. These parameters are defined as

$$P = \frac{t_{co} - t_{ci}}{t_{hi} - t_{ci}} \quad \text{and} \quad R = \frac{t_{hi} - t_{ho}}{t_{co} - t_{ci}} \quad (8)$$

By combining Equations 4, 5, 6 and 7, we can conclude that:

i. $\varepsilon = P$ if $R<1$

ii. $\epsilon = P*R$ if $R \geq 1$

Heat exchanger capacity is given by,

$$\dot{Q} = \dot{m}_{ref} * (h_{in} - h_{out}) \quad (9)$$

The effect of discharge and intermediate pressures on these characteristics were researched for the four heat exchangers, which are gas cooler, intercooler, SLHX and IHX.

The effectiveness is calculated for SLHX and IHX and the approach temperature is calculated for gas cooler and intercooler. Capacity values are calculated for all the heat

exchangers. Heat exchanger characteristics are investigated for split cycle option for all heat exchangers at different evaporating temperatures.

For a better understanding of performance of individual heat exchangers, the term "pseudo-critical temperature" is defined here. Pseudo-critical temperature is the temperature which provides the maximum specific heat value at a constant pressure. Figure 23 shows the specific heat values for CO_2 at different temperatures and pressures. The critical pressure for CO_2 is 7.4 MPa, and the critical temperature is 31.1 °C. By definition, the specific heat of the refrigerant becomes infinite at this point.

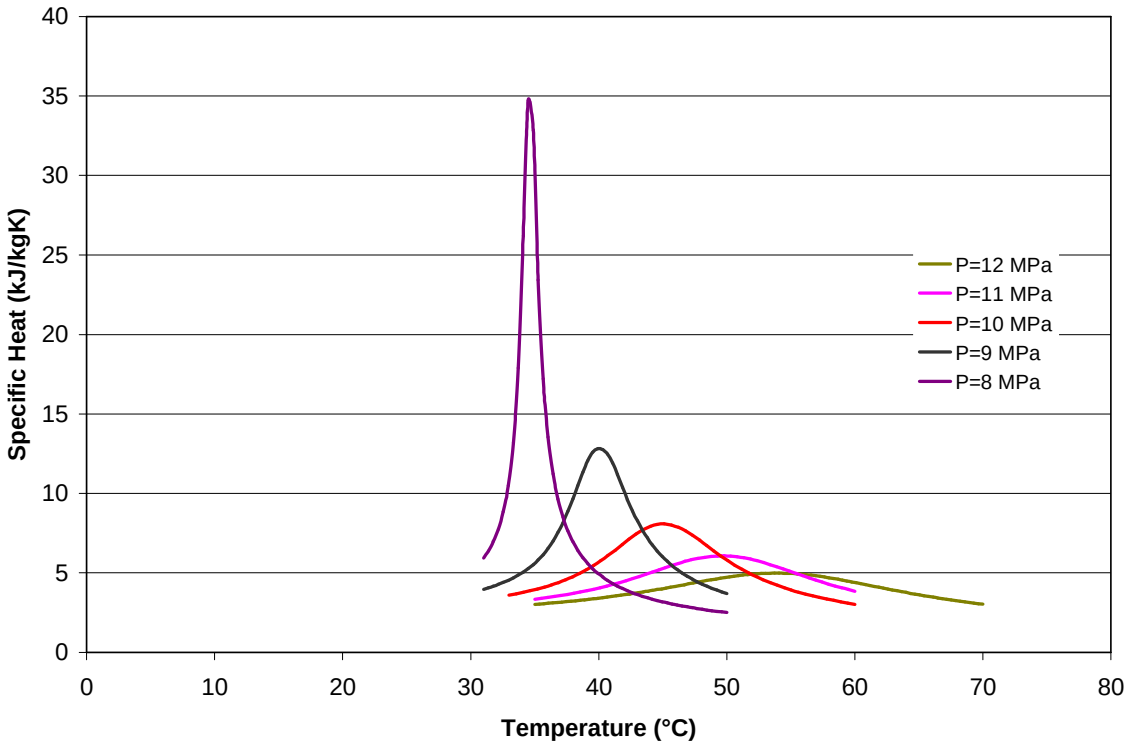

Figure 23: Specific heat variation of CO_2 with pressure and temperature

Pseudo-critical temperatures for CO_2 at different pressures are shown in Figure 24.

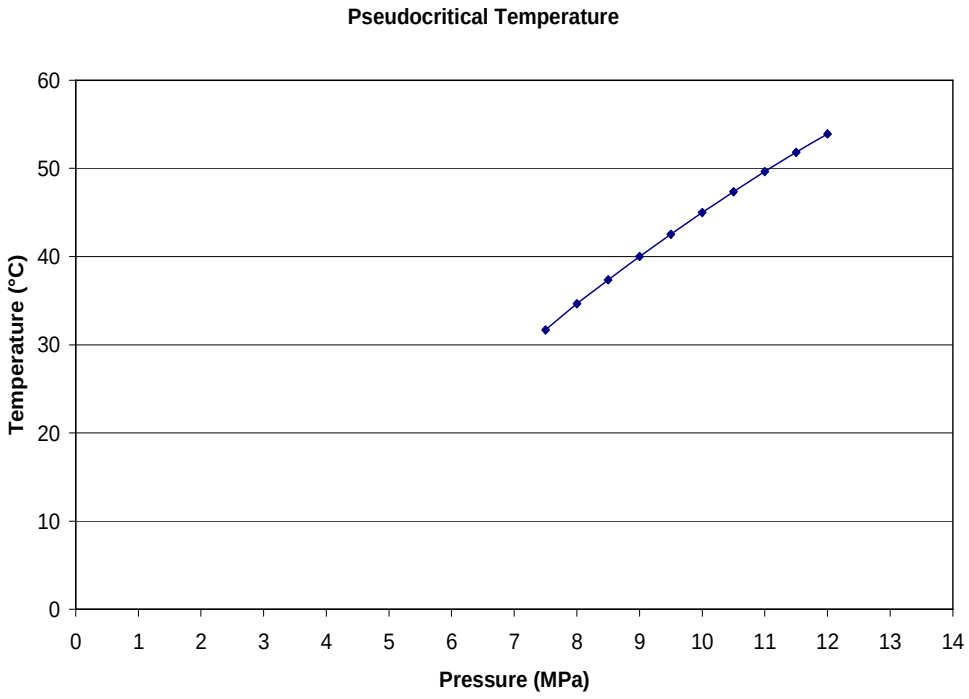

Figure 24: Pseudo-critical temperatures at different pressures

6.1 Gas Cooler

Figure 25 shows the approach temperature values at different gas cooling pressure (at the inlet) for different test conditions.

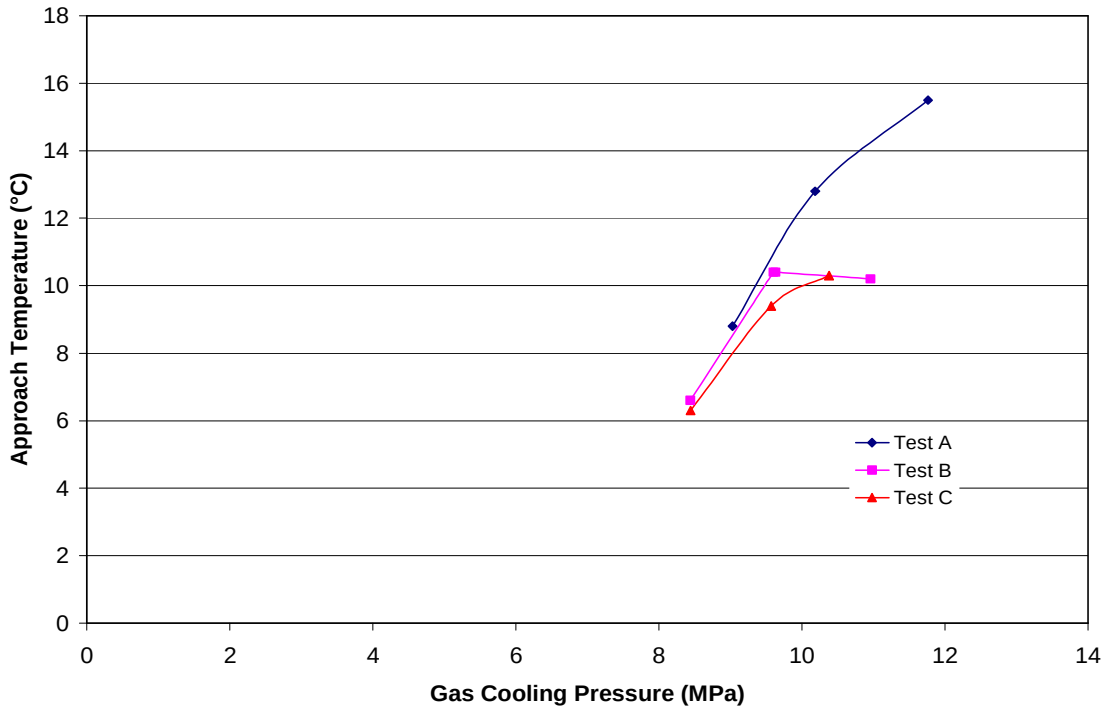

Figure 25: Approach temperature vs. gas cooling pressure

As the evaporating pressure decreases, the refrigerant suction density decreases, decreasing the mass flow rate of the refrigerant. So, the mass flow rate of the refrigerant flowing through the gas cooler is higher for Test A condition than Test B and Test C conditions. Therefore, the approach temperature increases more for Test A condition. It also shows that if a test condition is set for an approach temperature of 10°C, then the heat exchanger area should be increased to maintain that approach temperature. In our test conditions, this approach temperature was not set. Figure 26 shows the gas cooling capacity values calculated by Equation 9 at different gas cooling pressure (inlet) for different test conditions.

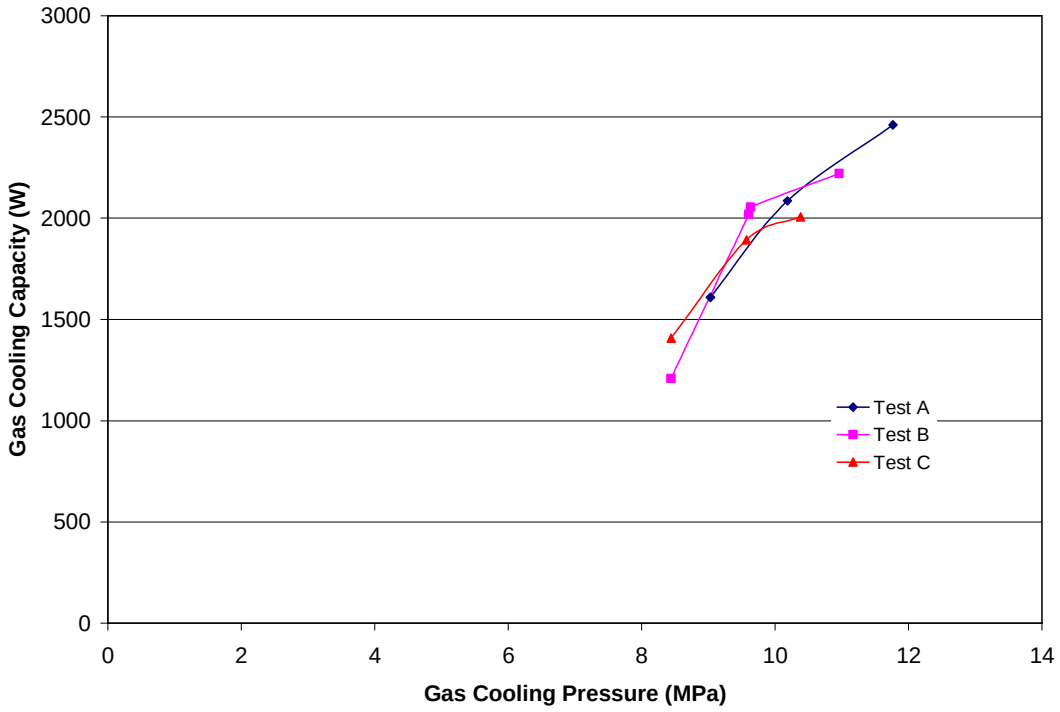

Figure 26: Gas cooling capacity vs. gas cooling pressure

Since the specific heat value becomes a maximum at the pseudo-critical temperature, as the refrigerant temperature decreases to this value, more heat needs to be removed. Moreover, it is known that pseudo-critical temperature increases with increasing pressure. Therefore, the slope of the gas cooling capacity curve is decreasing with the increasing gas cooling pressure. Note that the gas cooling capacity is increasing in the above figure because the total mass flow rate of the refrigerant entering the gas cooler is increasing.

6.2 Intercooler

Figure 27 shows the approach temperature values at different intercooling pressures (inlet) for different test conditions. Intercooling pressure is also the 1st stage compressor outlet pressure, known as the intermediate pressure.

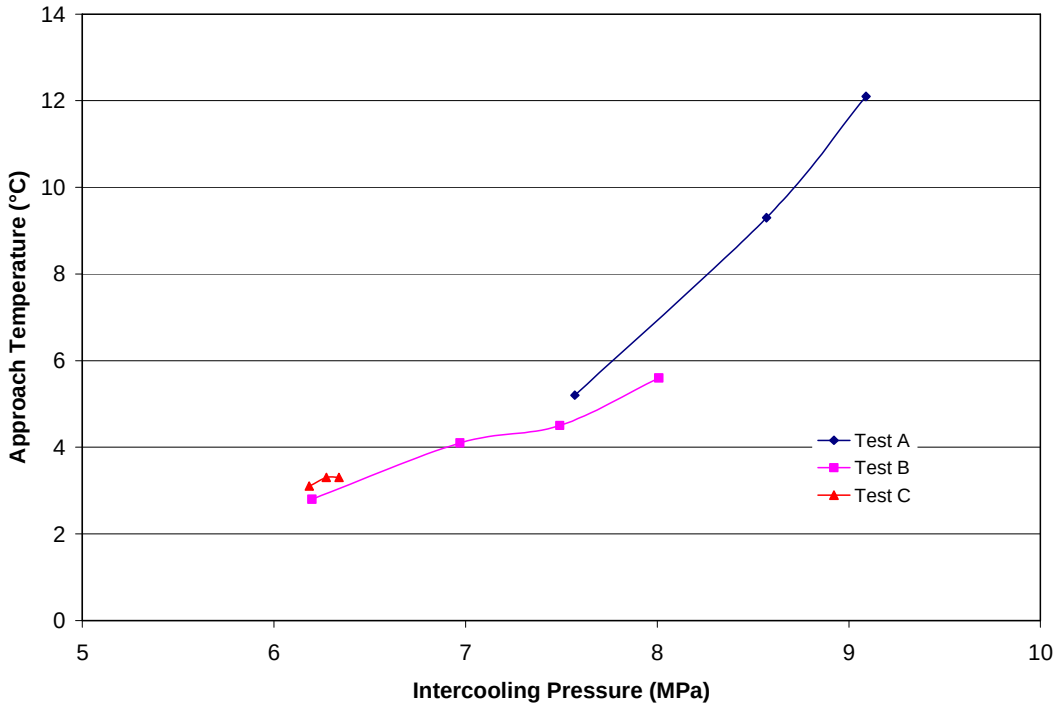

Figure 27: Approach temperature vs. intercooling pressure

As shown in this figure, the intercooler provides higher approach temperatures at condition A than at conditions B and C because of higher refrigerant mass flow rate at that condition. Increasing either the heat transfer area or air mass flow rate can lower approach temperature at this test condition.

Figure 28 shows the intercooler capacity values at different intercooling pressures (inlet) for different test conditions. The intercooler capacity range for test condition C is small because the approach temperature for the intercooler doesn't change with intercooling pressure at that test condition as shown in Figure 27. The intercooler provides the maximum possible cooling at all intercooling pressures because of low refrigerant mass flow rates at this condition.

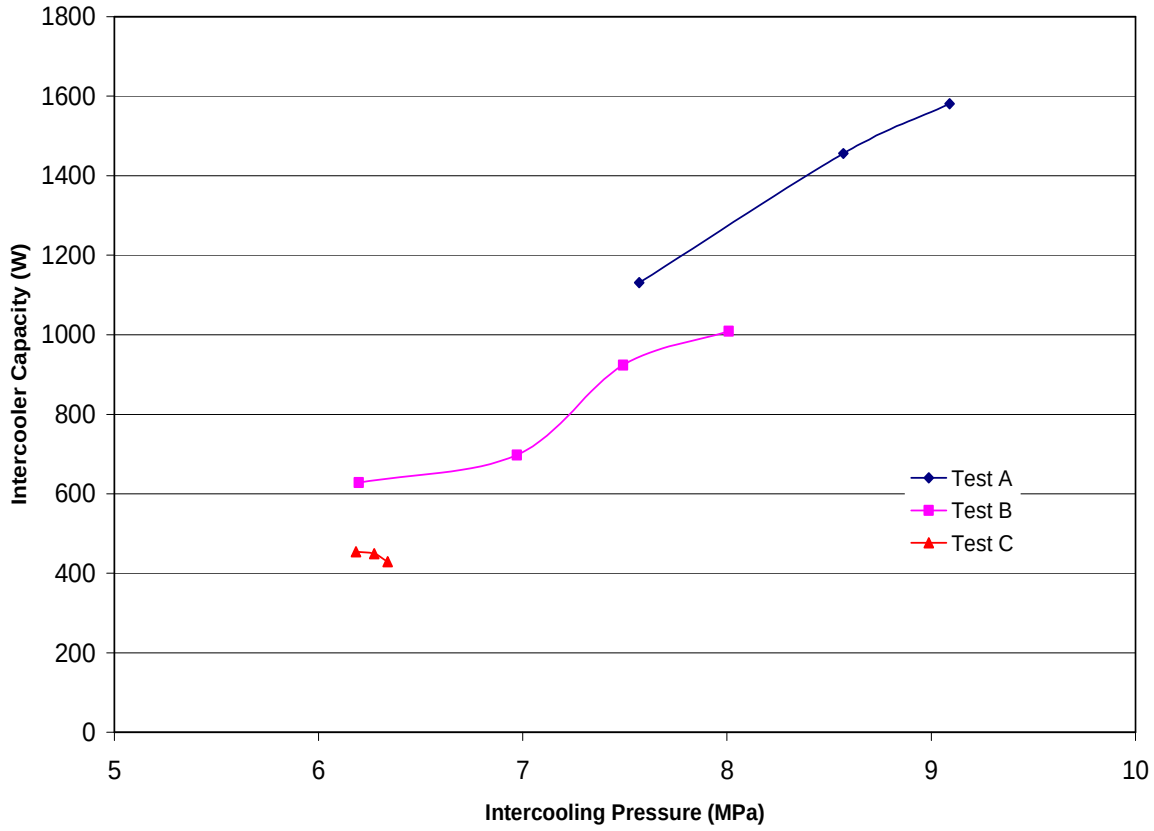

Figure 28: Intercooler capacity vs. intercooling pressure

For test conditions A and B, the intercooler capacity is increasing by increasing intercooling (compressor 1st stage outlet) pressure. However, intercooling capacity

decreases with increasing pressure under test condition C. The reason for this behavior is that the volumetric efficiency of the first stage decreases as the intercooling pressure increases. Therefore, the mass flow rate of the refrigerant decreases. The mass flow rate of the refrigerant for test condition C is half of that for test condition B and a third of that for test condition A. Although the enthalpy difference increases for test conditions A and B, it becomes constant for test condition C. Hence, the intercooler capacity decreases by increasing intercooling pressure for test condition C.

6.3 SLHX

6.3.1 Condition 1

Figure 29 shows the change in the effectiveness of the SLHX with respect to the refrigerant mass flow rate. Figure 30 shows the changes in the effectiveness of the SLHX and the refrigerant mass flow rate with respect to the gas cooler outlet pressure. The result shows that the effectiveness is affected by the refrigerant mass flow rate and gas cooling pressure. The maximum effectiveness occurred at around 9 MPa and 17 g/s. The effectiveness ranges from 0.70 to 0.79 in this condition.

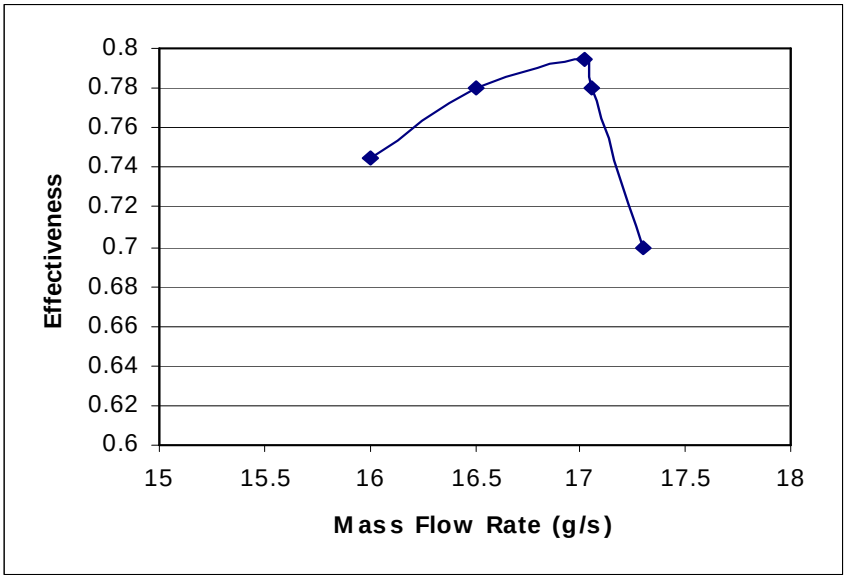

Figure 29: SLHX effectiveness vs. refrigerant mass flow rate at condition 1

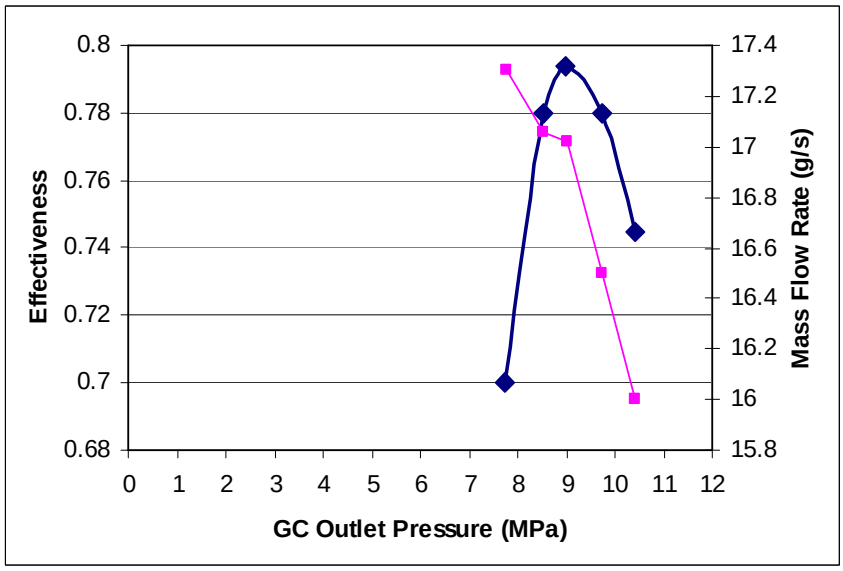

Figure 30: SLHX effectiveness and refrigerant mass flow rate vs. gc outlet pressure at condition 1

6.3.2 Condition 2

If the effectiveness of the transcritical cycle cases is considered, it ranges from 0.67 to

0.74, which is lower than that of the Condition 1. Figure 31 shows the change in the effectiveness of the SLHX with respect to the refrigerant mass flow rate. Figure 32 shows the change in the effectiveness of the SLHX and the refrigerant mass flow rate with respect to the gas cooler outlet pressure. The result shows that the effectiveness is affected by both the refrigerant MFR and the gas cooling pressure.

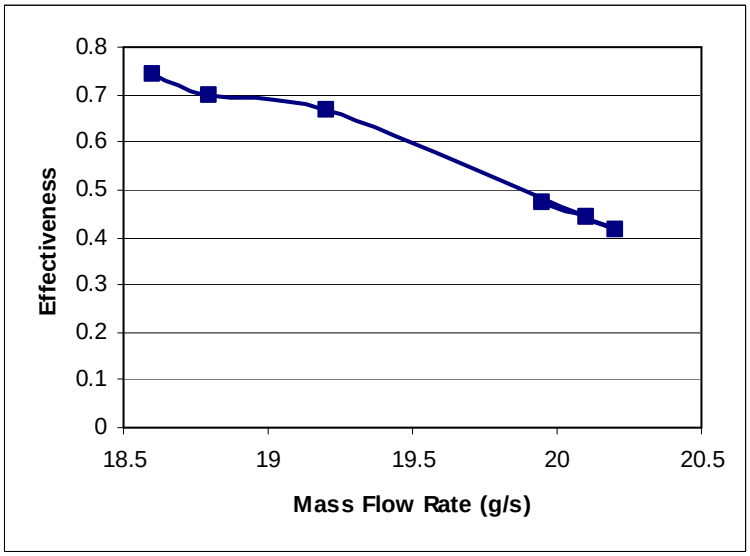

Figure 31 SLHX effectiveness vs. refrigerant mass flow rate at condition 2

For the transcritical cycle, the refrigerant mass flow rate decreased and the effectiveness increased as the gas cooling pressure increased. The maximum effectiveness was not reached until the gas cooling pressure reached 12 MPa.

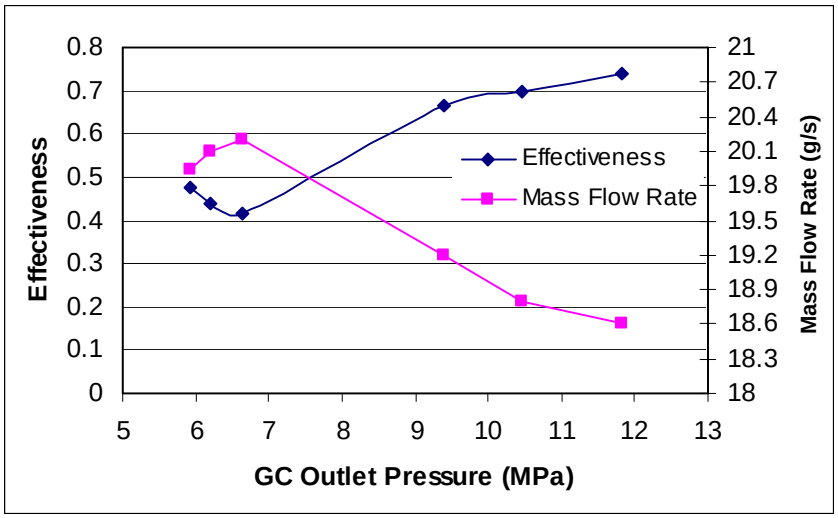

Figure 32: SLHX effectiveness and refrigerant mass flow rate vs. gc outlet pressure at condition 2

SLHX has a better efficiency at condition 1 than at condition 2. More importantly, SLHX cycle at condition 1 provided better cycle performance than at condition 2 in terms of COP. Therefore, testing SLHX cycle at condition 1 is recommended.

6.4 IHX

Figure 33 shows the capacity of internal heat exchanger at different internal HX inlet pressure (inlet) for different test conditions.

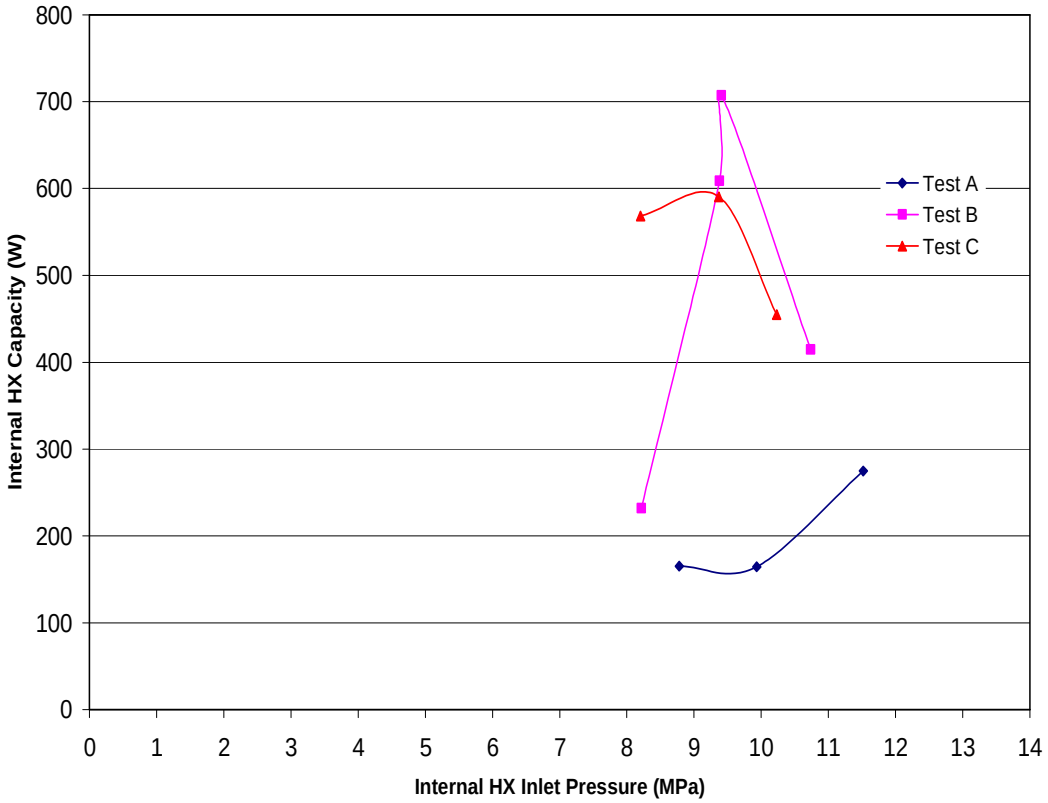

Figure 33 Internal heat exchanger capacity vs. internal heat exchanger inlet pressure

Internal heat exchanger capacity has its maximum at 9.4 MPa for test conditions B and C. Note that, this was also the internal heat exchanger inlet pressure (high side) where the optimum COP was obtained. For test condition A, at 9.9 MPa inlet pressure, the internal heat exchanger inlet temperature was very close to the pseudo-critical temperature (0.5°C above). Therefore, the internal heat exchanger capacity is low at that point. The capacity of the IHX is lower at condition A then conditions B and C. IHX capacity directly affects the cooling capacity. Therefore, the capacity increase at condition A does not depend mainly on IHX.

7 Compressor Performance Data

In this chapter, performance of the compressor is investigated in terms of efficiency. Two different efficiencies are defined for analyzing the performance of the compressor. These are volumetric efficiency and compressor efficiency. Volumetric efficiency is the ratio of actual mass flow rate to the ideal mass flow rate. Since there is two-stage compression, this volumetric efficiency can be defined for each stage.

1st stage volumetric efficiency was calculated by the following equation:

$$\eta_{vol,1} = \frac{mfr_m}{\rho_2 * (RPM/60) * DISPvol_1} \quad (10)$$

where

$\eta_{vol,1}$: Volumetric efficiency of the first stage

mfr_m : Main flow mass flow rate (kg/s)

ρ_2 : Refrigerant density at 1st stage inlet (kg/m^3)

RPM : Compressor speed (rpm)

$DISPvol_1$: 1st stage displacement volume (m^3)

2nd stage volumetric efficiency was calculated by the following equation:

$$\eta_{vol,2} = \frac{mfr_t}{\rho_5 * (RPM/60) * DISPvol_2} \quad (11)$$

where

$\eta_{vol,2}$: Volumetric efficiency of the first stage

mfr_t: Total mass flow rate (kg/s)

ρ_5 : Refrigerant density at 2nd stage inlet (kg/m^3)

RPM : Compressor speed (rpm)

$DISPvol_2$: 2nd stage displacement volume (m^3)

Compressor efficiency considers only what happens in the compressor volume and is a measure of the deviation of actual compression from ideal compression. It is defined as the ratio of the work required for the isentropic compression of the gas to the work delivered to the gas within the compression volume. (Ashrae Handbook, 2000)

Compressor efficiency was calculated by the following equation:

$$\eta_{comp} = \frac{mfr_m * (h_{1,dis,ise} - h_{1,suc}) + mfr_t * (h_{2,dis,ise} - h_{2,suc})}{P_{comp}} \quad (12)$$

where

η_{comp} : Compressor efficiency

$h_{1,dis,ise}$: Refrigerant enthalpy at 1st stage discharge (J/kg)

$h_{1,suc}$: Refrigerant enthalpy at 1st stage suction (J/kg)

$h_{2,dis,ise}$: Refrigerant enthalpy at 2nd stage discharge (J/kg)

$h_{2,suc}$: Refrigerant enthalpy at 2nd stage suction (J/kg)

P_{comp} : Compressor power (W)

Pressure ratio is defined as the ratio of the discharge pressure to the suction pressure for each stage.

$$PR = \frac{P_{dis}}{P_{suc}} \quad (13)$$

where PR is the pressure ratio, P_{dis} is the discharge pressure and P_{suc} is the suction pressure.

7.1 Volumetric Efficiencies

Figure 34 shows the 1st stage volumetric efficiency values for different pressure ratios at the first stage. 1st stage volumetric efficiency varies from 0.8 to 0.95 depending on the pressure ratio across the first stage.

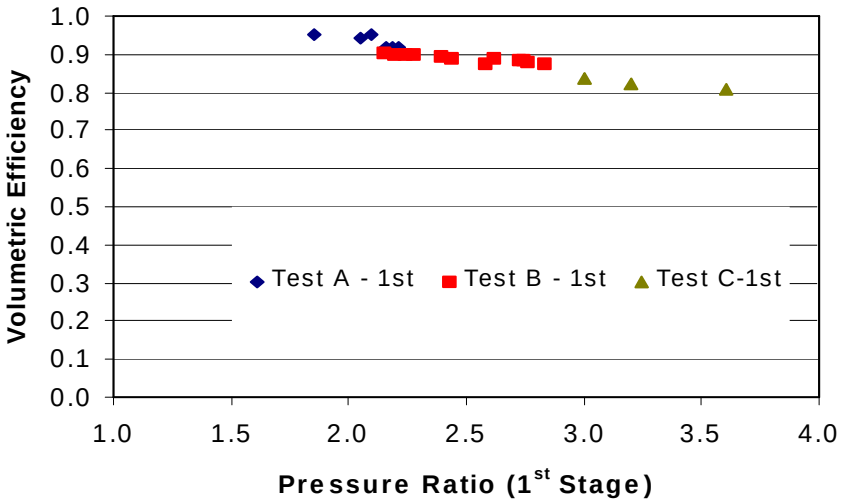

Figure 34 Volumetric efficiency of 1st stage at different test conditions

2nd stage volumetric efficiency values at different discharge pressures and test conditions are shown in Figure 35. 2nd stage volumetric efficiency varies from 0.75 to 0.95 depending on the pressure ratio across the second stage. 1st and 2nd stage volumetric efficiencies slightly differ from each other because of different displacement volumes and operating pressure ranges for these stages.

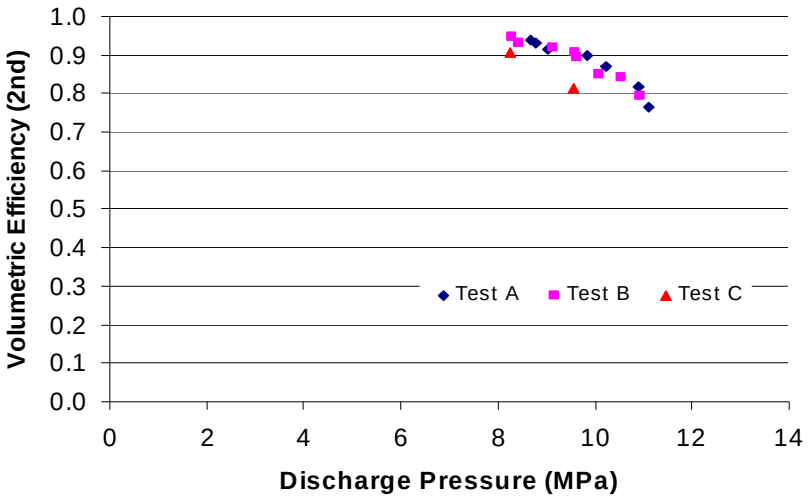

Figure 35 Volumetric efficiency of the 2nd stage for different test conditions

7.2 Compressor Efficiency

Figure 36 shows the compressor efficiency values for different overall pressure ratios and test conditions. Compressor efficiency decreases from 0.7 to 0.55 by increasing the overall pressure ratio.

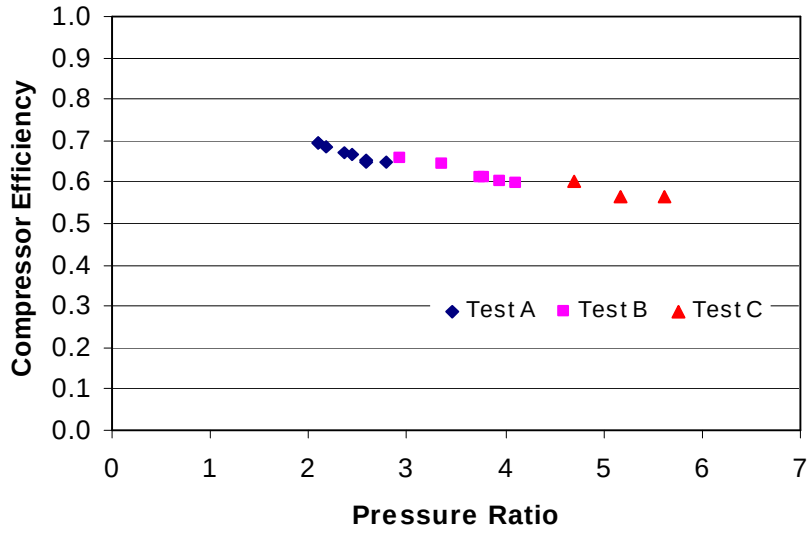

Figure 36 Compressor efficiency at different test conditions

8 Optimization of Split Cycle

The state points in a split cycle are shown on Figure 37.

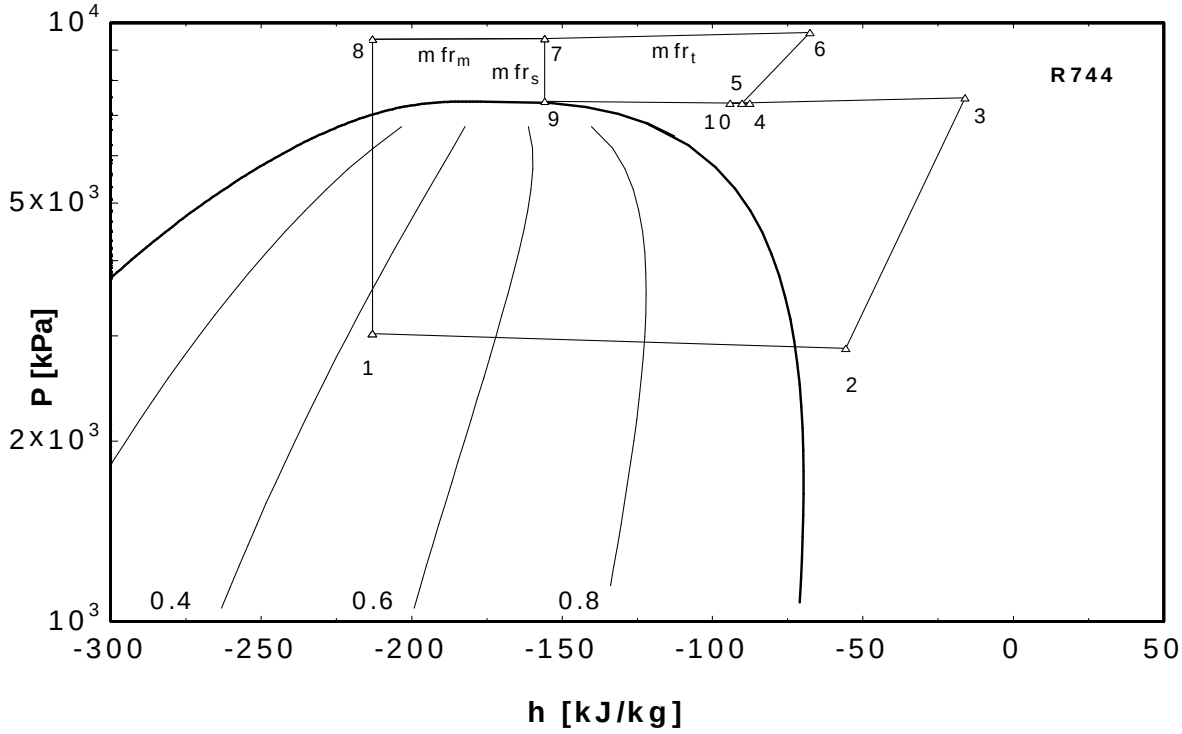

Figure 37 State points of split cycle on p-h diagram

In this figure:

mfr_t : Total refrigerant mass flow rate (g/s)

mfr_m: Main cycle refrigerant mass flow rate (g/s)

mfr_s: Sub cycle refrigerant mass flow rate (g/s)

1: Evaporator Inlet

2: Compressor Inlet

3: Compressor 1st Stage Outlet

4: Intercooler Outlet

5: Compressor 2nd Stage Inlet

6: Compressor 2nd Stage Outlet

7: Gas Cooler Outlet

8: Main Cycle Expansion Valve Inlet

9: Sub Cycle Expansion Valve Outlet

10: Internal Heat Exchanger Outlet

Evaporator capacity can be calculated by the following equation:

$$\dot{Q}_{evap} = mfr_m * (h[2] - h[1]) \quad (14)$$

where h represents the enthalpy value for the given state point, and

$\dot{Q}_{evap}$ represents evaporator capacity.

Compressor power can be calculated by the following equation:

$$P_{comp}=\{mfr_m* (h[3]ise-h[2]) + mfr_t * (h[6]ise-h[5])\}/\eta_{comp} \quad (15)$$

where

h[3]ise: Isentropic enthalpy at state point 3

h[6]ise: Isentropic enthalpy at state point 6

η_{comp}: Compressor efficiency

P_{comp}: Compressor power

Coefficient of performance (COP) can be calculated by the following equation:

$$COP = \frac{\dot{Q}_{evap}}{P_{comp} + P_{fan}} \quad (16)$$

where P_{fan} represents the fan power.

By substituting Equations 14 and 15 into 16, one may get the following equation:

$$\frac{1}{COP} = \frac{1}{\eta_{comp}} * \{\{\frac{h[3]ise - h[2]}{h[2] - h[1]} + [1 + \frac{mfr_s}{mfr_m} * (\frac{h[6]ise - h[5]}{h[2] - h[1]})]\} + \{\frac{P_{fan}}{mfr_m * (h[2] - h[1])}\}\} \quad (17)$$

From this equation, we define “mass flow rate ratio” as the ratio of the sub cycle’s mass flow rate to the main cycle’s mass flow rate.

$$mfr_{ratio} = \frac{mfr_s}{mfr_m} \quad (18)$$

We also define “power ratio” as the ratio of the power required for first stage compression to the power required for second stage compression.

$$P_{comp1} = \frac{mfr_m * (h[3]ise - h[2])}{\eta_{comp}} \quad (19)$$

$$P_{comp2} = \frac{mfr_t * (h[6]ise - h[5])}{\eta_{comp}} \quad (20)$$

$$Ratio_{power} = \frac{P_{comp1}}{P_{comp2}} \quad (21)$$

From Equation 17, decreasing mass flow rate ratio may seem to increase the COP. However, when the mass flow rate ratio is decreased, the sub cycle’s mass flow rate decreases. Therefore, the intermediate pressure (P[3]) decreases, and the discharge pressure (P[6]) increases. This causes the COP value to decrease.

Increasing mass flow rate causes the increase in intermediate pressure and decrease in

discharge pressure. Although increase in mass flow rate and intermediate pressure causes the COP value to decrease, the decrease in discharge pressure helps to increase the COP value. Hence, this becomes an optimization problem of mass flow rate ratio to maximize the COP value.

The cycle can also be optimized by adjusting the intermediate pressure. To simplify this optimization, geometric mean pressure is defined in Eq. 22.

$$GMP = \sqrt{P_{suc} * P_{dis}} \tag{22}$$

where GMP is the geometric mean pressure (MPa).

Optimum intermediate pressure ($P_{int,opt}$) is given by;

$$P_{int,opt} = k_{int,opt} * GMP \tag{23}$$

where $k_{int,opt}$ is the optimum intermediate pressure coefficient.

8.1 Optimum Mass Flow Ratio

Optimized mass flow rate ratios at different suction pressures are shown in Figure 38.

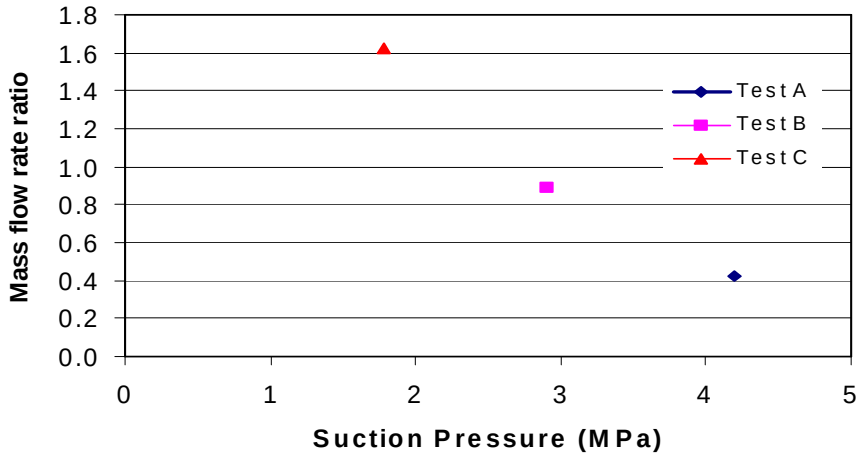

Figure 38: Optimum mass flow rate ratios

Optimum mass flow rate ratio decreases as the suction pressure decreases. From the definition of the mass flow rate ratio given in Eq. 18, it can be stated that the sub cycle becomes the dominant cycle as the suction pressure decreases. Therefore, IHX becomes an essential component of the system at lower suction pressures. A "0" value of mass flow rate ratio implies that there is no sub flow such as the baseline, SLHX and intercooler cycles. The optimum mass flow rate ratio becomes "0" above 5 MPa suction pressure. Therefore, above this pressure there is no need for IHX.

8.2 Optimum Intermediate Pressure Coefficient

Optimized intermediate pressure coefficients at different suction pressures are shown in Figure 39.

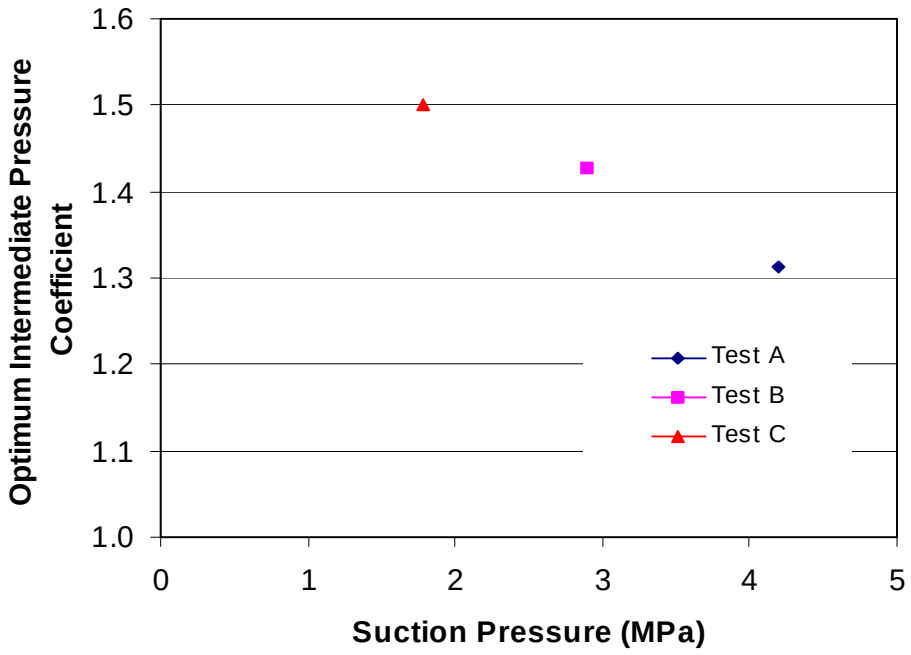

Figure 39: Optimum intermediate pressure coefficients

The optimum intermediate pressure coefficient decreases as the suction pressure increases. It varies from 1.3 to 1.5 in the given suction pressure range. As the suction pressure increases, the square-root of suction pressure is increasing more than the decrease in optimum intermediate pressure coefficient. Therefore, optimum intermediate pressure increases even though the optimum intermediate pressure coefficient decreases for increasing suction pressure.

The optimum intermediate pressure coefficient can be related to the pressure ratios. Substituting Eq. 22 in 23 yields;

$$k_{\text{int},opt} = \frac{P_{\text{int},opt}}{\sqrt{P_{suc} * P_{dis}}} \tag{24}$$

This equation can be arranged such that,

$$k_{\text{int},opt}{}^{2} = \left(\frac{P_{\text{int},opt}}{P_{suc}} \right) * \left(\frac{P_{\text{int},opt}}{P_{dis}} \right) \tag{25}$$

If the pressure drop across the intercooler is neglected, then the pressure ratios can be formulated by these equations:

$$PR_1 = \frac{P_{\text{int},opt}}{P_{suc}} \tag{26}$$

$$PR_2 = \frac{P_{dis}}{P_{\text{int},opt}} \tag{27}$$

Substituting equations 26 and 27 into 25 yields;

$$k_{\text{int},opt}{}^{2} = \frac{PR_1}{PR_2} \tag{28}$$

or,

$$k_{\text{int},opt} = \sqrt{\frac{PR_1}{PR_2}} \tag{29}$$

The last equation states that if the optimum intermediate pressure coefficient is increasing, then the ratio of the pressure ratios should also be increasing. This is proved to be the case for decreasing suction pressures.

8.3 Optimum Power Ratio

Optimized power ratios at different suction pressures are shown in Figure 40.

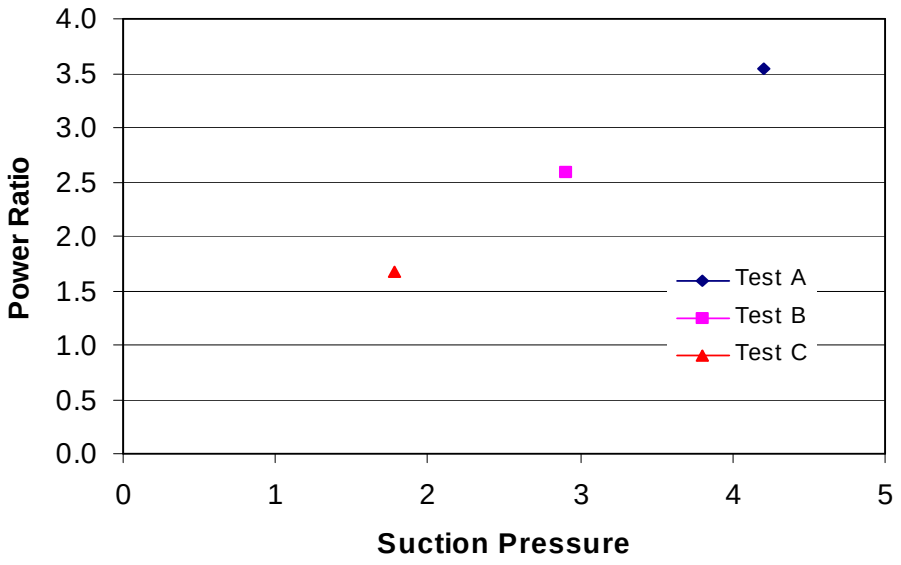

Figure 40: Optimum power ratios at different suction pressures

The optimum power ratio increases as the suction pressure increases. It varies from 1.7 to 3.5 in the given suction pressure range. Therefore, 1st stage compression consumes more power than 2nd stage compression. In the previous analysis, it was found that a lower ratio between pressure ratios was needed for optimum performance at higher suction pressures. Therefore, the optimum ratio of the compression enthalpy differences of the 1st and 2nd

stages decreases as the suction pressure increases. However, the refrigerant mass flow rate in the 1st stage increases by 233% over the given suction pressure range. Therefore, it dominates the power ratio, which is directly related to the suction pressure.

9 Cycle Modeling

Baseline, SLHX, intercooler and two-stage split CO_2 cycles were modeled by Engineering Equation Solver (EES) software. The basic function provided by EES is the numerical solution of a set of algebraic equations. EES can also be used to solve differential and integral equations, for optimization, to provide uncertainty analyses and linear and non-linear regression, and to generate publication-quality plots. There are two major differences between EES and other equation-solving programs. First, EES allows equations to be entered in any order with unknown variables placed anywhere in the equations; EES automatically reorders the equations for efficient solution. Second, EES provides many built-in mathematical and thermophysical property functions useful for engineering calculations. For cycle modeling, enthalpy, entropy and density of CO_2 at each state point were calculated by EES. EES has the capability to plot T-s, P-v, P-h, and other types of property plots and also to do parametric studies with spreadsheet-like table which were used during the cycle modeling (EES Manual 2004).

Two different approaches were used which were ideal case and the parametric analysis. Ideal case has the following characteristics:

- Steady state
- Isenthalpic expansion
- Isentropic compression
- No pressure drop across heat exchangers
- Volumetric and compressor efficiencies are 1

- Effectiveness of the SLHX and IHX is 1
- The CO_2 temperature at gas cooler outlet and intercooler outlet is equal to the ambient temperature which is 32.2°C (90°F)
- Fan power is neglected

Modeling of the ideal case gives the maximum COP with CO_2 cycles.

Parametric analysis has the following characteristics:

- Steady state
- Isenthalpic expansion
- Variable isentropic efficiencies of 1^{st} and 2^{nd} stages
- Variable pressure drops across heat exchangers
- Variable volumetric efficiencies
- Variable effectiveness of the SLHX and IHX
- The CO_2 temperature at gas cooler outlet and intercooler outlet is also variable

There are two goals for the parametric analysis. First goal is to simulate the experimental conditions. This will provide a comparison between experimental results and EES software results. The second goal is to determine the effect of each variable to the system efficiency. From this information, the major variable or variables can be determined for COP maximization.

During these analyses, both discharge and intermediate pressure were varied for baseline, SLHX, intercooler cycles and discharge pressures. For the first three cycles, intermediate

pressure is a function of compressor discharge pressure, while it is independent from the compressor discharge pressure for two-stage split cycle.

9.1 Baseline Cycle

First, sensitivity analysis was made for analyzing the effect of the parameters on the COP of the baseline cycle. Sensitivity is the percentage of the change in the dependant variable by the 1% of the change in the effective parameter. Therefore, sensitivity of COP to other system parameters can be given as;

$$Sensitivity = \frac{\partial(COP\,(\%))}{\partial(Parameter\ (\%))} \tag{30}$$

The maximum COP was obtained at 11.4 MPa of discharge pressure, 17K of gas cooler approach temperature and 130 kPa of gas cooler pressure drop for the baseline cycle. The result of sensitivity analysis for these conditions is shown in Table 30.

Table 30: Sensitivity analysis for the baseline cycle

Parameters	Sensitivity of COP
Compressor Efficiency	1.000
Gas Cooler Approach Temperature	-0.878
Gas Cooler Pressure Drop	-0.028
Discharge Pressure	0.773

This table shows that the COP is sensitive to the compressor efficiency, the gas cooler

approach temperature and the discharge pressure in this order. Gas cooler pressure drop has a small effect on the COP.

Change in gas cooler pressure drop determines the change in gas cooler outlet pressure. Gas cooler approach temperature is an indicator of the gas cooler outlet temperature. Since the compressor power is the same for the same discharge pressure, it can be said that the system capacity is affected mostly by the temperature changes at the gas cooler outlet (for the baseline cycle also the expansion valve inlet) rather than the pressure changes. The effect of gas cooler approach temperature and pressure drop on COP is also valid for other CO_2 cycle options since those cycles also have the gas cooler as a cycle component.

The maximum COP with baseline cycle at the ideal case was obtained at 7.87 MPa discharge pressure where the COP was 5.50. The refrigerant mass flow rate was varied between 10 g/s and 50 g/s with 10 g/s increments. The system capacity range for this modeling was 1.46 kW to 7.31 kW, and the compressor power range was 0.27 kW to 1.33 kW.

For the parametric analysis, first gas cooler approach temperature was varied between 0K and 12K with 3K increments. Figure 41 shows the effect of gas cooler approach temperature to COP. As shown in this figure, the performance of CO_2 cycles is highly sensitive to gas cooler approach temperature. The COP of the cycle becomes 54% of the ideal cycle at 12K gas cooler approach temperature. This information can also be used in

terms of ambient temperature. Gas cooler outlet temperature was defined as the sum of ambient temperature and gas cooler approach temperature. Therefore, 12K approach temperature makes the gas cooler outlet temperature as 44.2°C. The cycle with this approach temperature behaves as same as the ideal cycle (0K approach temperature) at 44.2°C ambient temperature for modeling purposes. Therefore, the COP value here can also be used for determining the performance degradation by ambient temperature, which is 3.83% for 1K ambient temperature increase as an average value over the given range.

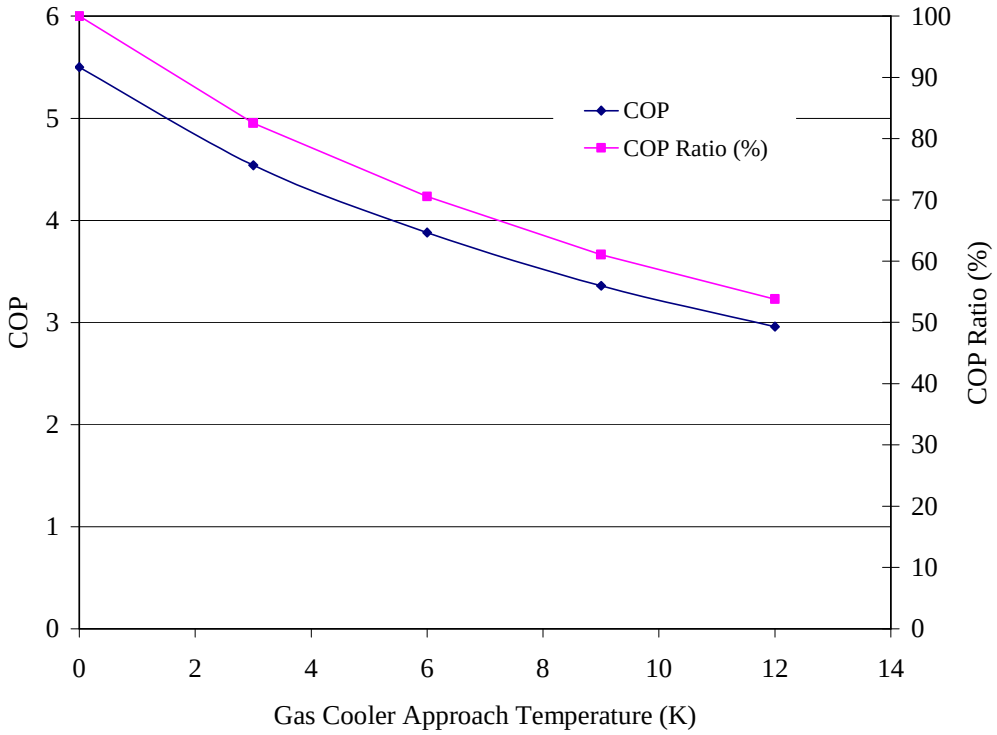

Figure 41: Effect of gas cooler approach temperature to COP

As described earlier, COP is the ratio of evaporator capacity to compressor power for the ideal case (fan power neglected). Therefore, it is important to investigate this degradation

in COP with evaporator capacity and compressor power. Figure 42 shows the change in evaporator capacity for increasing gas cooler approach temperature for 10 g/s refrigerant mass flow rate. Figure 43 shows the compressor power behavior within the same range of gas cooler approach temperature for the same refrigerant mass flow rate.

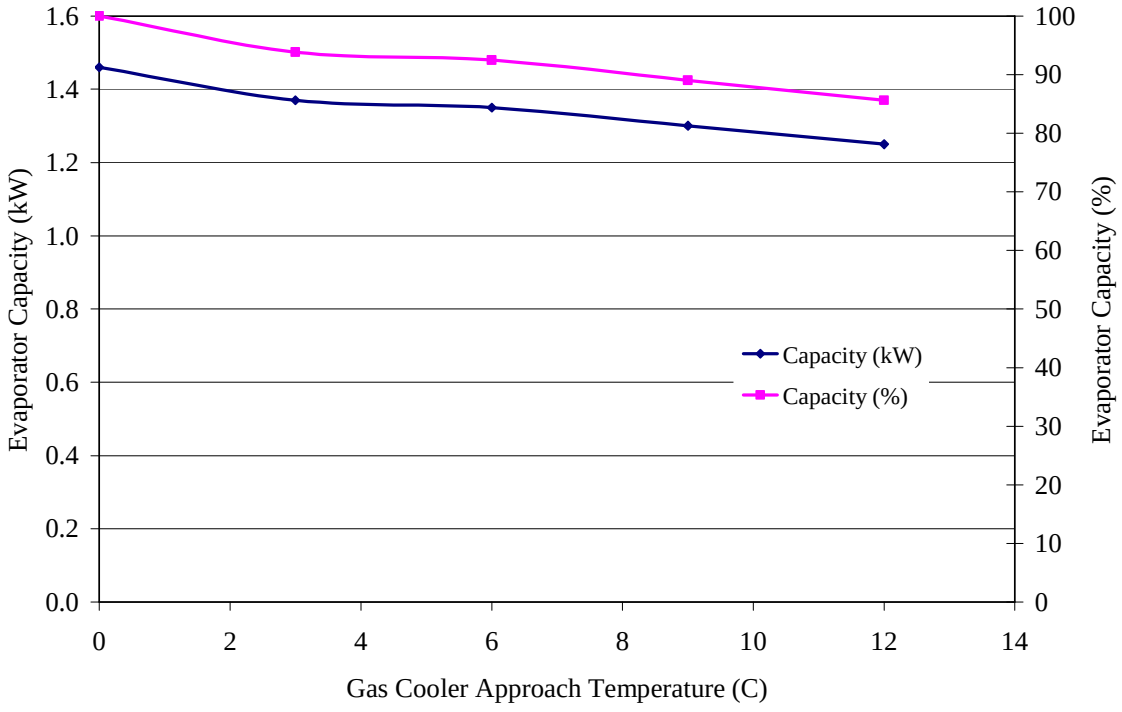

Figure 42: Effect of gas cooler approach temperature to the capacity

Within the given range of gas cooler approach temperature, evaporator capacity is decreasing by 14.4 % while compressor power is increasing by 55.6%. The decrease in evaporator capacity is because of higher gas cooler outlet and evaporator inlet temperatures. This will lead to lower evaporator capacities as given in Eq. 1 for the same refrigerant mass flow rate because the evaporator outlet enthalpy is kept constant.

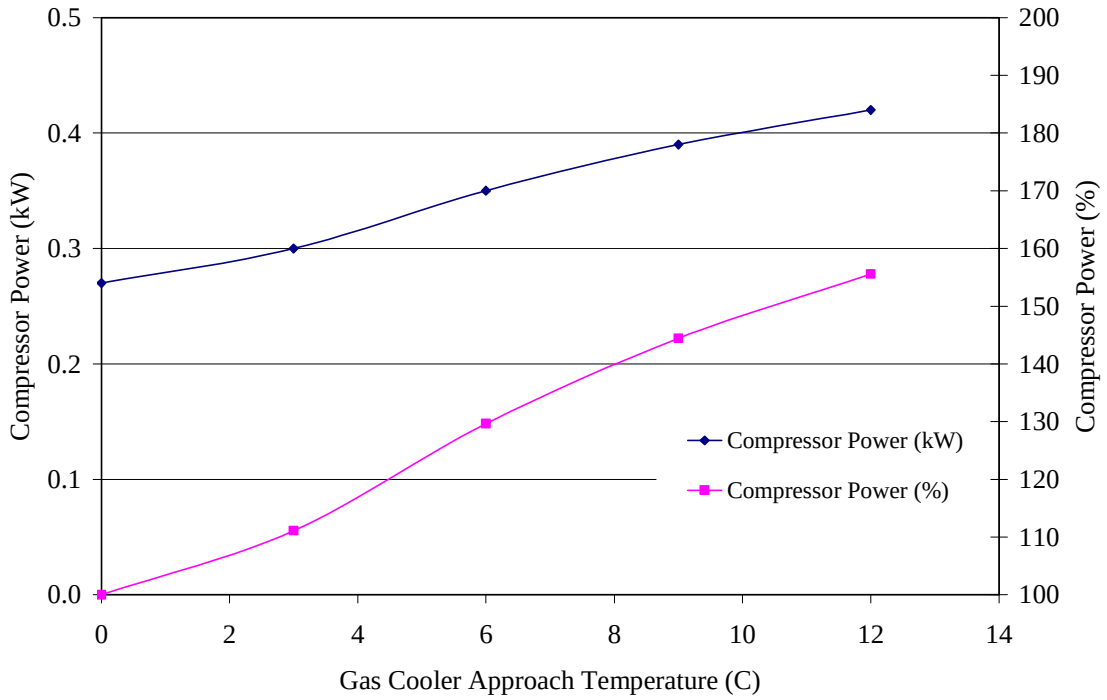

Figure 43: Effect of gas cooler approach temperature to the compressor power

However, the increase in compressor power is not directly related with gas cooler approach temperature. Figure 44 shows the enthalpy changes of CO_2 with temperature and pressure.

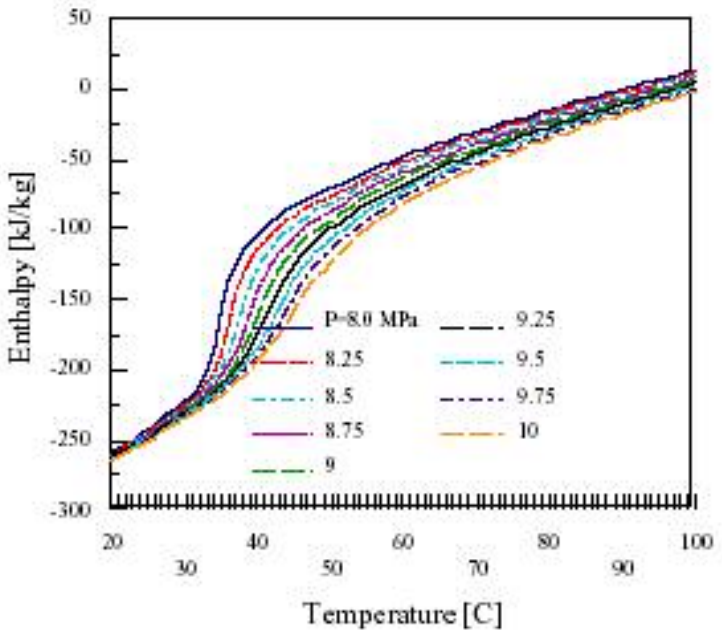

Figure 44: Enthalpy-pressure and temperature relationships for CO_2

For 3K approach temperature, which corresponds to 35.2°C gas cooler outlet temperature, increasing gas-cooling pressure will result in lower enthalpies. At the same pressure, if the refrigerant temperature increases or in other words gas cooler approach temperature increases, the refrigerant enthalpy will increase. This will cause the evaporator capacity to decrease. Therefore, the system has to optimize itself at a higher pressure to negate the effect of decreasing capacity. When the gas-cooling or compressor discharge pressure increases, since compressor suction is constant, compressor power will increase causing the COP to decrease. Therefore, the COP value at higher approach temperatures will be lower. Table 31 shows the capacity, compressor power and COP values at two different approach temperatures for 10 g/s refrigerant mass flow rate, which supports this argument.

Table 31: System performance at two different approach temperatures

	AT_{gc}=3K	AT_{gc}=6K
Optimum Pressure (MPa)	8.52	9.39
Optimum Capacity (kW)	1.37	1.35
Optimum Compressor Power (kW)	0.30	0.35
Optimum COP	4.54	3.88
Capacity at 7.8 MPa (kW)	1.37	0.92
Compressor Power at 8.52 MPa (kW)	0.30	0.30
COP at 8.52 MPa	4.54	3.05

As shown in this table, at higher approach temperature, if the system was kept at the same discharge pressure as 3K approach temperature case, then the compressor power would be the same, but the system capacity would be lower. Therefore, COP of the system would be lower.

Figure 45 shows the optimum gas cooler outlet pressures for each gas cooler approach temperatures. Optimum gas cooler outlet pressure curve shows a linear behavior with gas cooler approach temperature, which can be expressed as:

$$P_{gc,out,opt} = 0.2623 * AT_{GC} + 7.812 \quad (31)$$

In this equation $P_{gc,out,opt}$ is optimum gas cooler outlet pressure and AT_{GC} is gas cooler approach temperature.

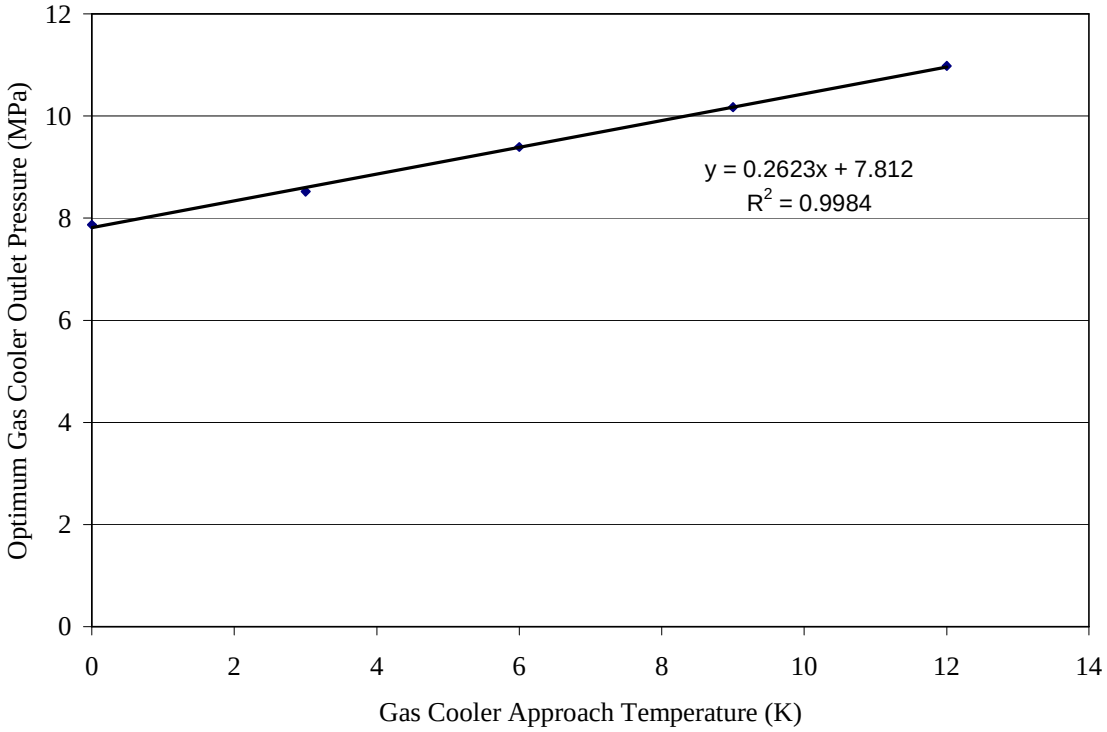

Figure 45: Optimum gas cooler outlet pressures for the baseline cycle

Note that, optimum discharge pressure can be found by adding gas cooler pressure drop to the optimum gas cooler outlet pressure given by Equation 31.

Next, the effect of gas cooler pressure drop to system performance was investigated. Figure 46 shows the effect of gas cooler pressure drop to system capacity and COP for optimum cases at 10 g/s refrigerant mass flow rate and ideal conditions. As seen from this figure, the system capacity remains constant. Because, there is an optimum pressure for the gas cooler outlet pressure, and the system will optimize itself at that pressure regardless of the gas cooler pressure drop. However, since optimum gas cooler outlet

pressure is same, increasing pressure drop will increase compressor discharge pressure. Therefore, the compressor power consumption will increase.

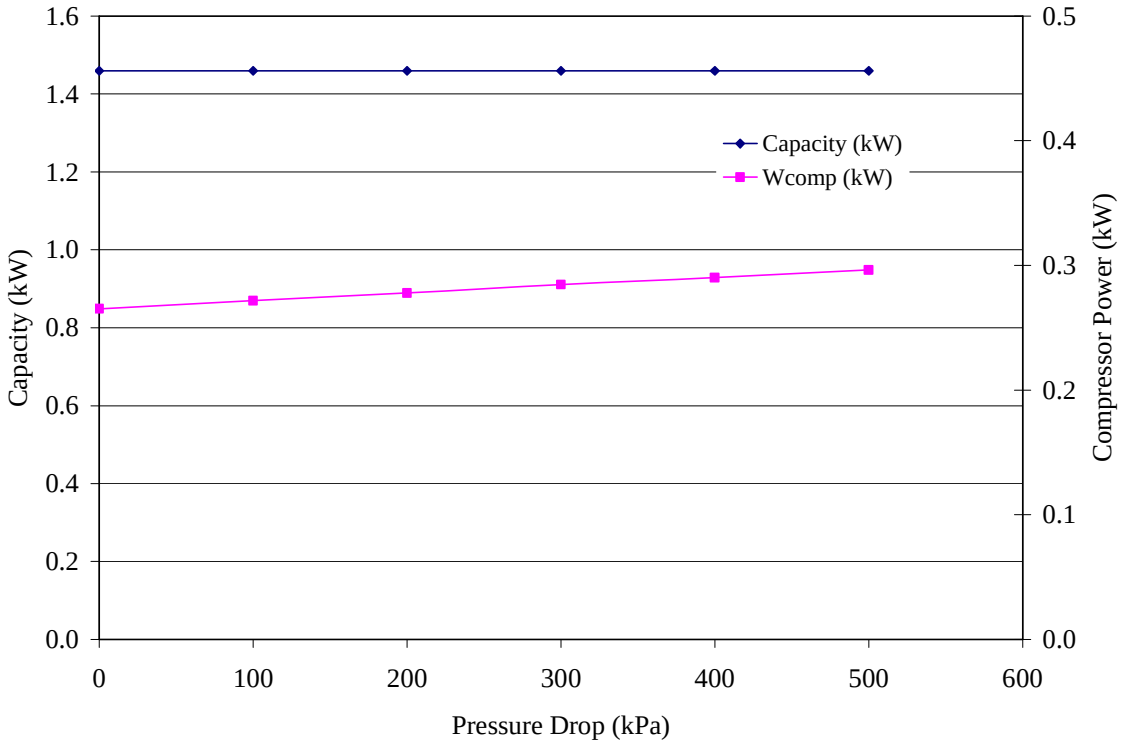

Figure 46: Effect of gas cooler pressure drop to capacity and compressor power

This figure also shows that compressor power is increasing by 10% when the pressure drop is 500 kPa instead of the ideal case. This means that compressor power increases by 2% as for each 100 kPa pressure drop at the gas cooler. Because of the definition of COP, this results a COP degradation of 2% for each 100 kPa pressure drop at the gas cooler. Compared with gas cooler approach temperature's effect on COP, gas cooler pressure drop has a smaller effect. Figure 47 shows the COP variation by gas cooler pressure drop for different gas cooler approach temperatures.

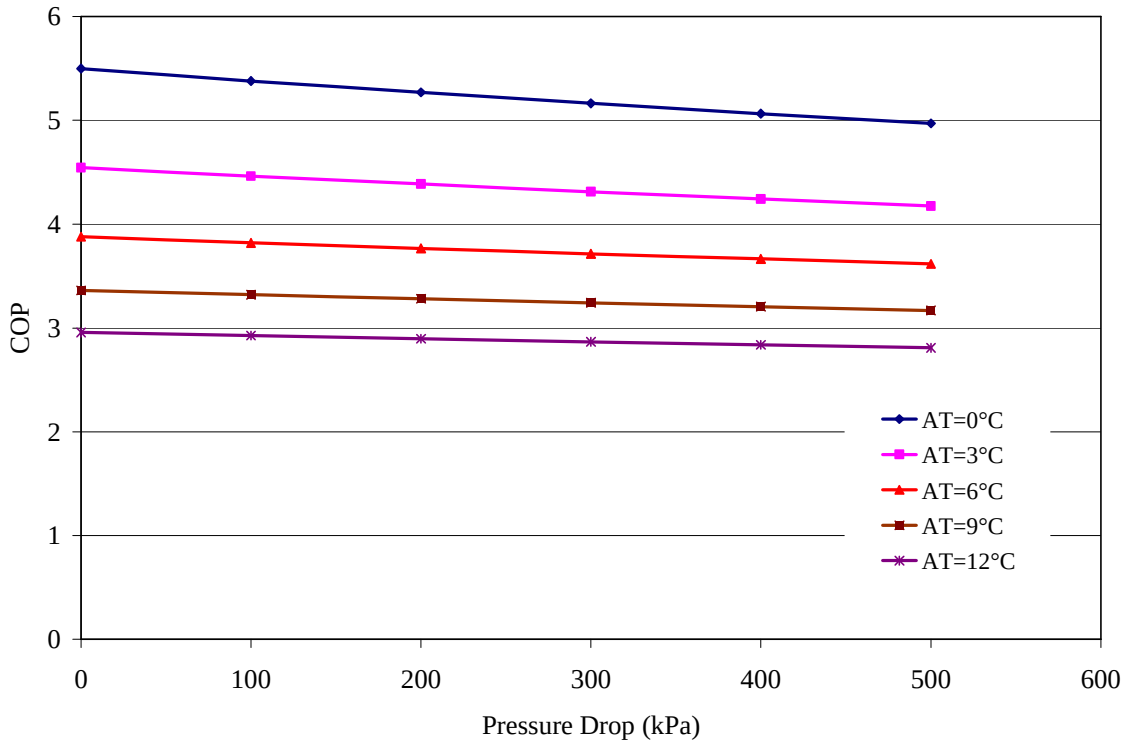

Figure 47: COP variation with gas cooler pressure drop and approach temperature

This figure shows that optimum COP decreases by 2% for each 100 kPa pressure drop at the gas cooler independent from gas cooler approach temperature.

Third variable that affects the system performance is compressor efficiency. If we neglect the interactions between compressor efficiency and other variables, then the optimum gas cooler outlet pressure and system capacity for varying compressor efficiencies are the same as ideal case. However, compressor power increases as given in Equation 12. Therefore, COP of the system decreases with decreasing compressor efficiency. Figure

48 shows the change in COP by the compressor efficiency at 10 g/s refrigerant mass flow rate and ideal case.

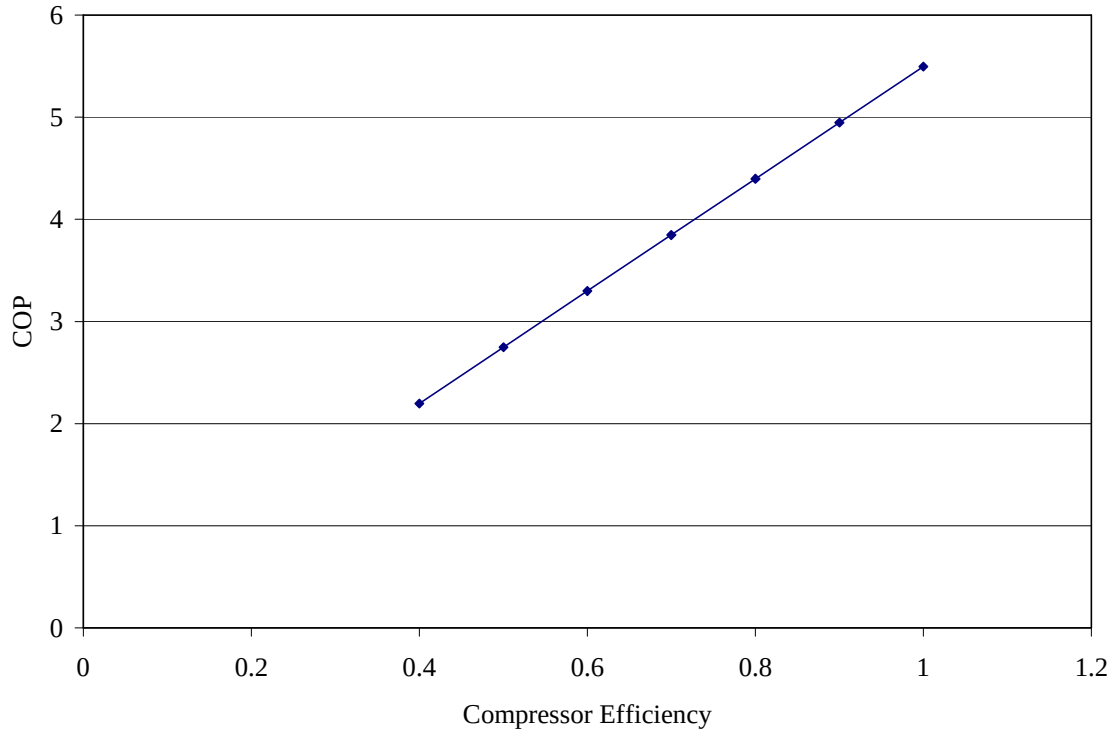

Figure 48: Effect of compressor efficiency to COP

Figure 48 shows the linear behavior of COP with compressor efficiency. However, in real cases, compressor efficiency interacts with pressure ratio as shown in Figure 49. As the pressure ratio increases, the compressor efficiency decreases which results in higher compressor power consumption and lower COP. Therefore, the system optimizes itself at a lower discharge pressure when this interaction is not neglected. For the same approach temperature, lower discharge pressure results less compression work and lower system capacity.

Following equation was obtained for compressor efficiency from the experimental data.

$$\eta_{comp} = -0.0361 * PR + 0.756 \qquad (32)$$

This equation is used for simulation of the baseline cycle to analyze the effect of the interaction between the compressor efficiency and the pressure ratio.

Figure 49 shows a comparison of constant and variable compressor efficiency cases for different gas cooler approach temperatures.

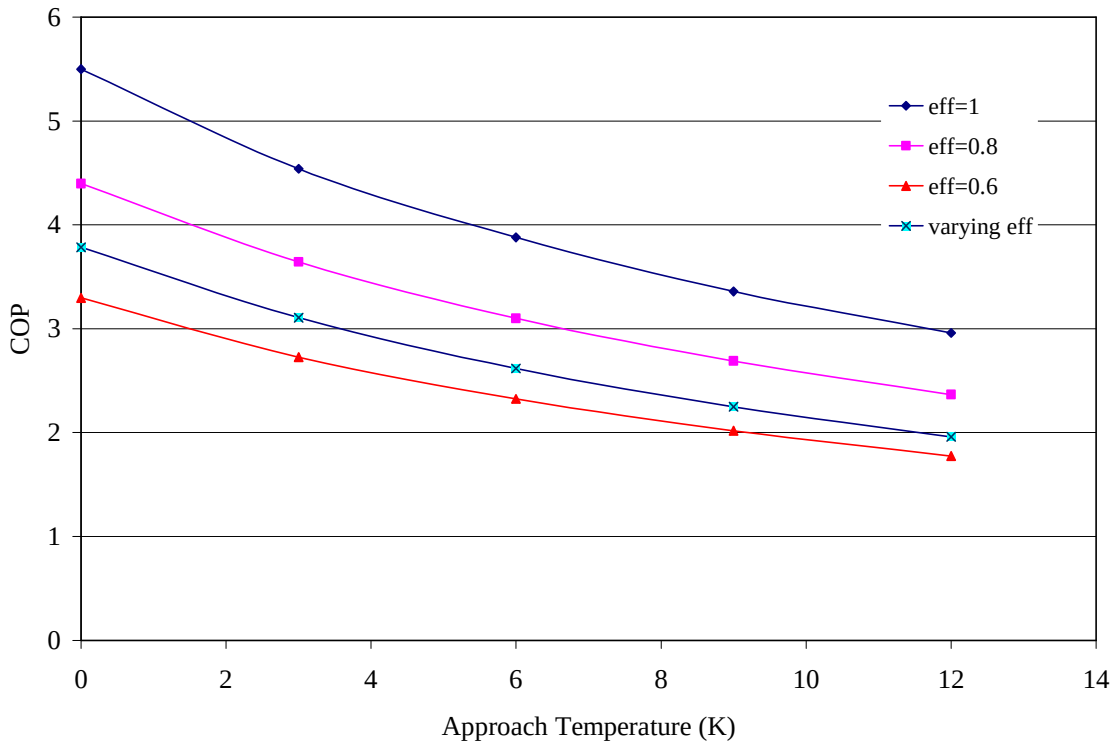

Figure 49: Effect of variable compressor efficiency to COP

As shown in this figure, there is a slight change in the COP curve pattern for variable

compressor efficiencies, which is because of lower optimum discharge pressures. Figure 50 shows the optimum discharge pressures for both constant and variable compressor efficiency cases.

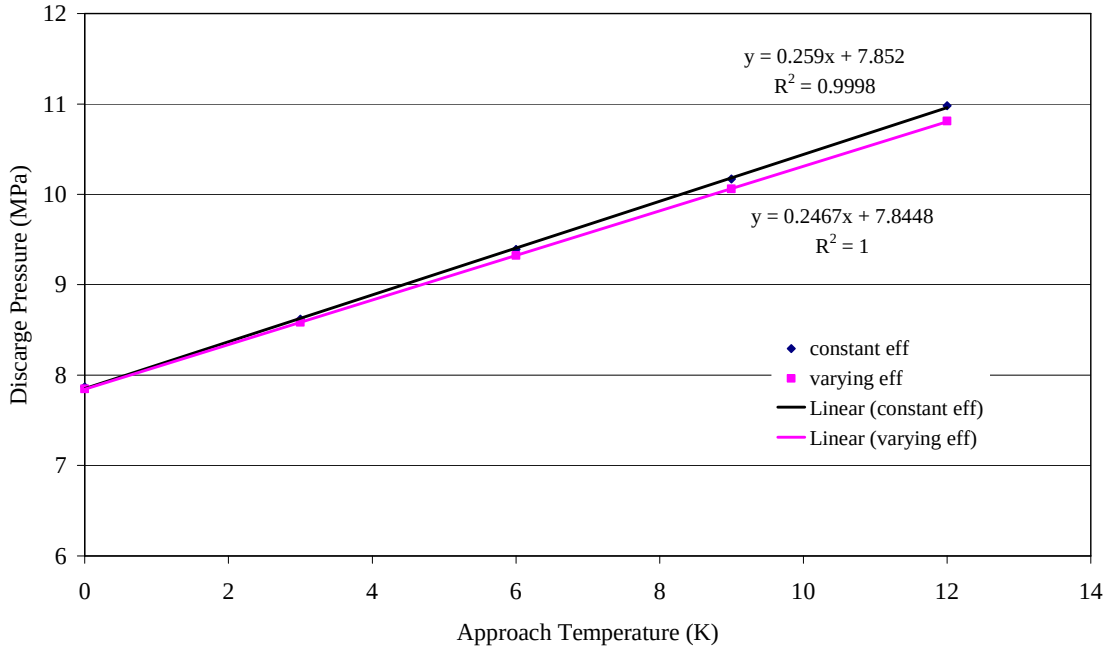

Figure 50: Effect of compressor efficiency to the optimum discharge presssure

For all approach temperatures, the optimum discharge pressure for constant compressor efficiency case is higher than the optimum discharge pressure for the variable compressor efficiency case. As the gas cooler approach temperature decreases, this difference becomes smaller because of the slope of the refrigerant enthalpy diagram shown in Figure 44 at lower discharge pressures.

Correlations can be written for baseline cycle for optimum discharge pressure.

For constant compressor efficiency case,

$$P_{dis,opt} = 0.259 * AT_{gc} + 7.852 \quad (33)$$

For variable efficiency case (experimental data),

$$P_{dis,opt} = 0.2467 * AT_{gc} + 7.8448 \quad (34)$$

Note that, these equations assume no pressure drop in the gas cooler. If pressure drop is also considered, then these equations give the gas cooler outlet pressure.

As discussed earlier, the maximum COP for the ideal baseline cycle is “5.5”. Compared with the actual refrigeration systems, this value might seem too high. However, this value doesn’t include the effect of the system parameters. For example, for a compression efficiency of “0.6”, the maximum COP drops to “3.3”. Also, it is found that the COP of the cycle at 12K gas cooler approach temperature becomes 54% of the ideal cycle. Therefore, for this value of gas cooler approach temperature, the COP becomes “1.78”. Finally, the COP decreases by 2% for each 100 kPa pressure drop at the gas cooler. Therefore, the COP of the system becomes “1.67” which is only 30% of the ideal COP with assuming a pressure drop of 300 kPa in addition to the above assumptions. Since the gas cooler is used for all CO_2 cycle options, the gas cooler approach temperature and pressure drop are also effective on COP for the other cycle options.

Experimental data and simulation results are compared in Table 32 for baseline cycle for the optimum discharge pressure of 11.4 MPa and gas cooler approach temperature of 17K. The actual displacement volumes of the compressor are used. The pressure and

temperature values are taken from Table 12, and these values are used for the thermodynamic calculation of the evaporator capacity. Compressor efficiency is found from Equation 32. Compressor power is calculated from the compressor suction and discharge temperatures, pressures and the compressor efficiency. Fan power is added to the COP calculation, which is obtained from Table 13.

Table 32: Comparison of experimental and simulation results for the baseline cycle

	Experimental Results	Simulation Results
P_{dis} (MPa)	11.4	11.4
Q_{evap} (kW)	1.96	2.01
W_{comp} (kW)	1.29	1.31
COP	1.42	1.43

The difference in evaporator capacity and compressor power is less than 2%. Optimum COP values differ by only 0.7%. This table shows that the experimental results match with the simulation results.

9.2 SLHX Cycle

The effect of SLHX efficiency to the system performance is investigated in this section. The highest efficiency with SLHX ideal cycle was 5.6, which was only 1% higher than that of baseline cycle. Figure 51 shows the COP values at various SLHX effectiveness values. As seen from this figure, increasing heat exchanger effectiveness has a positive influence on COP. However, this result is also related to the gas cooler approach temperature. For example, for the ideal case, the COP gain is only 1% while it is 6% at 12K approach temperature. As the approach temperature increases, the COP gain

becomes increasingly dependent upon the heat exchanger effectiveness. As the approach temperature increases, the temperature of the hot side inlet for the SLHX increases. This results in a larger enthalpy difference with the cold side. Thus, the effectiveness becomes important.

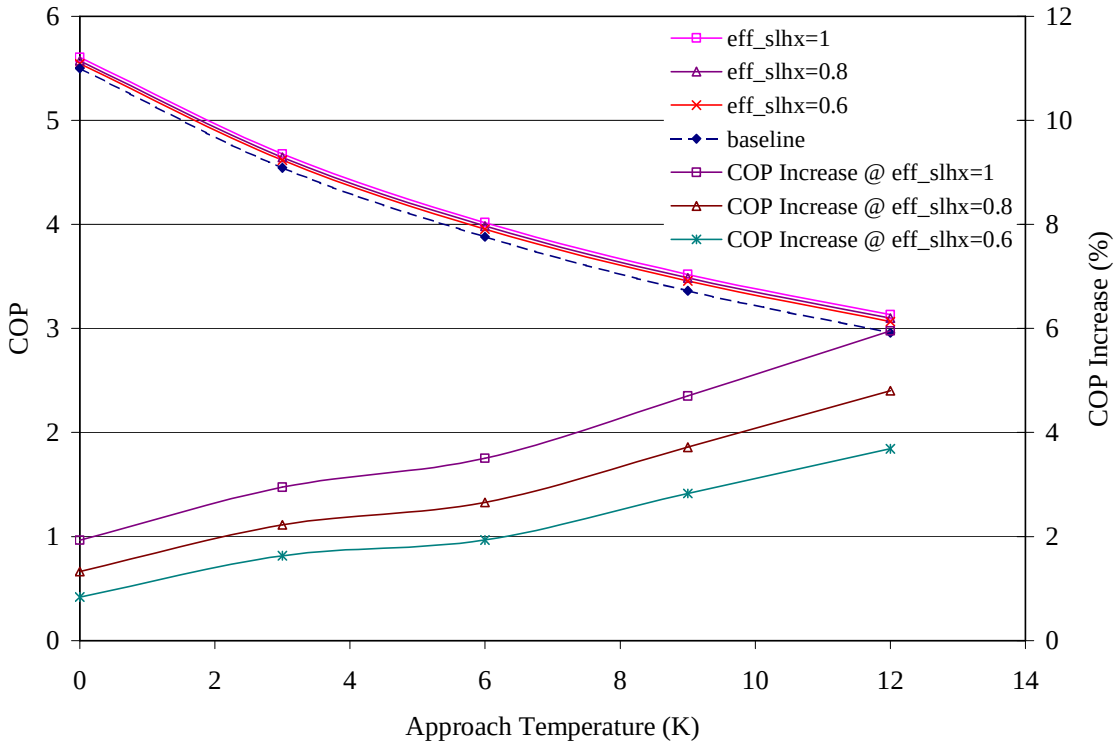

Figure 51: Effect of SLHX effectiveness to COP

The capacity of the system for baseline and SLHX cycles are compared as shown on Figure 52. The values are calculated for 10 g/s refrigerant mass flow rate. The system (evaporator) capacity for SLHX cycle is higher than baseline cycle due to the capacity increase by the SLHX. Similar to COP, the capacity gain increases with approach temperature and heat exchanger effectiveness.

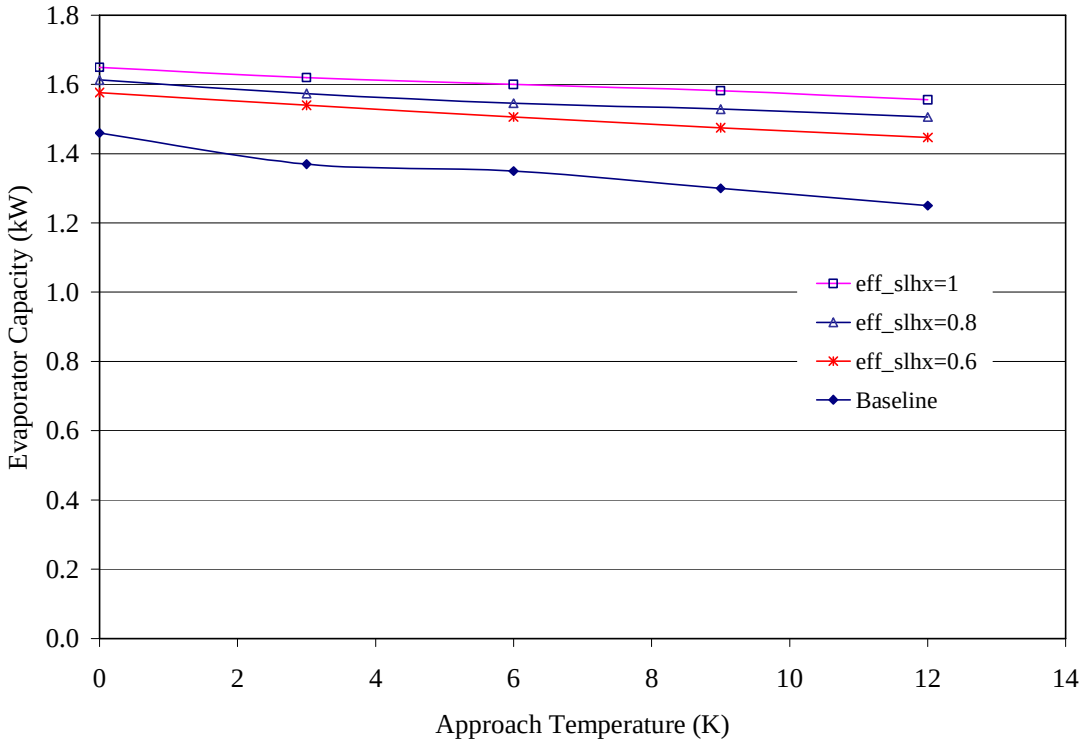

Figure 52: Effect of SLHX effectiveness to system capacity

Although the COP of the SLHX cycle is 6% higher than that of the baseline cycle at 12K gas cooler approach temperature, the capacity of the ideal SLHX cycle is 24.5% higher than that of the ideal baseline cycle. The COP gain is less for SLHX cycle because of greater compressor work requirement for higher suction and discharge temperatures. The required compressor power for the baseline and SLHX cycles are compared as shown in Figure 53. The values are calculated for 10 g/s refrigerant mass flow rate. The required compressor power for the ideal SLHX cycle is 19% higher than for the ideal baseline cycle at 12K gas cooler approach temperature.

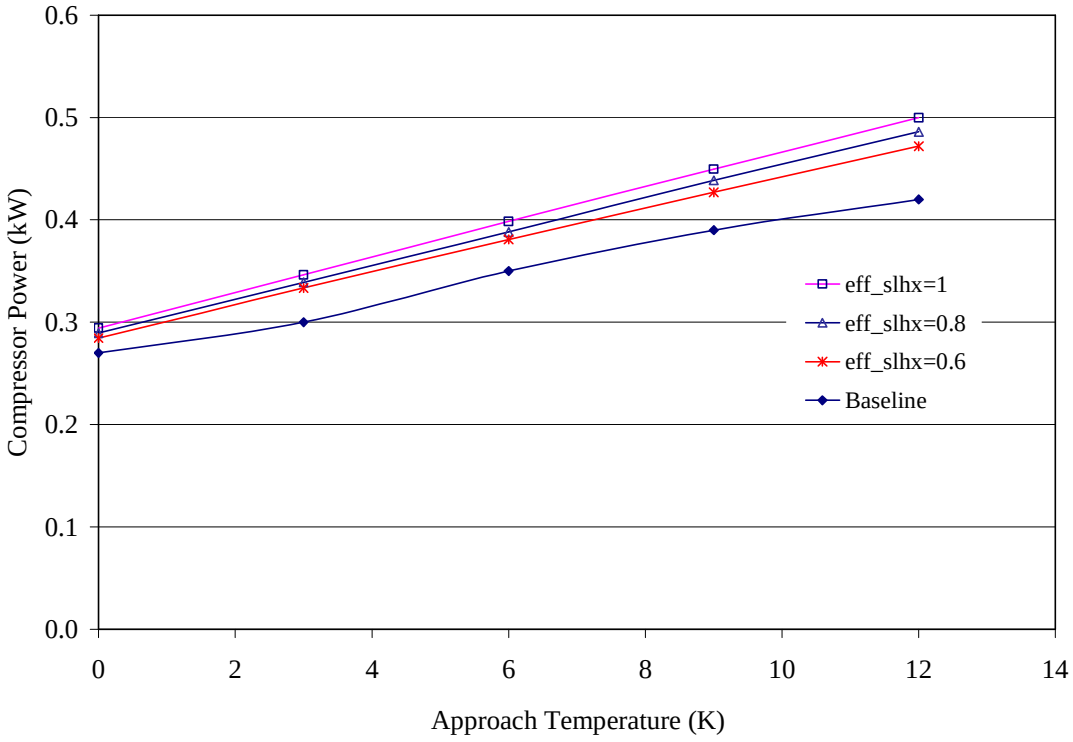

Figure 53: Effect of SLHX effectiveness to compressor power

Experimental data and simulation results are compared in Table 33 for the SLHX cycle for the optimum discharge pressure of 10.5 MPa and gas cooler approach temperature of 15.7K. The actual displacement volumes of the compressor are used. The pressure and temperature values are taken from Table 16, and these values are used for the thermodynamic calculation of the evaporator capacity. Compressor efficiency is found from Equation 32. Compressor power is calculated from the compressor suction and discharge temperatures, pressures and the compressor efficiency. Fan power is added to the COP calculation, which is obtained from Table 17.

Table 33: Comparison of experimental and simulation results for the SLHX cycle

	Experimental Results	Simulation Results
P_{dis} (MPa)	10.5	10.5
Q_{evap} (kW)	2.11	2.08
W_{comp} (kW)	1.17	1.19
COP	1.67	1.63

The difference in evaporator capacity and compressor power is less than 2%. Optimum COP values differ by only 2.5%. This table shows that the experimental results match with the simulation results.

9.3 Intercooler Cycle

Intercooler has two effects to the system performance. First, it is decreasing the discharge temperature by decreasing the suction temperature for the second stage compression. This decreases the compression work required for the second-stage, decreasing the total compression work. It is also indirectly increasing the system capacity. Since the intercooler cools down the refrigerant and the decreases the discharge temperature, the gas cooler can cool down the refrigerant to lower temperatures providing higher evaporator capacities. This effect is shown on P-h diagram in Figure 54.

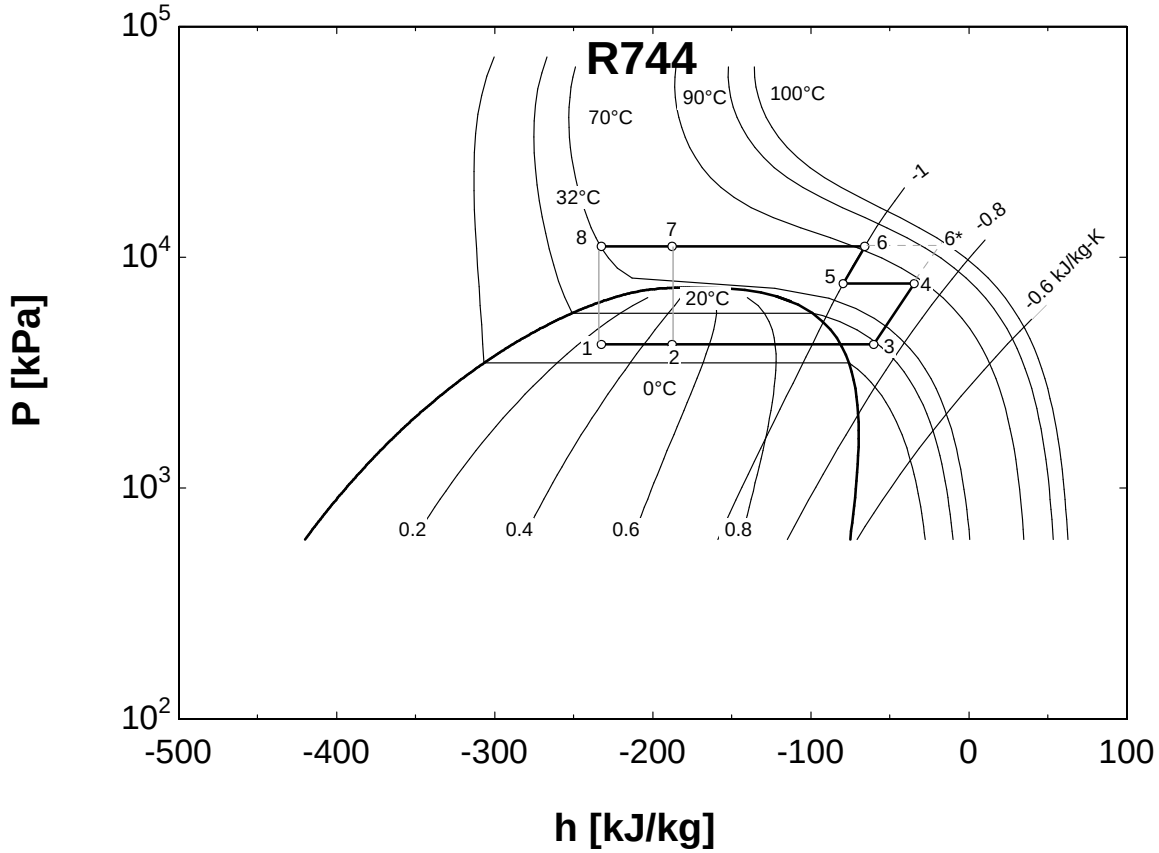

Figure 54: P-h diagram of ideal intercooler cycle

Similar to the gas cooler, approach temperatures are used for the intercooler cycle modeling. Two different modeling approaches are used for the intercooler. These are:

1. Using the same heat exchanger for the gas cooler as the baseline cycle and using a separate heat exchanger for the intercooler for extra cooling
2. Using part of the gas cooler as the intercooler for providing the same gas cooler approach temperature

The COP variation with intercooler and gas cooler approach temperatures with the first approach is given in Figure 55 (the other parameters are ideal).

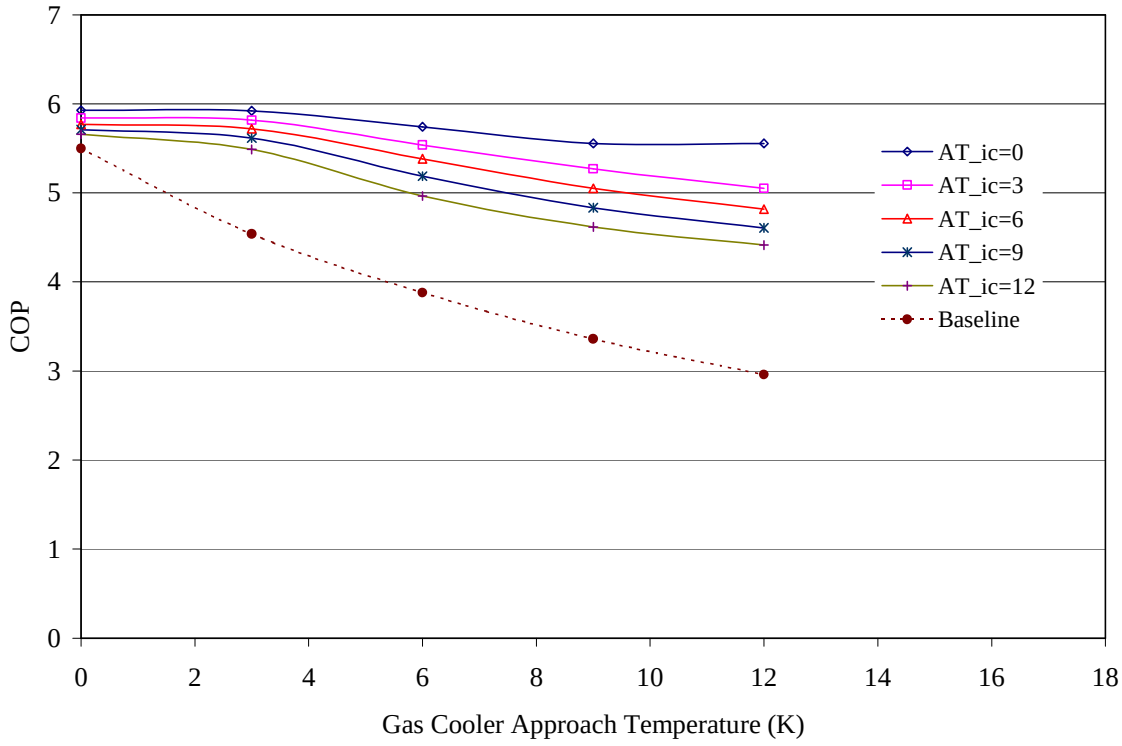

Figure 55: COP variation with gas cooler and intercooler approach temperatures

As shown in this figure, the ideal intercooler cycle has a COP of 5.95, which is 7.8% higher than ideal baseline cycle. Also, the COP degradation with increasing gas cooler approach temperature is not as fast as baseline cycle for intercooler cycle. Because, the intercooler is providing additional cooling where needed. Compared with ideal case, COP for 12K gas cooler approach temperature is lower by 6-22%, which is decreasing more for higher intercooler approach temperatures. Moreover, as the gas cooler approach temperature increases from 0K to 3K, the COP decreases by less than 1%. Thus, a smaller heat exchanger for either gas cooler or intercooler can be used for 3K approach temperature without affecting the COP significantly.

The COP variation with intercooler and gas cooler approach temperatures with the second method is given in Figure 56 (the other parameters are ideal). This figure shows that the maximum COP with the integrated gas cooler and intercooler design at the ideal conditions is the same as the first approach. This is because both approaches are the same at the ideal conditions. However, the COP degradation of intercooler cycle with increasing gas cooler approach temperature is faster than in the first approach. This is due to the fact that the same heat exchanger area is used for both intercooler and gas cooler instead of using additional heat exchanger area for the intercooler. Compared with ideal case, COP for 12K gas cooler approach temperature is lower by 30-41%. Moreover, as the gas cooler approach temperature increases from 0K to 3K, the COP decreases by 10-15%. Thus, use of a smaller heat exchanger cannot be justified as in the first design approach.

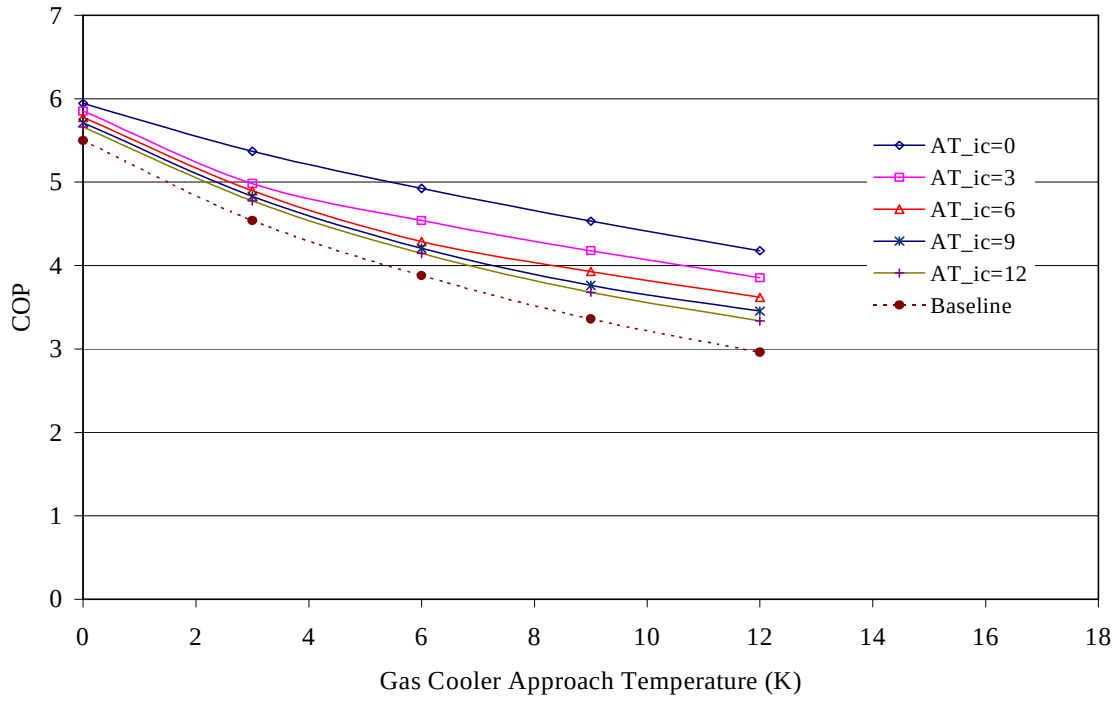

Figure 56: Results for 2nd approach of intercooler cycle modeling

Optimum discharge pressures for the intercooler cycle (no pressure drops) are shown in Figure 57.

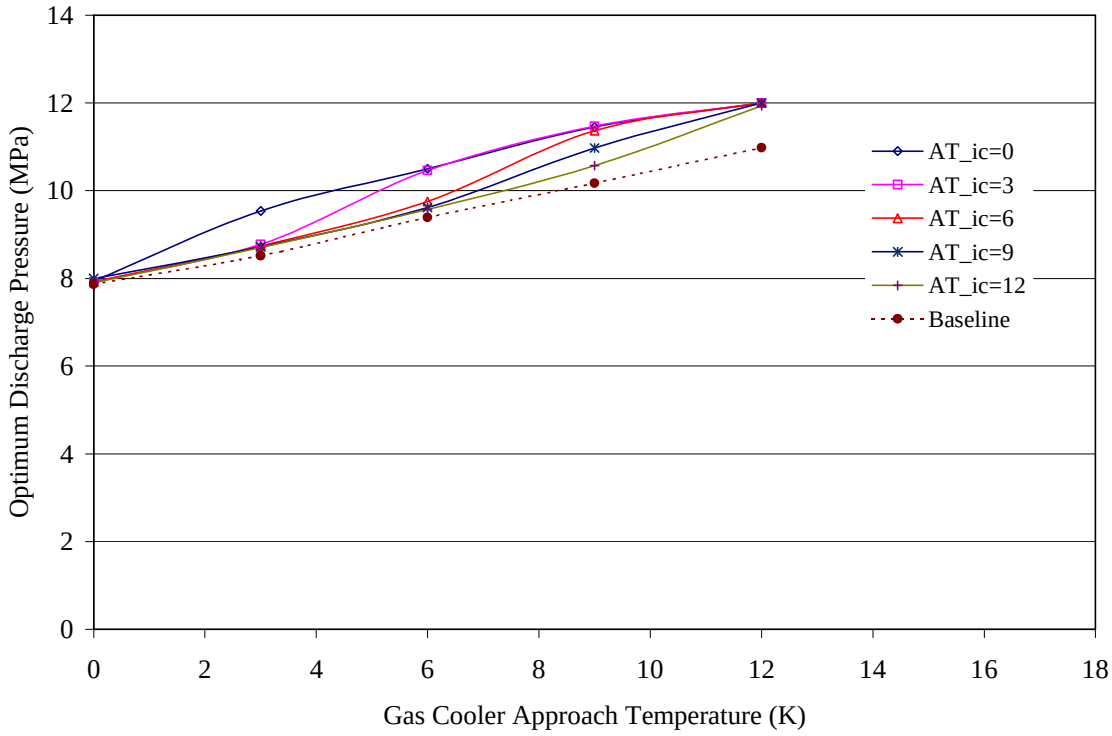

Figure 57: Optimum discharge pressures for the intercooler cycle

This figure shows that intercooler cycle optimizes itself at a higher discharge pressure than baseline cycle. Lower optimum discharge pressures are obtained with higher intercooler approach temperatures, while higher optimum discharge pressures are obtained with higher gas cooler approach temperatures.

As the gas cooler approach temperature increases, the capacity of the gas cooler decreases, while the capacity of the intercooler increases. This is shown in Figure 58 for intercooler approach temperature of 9K and at 10 g/s refrigerant mass flow rate. In this figure, gas cooler capacity (%) is the ratio of the gas cooler capacity to the total capacity of the gas cooler and intercooler.

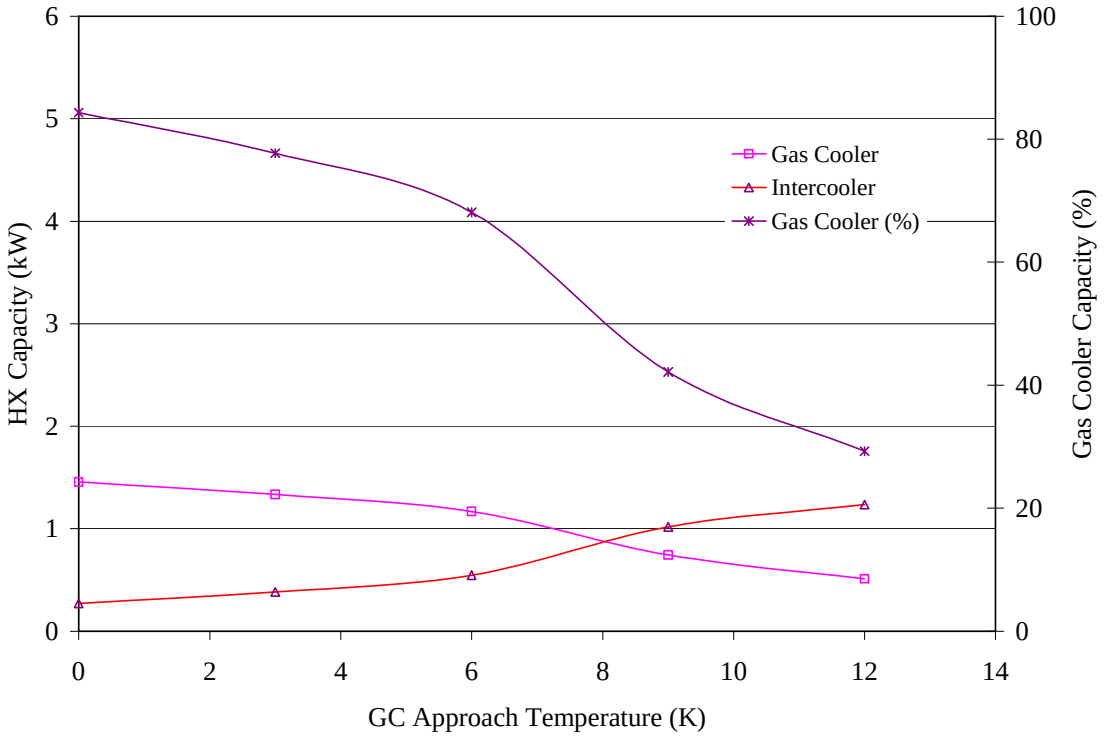

Figure 58: Required heat exchanger capacities for AT_{ic}=0K

The effect of intercooler approach temperature upon the gas cooler capacity (%) is shown in Figure 59. As the intercooler approach temperature increases, the gas cooler becomes dominant and the percentage of gas cooler capacity increases. Moreover, the intercooler capacity becomes as same as the gas cooler capacity at higher gas cooler approach temperatures. This figure can be used for designing an optimum integrated heat exchanger under the desired conditions.

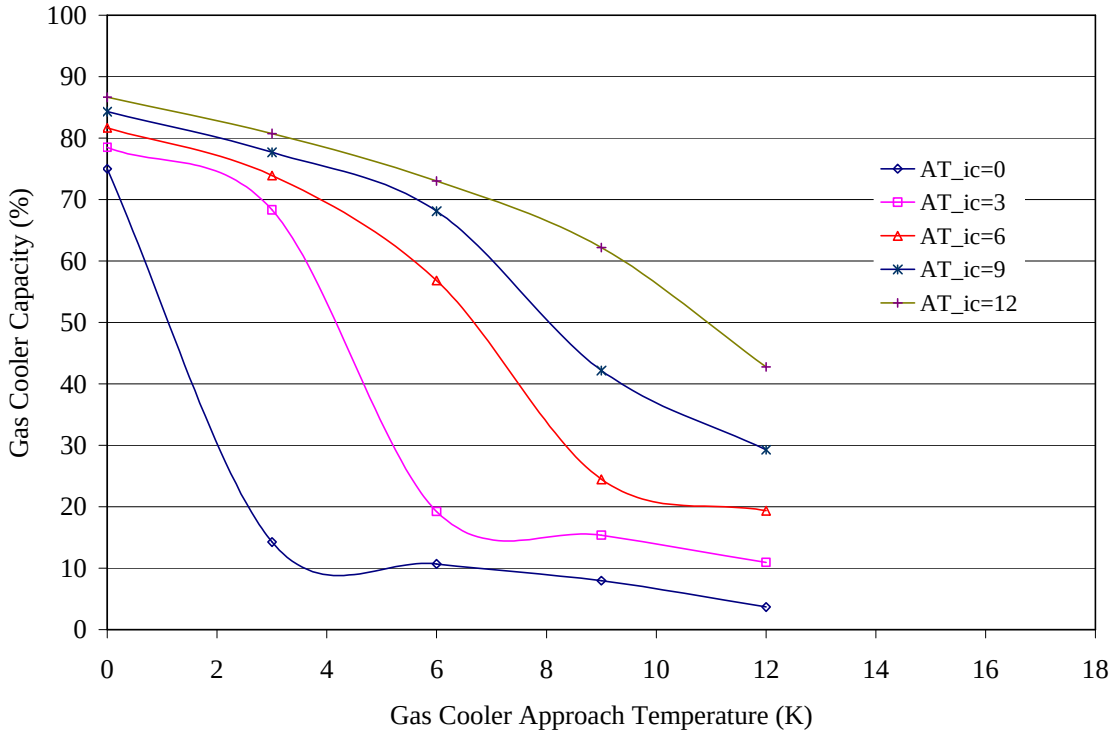

Figure 59: Required gas cooler capacity ratios for the intercooler cycle

Experimental data and simulation results are compared in Table 34 for the intercooler cycle for the optimum discharge pressure of 11.4 MPa and gas cooler approach temperature of 15.7K. The actual displacement volumes of the compressor are used. The pressure and temperature values are taken from Table 20, and these values are used for the thermodynamic calculation of the evaporator capacity. Compressor efficiency is found from Equation 32. Compressor power is calculated from the compressor suction and discharge temperatures, pressures and the compressor efficiency. Fan power is added to the COP calculation, which is obtained from Table 21.

Table 34: Comparison of experimental and simulation results for the intercooler cycle

	Experimental Results	Simulation Results
P_{dis} (MPa)	11.4	11.4
Q_{evap} (kW)	2.44	2.42
W_{comp} (kW)	1.26	1.22
COP	1.76	1.79

The difference in evaporator capacity and compressor power is less than 2%. Optimum COP values differ by only 1.7%. This table shows that the experimental results match with the simulation results.

9.4 Split Cycle

Modeling of the split cycle is much more complicated than the modeling of the other cycles because of the number of heat exchangers and interactions between them. Split cycle can be thought simply as the addition of sub cycle to the intercooler cycle. However, there is an interaction between the sub cycle and the intercooler, because the sub cycle is controlling the intermediate pressure, which is an input parameter for the intercooler. Therefore, it is affecting the performance of the intercooler.

The internal heat exchanger (IHX) is modeled first. There are two major differences between SLHX and IHX. First, SLHX operates between the low and high side pressures, while IHX operates between the intermediate and high side pressures. The second difference is that, the intermediate pressure of the cycle varies for the IHX by the effect of secondary expansion valve on the sub cycle while SLHX works with constant

intermediate pressure at the same discharge pressure.

Heat exchanger effectiveness is used as a variable for IHX performance similar to the SLHX. However, as shown in Figure 37, the cold side inlet of the IHX can be at subcritical or supercritical state. Therefore, the effectiveness equations (Eq. 5-8) can only be used if only that point is in the supercritical region. If the cold side inlet is in the subcritical region, then the effectiveness equations should be changed to provide a fair comparison. Effectiveness calculated by the enthalpy values is much more accurate in this region.

For the subcritical region, the effectiveness of the IHX is calculated from:

$$\varepsilon = \frac{h_{co} - h_{ci}}{h_{co,ideal} - h_{ci}} \tag{40}$$

In this equation;

h_{co}: Refrigerant enthalpy at the cold side outlet (mixer inlet, kJ/kg)

h_{ci}: Refrigerant enthalpy at the cold side inlet (expansion valve outlet, kJ/kg)

$h_{co,ideal}$: Ideal or maximum refrigerant enthalpy at the cold side outlet (kJ/kg)

For the ideal case, refrigerant temperature at the cold side outlet can reach the refrigerant temperature at the hot side inlet. Therefore, ideal refrigerant enthalpy at the cold side outlet can be calculated by EES at that temperature and at the optimized pressure.

The intermediate pressure is also optimized for the maximum COP. Unlike other cycles, it is not related directly to the discharge pressure in the split cycle. Therefore, it is not

possible to directly determine the optimum displacement volume ratio for the split cycle.

Split cycle has one more independent variable than the other cycles. This variable is the mass flow rate of the sub cycle. At a fixed effectiveness of the IHX, an increased mass flow rate will increase the capacity of the IHX and thus the COP of the system. Therefore, any optimization of the displacement volumes leads to infinite displacement volumes. To solve this problem, either the IHX capacity or the refrigerant condition exiting the IHX can be fixed. Fixing the IHX capacity is not providing a good comparison for different evaporator capacities. Therefore, the refrigerant condition at the IHX outlet is fixed for modeling the split cycle. Moreover, the cooling capacity of the two-stage split CO_2 cycle is set same as the intercooler cycle.

The optimum intermediate and discharge pressures for both cycles are shown in Figure 60. The optimum discharge pressures for both the intercooler cycle and two-stage split cycle are increasing with the gas cooler approach temperature. However, the intercooler cycle has higher optimum discharge pressures than the two-stage split cycle for all values of gas cooler approach temperature. The difference in optimum discharge pressures between these two cycles reaches 2 MPa for 12K of gas cooler approach temperature. Both cycles have the same optimum intermediate pressure values above 3K of gas cooler approach temperature.

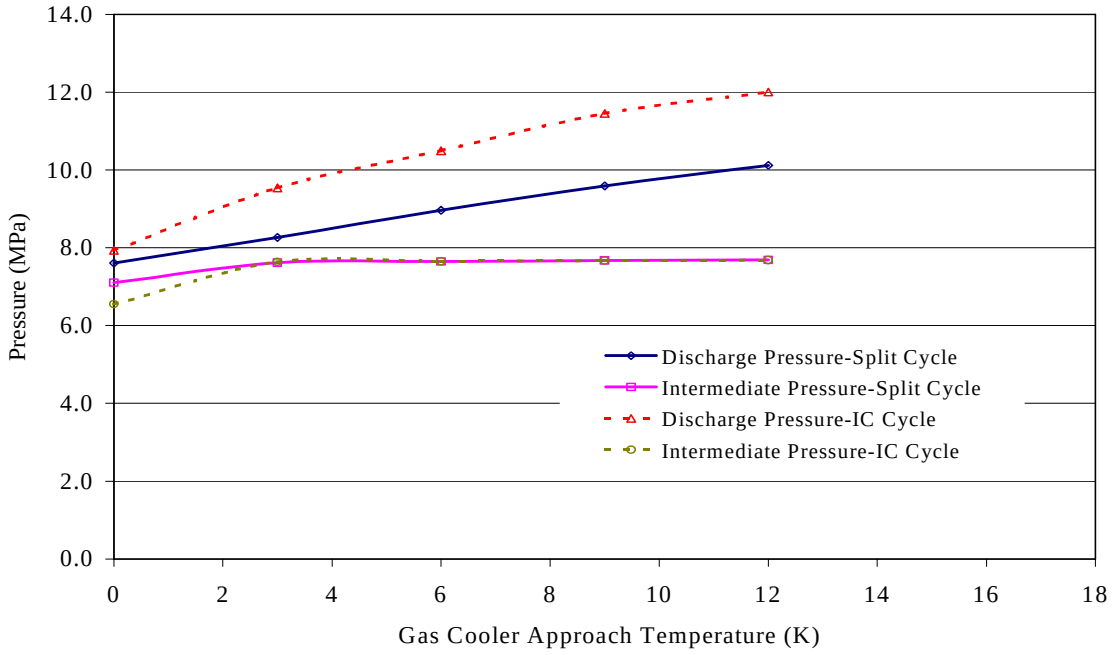

Figure 60: Comparison of optimum pressures for intercooler and split cycles

The compressor power consumption of the split cycle is less than the intercooler cycle because of the lower optimum discharge pressures. Therefore, the COP of the split cycle is higher than the intercooler cycle at all gas cooler approach temperatures as shown in Figure 61.

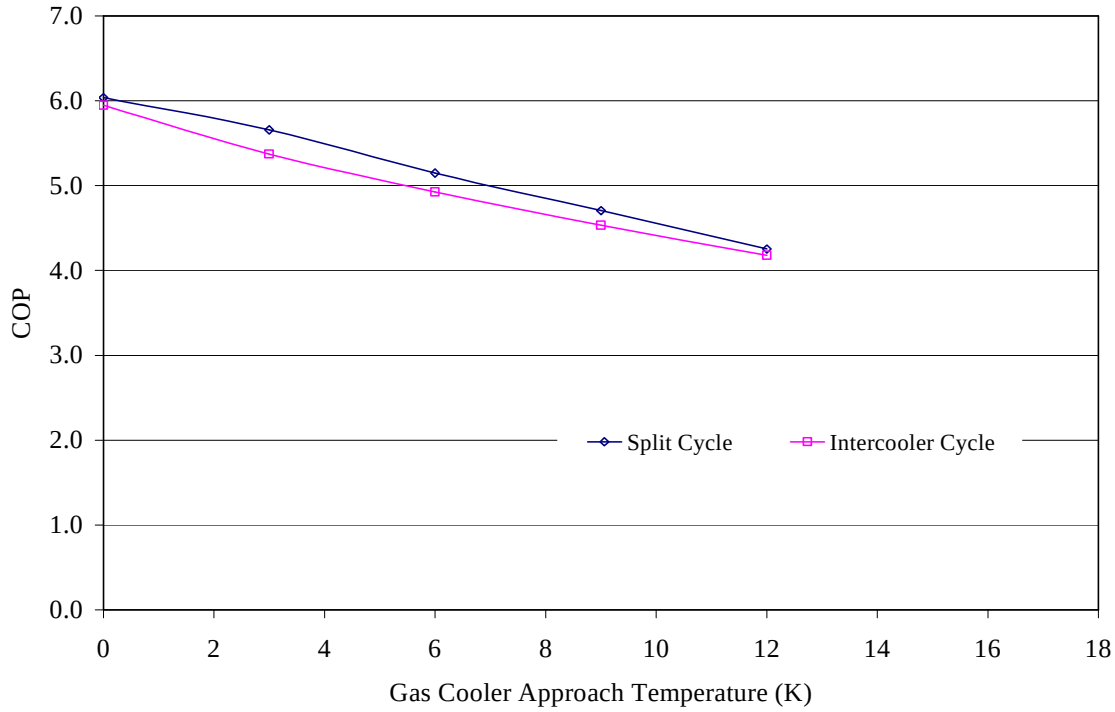

Figure 61: Comparison of COP values for intercooler and split cycles

Effectiveness of the internal heat exchanger and the compressor efficiency influence the COP as shown in Figure 62. Similar to the baseline cycle, the compressor efficiency has a dominant effect on the system COP. The effectiveness of the IHX does not have a significant effect on COP at the optimum conditions.

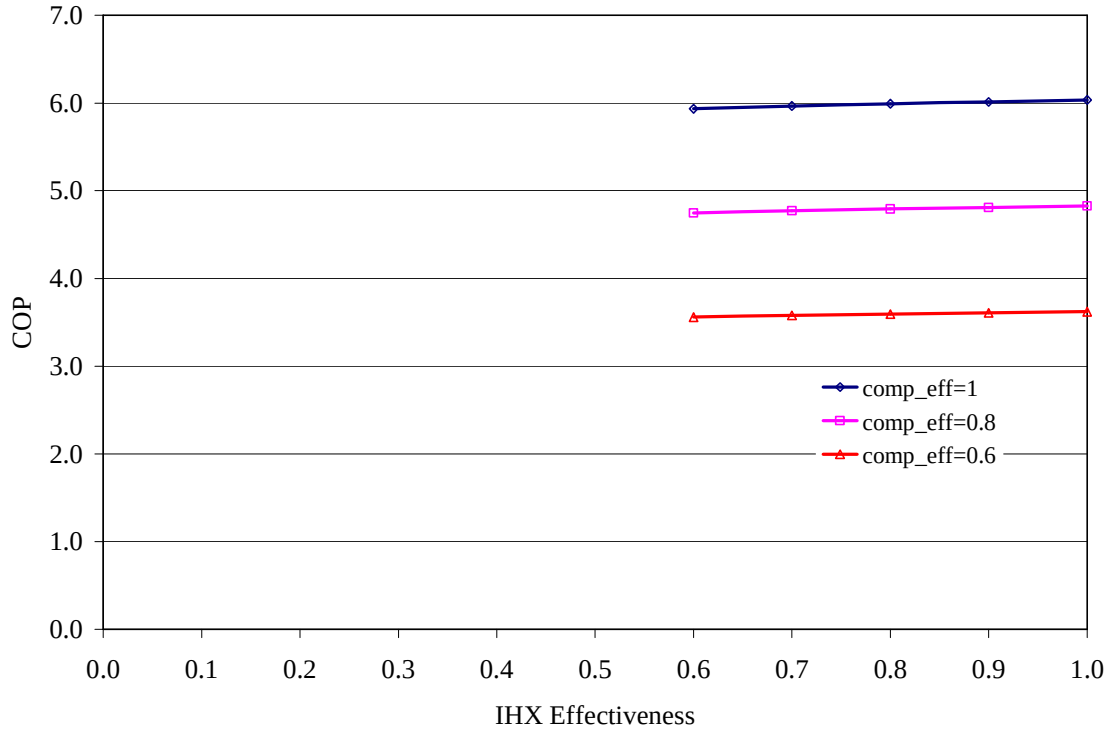

Figure 62: Effect of internal heat exchanger effectiveness on COP for the split cycle

Experimental data and simulation results are compared in Table 35 for the split cycle for the optimum discharge pressure of 10.2 MPa and gas cooler approach temperature of 12.8K. The actual displacement volumes of the compressor are used. The pressure and temperature values are taken from Table 24, and these values are used for the thermodynamic calculation of the evaporator capacity. Compressor efficiency is found from Equation 32. Compressor power is calculated from the compressor suction and discharge temperatures, pressures and the compressor efficiency. Fan power is added to the COP calculation.

Table 35: Comparison of experimental and simulation results for the intercooler cycle

	Experimental Results	Simulation Results
P_{dis} (MPa)	10.2	10.2
P_{int} (MPa)	8.57	8.52
Q_{evap} (kW)	2.43	2.42
W_{comp} (kW)	1.18	1.17
COP	1.86	1.87

This table shows that an optimum COP of 1.87 can be obtained instead of 1.86 at an intermediate pressure of “8.52 MPa” instead of “8.57 MPa”.

The difference in evaporator capacity and compressor power is less than 1%. Optimum COP values differ by only 0.5%. This table shows that the experimental results match with the simulation results.

10 Conclusions

The performance of four CO_2 cycles was tested for three different evaporating temperatures, 7.2, -6.7, and -23.3°C under the ARI Standard 520 for the condensing units. Four cycle options were the baseline cycle, the cycle with SLHX, the cycle with intercooler, and the two-stage split cycle. The compressor used in testing was a hermetic, rotary type two-stage compressor. Based on experimental results, the following conclusions are obtained.

- SLHX works better under the condition 1 (evaporator outlet 18.3°C) than under the condition 2 (suction 18.3°C) because of the additional cooling by the SLHX.
- Cycle with SLHX, intercooler and two-stage split cycle improve the COP by 18, 24 and 31% over the baseline CO_2 cycle under the test condition A. The improvement in COP by the SLHX cycle is a result of additional cooling provided directly by the SLHX. The improvement in COP by the intercooler cycle is a result of an indirect cooling effect of the intercooler while the split cycle also benefits from an additional internal heat exchanger.
- Cycle with intercooler and two-stage split cycle improve the COP by 10 and 40% over the baseline CO_2 cycle under the test condition B.
- Cycle with SLHX decreases the optimum discharge pressure where the COP is a maximum. However, this cycle option increases the optimum discharge temperature.
- Cycle with intercooler decreases the optimum discharge temperature, but has no effect on optimum discharge pressure.
- Split cycle decreases both the optimum discharge pressure and temperature by the

combined effect of the intercooler and additional refrigerant mass flow rate.

- Split cycle option allows operation at lower evaporating temperatures by decreasing the discharge temperatures.
- Two-stage CO_2 split cycle can compete with conventional condensing units.
- Volumetric efficiencies and compressor efficiencies are 0.80 to 0.95 and 0.55 to 0.70, respectively.
- The work required for first stage compression is significantly higher than the work required for second stage compression.
- Optimum intermediate pressure for Split CO_2 cycle is 30-50% higher than GMP.
- Gas cooler approach temperature and the compressor efficiency are the most important parameters for CO_2 system modeling and design.

Based on cycle modeling, the following conclusions are obtained.

- As the gas cooler approach temperature increases, the intercooler approach temperature becomes an important factor on COP.
- 3.83% degradation in COP for 1K of gas cooler approach temperature increase
- 2.4% degradation in COP for each 100 kPa of pressure drop at the gas cooler
- Increased capacity with SLHX cycle compared with baseline cycle
- The optimum intermediate pressures are same for the split and the IC cycles above 3K approach temperature
- Split cycle provides lower optimum discharge pressures than the intercooler cycle

11 Future Work

Recommended future work as the continuation of this study is listed below:

- Split cycle modeling and testing with SLHX
- Performing tests at different evaporator capacities or compressor sizes
- Designing the split cycle with integrated intercooler and gas cooler
- Optimizing the heat exchangers for the maximum COP
- More detailed analysis on cycle behaviors
- Investigating other cycle options such as flash cycle or split cycle with IHX and SLHX (without intercooler)
- Providing suggestions for system design at lower evaporating temperatures

12 Uncertainty Analysis

The uncertainty of these experiments was determined using the Pythagorean summation of the discrete uncertainties as shown in Equation 41.

$$u_f = \sqrt{\left(u_{x1} \cdot \frac{\partial f}{\partial x1}\right)^2 + \left(u_{x2} \cdot \frac{\partial f}{\partial x2}\right)^2 + ... + \left(u_{xn} \cdot \frac{\partial f}{\partial xn}\right)^2} \quad (41)$$

where

u_f: The overall uncertainty of function f resulting from individual uncertainties of $x_i..x_n$

x_i: Nominal values of variables

u_{xi}: Discrete uncertainties

The system capacity was calculated from Equations 1 and 3, which provided results for thermodynamic capacity and electrical heater capacity. Therefore, the sources of error for these two methods are investigated.

For the thermodynamic capacity, sources of error have been identified which are listed below:

- Pressure Measurement Errors
- Temperature Measurement Errors
- Mass Flow Rate Measurement Error

For the electrical heater capacity, sources of error have been identified which are listed

below:

- Time Measurement Errors
- Watt-hour Meter Measurement Errors

For the measurement of COP, both of these methods have also:

- Compressor Power Measurement (Wattmeter) Errors
- Fan Power Measurement (Wattmeter) Errors

The uncertainty associated with capacity and COP of the system is listed in Table 35.

Table 36: Estimated uncertainties of characteristic parameters

Parameter	Thermodynamic	Electrical heater
Capacity	± 2.89%	± 0.29%
COP	± 2.90%	± 0.35%

This table shows that the capacity and COP measurement by the electrical heaters provides an opportunity to improve the uncertainties in these parameters. The maximum difference between these two methods was 4% for all test conditions, cycle options and refrigerant charges.

13 References

Aarlien R. and Frivik P.E., 1998, "Comparison of Practical Performance Between CO_2 and R-22 Reversible Heat Pumps for Residential Use", *Preprints of Natural Working Fluids '98, IIR -Gustav Lorentzen Conference*, Oslo, Norway, pp. 341-350.

Air-Conditioning and Refrigeration Institute, 1997, Standard for Positive Displacement Condensing Units, ANSI/ARI Standard 520.

Allied Signal Chemicals, 1999, Genetron AZ-20 Product Brochure.

ASHRAE Handbook of HVAC Systems and Equipments, I-P 2000, Compressors, Chapter 34, pp. 34.9-34.11

Baek, J.S., Groll, E.A., and Lawless, P.B., 2002, "Effect of Pressure Ratios Across Compressors on the Performance of Transcritical Carbon Dioxide Cycle with Two Stage Compression and Intercooling", *Proceedings of the 5th IIR-Gustav Lorentzen Conference on Natural Working Fluids at Purdue.*

Bodinus. W.S. 1999, "The Rise and Fall of Carbon Dioxide Systems", ASHRAE Journal, Vol. 41, No. 4 (April). pp. 37-42.

Connaghan, M., 2002, "Experimental Investigation of a Breadboard Model of a Carbon Dioxide U.S. Army Environmental Control Unit", *Proceedings of the 5th IIR-Gustav Lorentzen Conference on Natural Working Fluids at Purdue*.

EES Manual for Microsoft Windows Operating Systems, 2004, Commercial and Professional Versions, F-chart Software, http://www.fchart.com

Fagerli, B.E., 1997, "CO_2 Compressor Development," Proc. IEA Heat Pump Centre/IIR Workshop on CO_2 Technology in Refrigeration, Heat Pump & Air Conditioning Systems, Trondheim, Norway, May 13-14.

Fagerli, B.E., 1996, "An Investigation of Possibilities for CO_2 Compression in a Hermetic Compressor," Proc. IIR Conf., Applications for Natural Refrigerants, Aarhus, Denmark, Sept. 3-6, pp. 639-649.

Fagerli, B.E., 1996, "Development and Experiences with a Hermetic CO_2 Compressor", Proc. 1996 Int. Compressor Eng. Conf. at Purdue, West Lafayette, IN, July 23-26, pp. 229-235.

Hafner A., Pettersen J., Skaugen G., and Nekså P., 1998, "An Automobile HVAC System with CO_2 as the Refrigerant", *Preprints of Natural Working Fluids '98, IIR - Gustav Lorentzen Conference*, Oslo, Norway, pp. 289-298.

Hirao T., Mizukami H., Takeuchi M., Taniguchi M., 2000, "Development of Air Conditioning System Using CO_2 for Automobile", *Preliminary Proceedings of the 4th IIR-Gustav Lorentzen Conference on Natural Working Fluids at Purdue*, pp. 193-200.

Hwang Y. and Radermacher R., 1998, "Experimental Evaluation of CO_2 Water Heater", *Preprints of Natural Working Fluids '98, IIR - Gustav Lorentzen Conferenc*e, Oslo, Norway, pp. 321-328.

Hwang, Y., and R. Radermacher, 1998, "Development of Hermetic Carbon Dioxide Compressor", Proc. 1998 Int'l Refrigeration Conf. at Purdue, West Lafayette, IN, July 14-17, pp. 171-176, 1998.

Hwang, Y., and R. Radermacher, 2000, Vapor Compression Heat Pumps with Refrigerant Mixtures, University of Maryland-CEEE, College Park, MD.

Koehler, J., Sonnekalb, M., and H. Kaiser, 1998, "A Transcritical Refrigeration Cycle with CO2 for Bus Air Conditioning and Transport Refrigeration", Proc. 1998 Int'l Refrigeration Conf. at Purdue, West Lafayette, IN, July 14-17, pp. 121-126.

Kruse, H., 1993, "European Research and Development Concerning CFC and HCFC Substitution", Proceedings of ASHRAE/NIST Refrigerants Conference, Gaithersburg, MD, pp. 41-57.

Lorentzen G. and Pettersen J., 1992, "New Possibilities for Non-CFC Refrigeration", *Refrigeration,, Energy, and Environment Proceedings*, pp. 147-163.

Lorentzen G. and Pettersen J., 1993, "A New and Environmentally Benign System for Car Air-Conditioning", *International Journal of Refrigeration*, Vol. 16, No. 1, pp. 4-12.

Mukaiyama H., Kuwabara O., Kazuhiro I., Ishigaki S., and Susai T., 2000, "Experimental Results and Evaluation of Residential CO_2 Heat Pump Water Heater", *Preliminary Proceedings of the 4th IIR-Gustav Lorentzen Conference on Natural Working Fluids at Purdue*, pp. 67-73.

Pettersen J., 1994, "An Efficient New Automobile Air-Conditioning System based on CO_2 Vapor Compression", ASHRAE Transactions, Vol. 100, Part 2, pp. 657-665.

Pettersen J. and Skaugen G., 1994, Operation of Trans-Critical CO_2 Vapor Compression Systems in Vehicle Air Conditioning, *IIR Conference on New Applications of Natural Working Fluids in Refrigeration and Air Conditioning*, pp. 495-505.

Preissner M., Cutler B., Singanamalla S., Hwang Y., and Radermacher R., 2000, Comparison of Automotive Air-Conditioning Systems Operating with CO_2 and R134a, *Preliminary Proceedings of the 4th IIR-Gustav Lorentzen Conference on Natural Working Fluids at Purdue*, pp. 185-192.

Reed, J.W., 1993, Environmental Overview: CFC and HCFC Regulatory Update, Proceedings of The 4th IEA Heat Pump Conference, Maastricht, The Netherlands, pp. 11-19.

Richter M.R., Song S.M., Yin J.M., Kim M.H., Bullard C.W., and Hrnjak P.S., 2000, Transcritical CO_2 Heat Pump for Residential Applications, *Preliminary Proceedings of the 4thIIR-Gustav Lorentzen Conference on Natural Working Fluids at Purdue*, pp. 9-16.

Tadano, M., Ebara, T., Oda, A., Susai, T., Takizawa, K., Izaki, H., and T. Komatsubara, 2000, "Development of the CO_2 Hermetic Compressor", *Proc. of the 4th IIR–Gustav Lorentzen Conference on Natural WorkingFluids*, Purdue University, West Lafayette, IN, July 25-28, pp. 323-330.

Yamasaki, H., Tadano, M., Sato, K., Matsuura, D., Ebara, T., 2001, "Hermetic CO_2 Compressor", SANYO Technical Review, Vol.33, No.2, pp.10-16